National Technical University of Athens

MSc. Computational Mechanics

Dissertation Thesis

“Ship’s hull response under extreme bending loading”

Supervisors: Prof. M. Papadrakakis
Prof. M. S. Samuelides

Christos Pollalis

ATHENS 2015

ACKNOWLEDMENTS

For the accomplishment of my thesis I would like, first of all, to thank professors M. Papadrakakis and M. S. Samuelides who supported me theoretically but also practically whenever problems occurred.

Furthermore, special thanks deserve colleagues I. Zilakos, A. Charitopoulos and P. Koroulakis who always provided me with high technological equipment and knowledge, necessary for the completion of my thesis.

Moreover, the assistance of C. Andriakopoulou and E. Kontoudakis was inevitable as it concerns the linguistic formulation.

Finally, as it happens always, my family supported and provided me with all the essentials so that my effort becomes more affordable.

DEEPLY GRATEFUL
CHRISTOS D. POLLALIS

TABLE OF CONTENTS

ABSTRACT

In April 2013, IACS first introduced the Draft Harmonized Rules for Tankers and Bulk Carriers, where it is also mentioned the study of the residual strength of a ship's hull after collision or grounding, including the proposed dimensions of a representative damage. In this thesis, the main part deals with this issue of ship's residual strength in case of collision. In Draft Harmonized Rules either the iterative-incremental method or the finite element method is proposed for the assessment of the ultimate bending capacity of a transverse cross-section.

In this work, we considered the sagging condition as the most severe in a ship's lifetime. The reason is that, in general, the part of a ship above neutral axis is less stiff than the part beneath the neutral axis as the double bottom provides increased strength and thus it faces greater risks to collapse. Moreover, the deck of a ship is usually more remote from the neutral axis than the bottom. Therefore, the normal stresses which are developed at deck plating and stiffeners are larger and can lead to buckling collapse of the structure.

We used the Finite Element Commercial package (ABAQUS *Version 6.13-4*) for our calculations. The models were simulated by applying explicit algorithm as deformations and rotations were quite large. In such cases, a static algorithm cannot be applied because the nonlinear response of the structure is too complicated and convergence is difficult to be achieved.

The second issue of interest in this thesis is to compare the numerical results to the results taken by the implementation of the incremental-iterative method.

CHAPTER ONE:

INTRODUCTION

1. INTRODUCTION

When we use the term “Ultimate Strength” we consider the limit state of a structure where static equilibrium does not exist anymore. An increase of the loading after that point is impossible when static behavior of the structure is considered. Ultimate strength is determined by buckling and yielding of a structural element, when compressive stresses are applied, and by yielding when tensile stresses are applied.

Nowadays, it is common that structures are designed so that will not collapse due to buckling or yielding. However, until 1850 the design criterion of structures was the stress of breakage. This was partially happened, because the main material of ship building was the hammered iron which is not so ductile when tensile forces are applied. Another reason is that buckling and its side effects were not considered as a failure criterion until ***Fairbaim’s tests*** *(ISSC 2006)* ***[17]*** *in 1845 (Timoshenko, 1953)* ***[18]****.* Afterwards, there was ***Bryan [1]]*** who tried to understand theoretically and calculate the buckling of plates and used the resistance against buckling as a criterion in order to determine the thickness of plates.

The first attempt for evaluating the ultimate strength of a ship was done by ***Caldwell [2]****.* Buckling was taken into account by reducing yield stress (ISSC 2006, Committee III.I. Ultimate Strength, 5).

In 1956 the first paper which referred to the Finite Element Method was published by ***Turner et al [3]****.* At first, this method was used for the analysis of the elastic response of structural members and systems, but it took more than two decades for the commercial software, which carried out complete analysis up to collapsed state, to be used widely.

Recent research on the issue of Ultimate strength has been made by several researchers. A grounding damage index was introduced by ***Paik et al. [4]*** which represented the loss of material of the inner and outer bottom plating with stiffeners. The procedures followed for the determination of the residual strength are a) The Paik-Mansour formula by ***Paik et al [5]***. , b) The incremental-iterative method described in CSR documents, c) A finite element approach using ANSYS and finally d) The ***ALPS/HULL [6]*** super-size finite element method. However, the above methods did not deal with the rotation of the neutral axis when an asymmetrical cross section is studied. ***Villavicencio et al. [7]*** also proposed a method, similar to what we have done in this work, where rotation was induced at a double bottom structure, connected to two rigid bodies aft and fore. The rest structure above double bottom was simplified in long plate elements with equivalent thicknesses. ***Notaro et al. [8]*** also investigated the residual strength of several ships, using

the commercial software ABAQUS in both sagging and hogging conditions. They also investigated the influence of several modeling aspects on the results such as the length of the model and the effect of initial imperfections. Finally, ***Koukounas et al. [9]***, ***Pollalis et al. [10]*** and ***Samuelides et al. [11]*** investigated the effect of several modeling parameters of the finite element method when dealing with the issue of Ultimate strength of intact and damaged hulls.

The present thesis consists of a continuation of this work with more details and also includes comparative results after using the incremental-iterative method. Through the implementation of numerical but also analytical methods, it is provided a methodology for estimating the residual strength of a ship after collision which can be useful in case of a real case scenario.

Apart from **Chapter II** which contains theoretical aspects, this thesis contains three more Chapters. In **Chapter III** results from the application of the Finite Element Method in two different ship sections can be seen and **Chapter IV** contains the results of the incremental-iterative method. Finally, in **Chapter V** the reader can see the final conclusions of my research.

CHAPTER TWO:

BACKGROUND

2. BACKGROUND

2.1 Explicit dynamic analysis

General

As we used only the explicit code for our simulations it is considered rational that we should present some basic attributes about its procedure of solving numerically problems using the Finite Element Method.

As it is mentioned in ***ABAQUS Tutorial [12]*** an explicit dynamic analysis:

- is computationally efficient for the analysis of large models with relatively short dynamic response times and for the analysis of extremely discontinuous events or processes;
- uses a consistent, large-deformation theory—models can undergo large rotations and large deformation;
- can use a geometrically linear deformation theory—strains and rotations are assumed to be small
- can be used to perform quasi-static analyses with complicated contact conditions; and
- allows for either automatic or fixed time incrementation to be used

The explicit dynamics procedure performs a large number of small time increments efficiently. An explicit central-difference time integration rule is used; each increment is relatively inexpensive because there is no solution for a set of simultaneous equations.in contrary to the dynamic implicit analysis where the integration operator matrix must be inverted and a set of nonlinear equilibrium equations must be solved at each time increment.
The explicit central-difference operator satisfies the dynamic equilibrium equations at the beginning of the increment, t; the accelerations calculated at time t are used to advance the velocity solution to time t+Δt/2 and the displacement solution to time t+Δt. ***[12]***

The explicit dynamics analysis procedure is based upon the implementation of an explicit integration rule together with the use of diagonal (“lumped”) element mass matrices. The equations of motion for the body are integrated using the explicit central-difference integration rule

$$\dot{u}^N_{(i+\frac{1}{2})} = \dot{u}^N_{(i-\frac{1}{2})} + \frac{\Delta t_{(i+1)} + \Delta t_{(i)}}{2} \ddot{u}^N_{(i)}$$

$$u^N_{(i+1)} = u^N_{(i)} + \Delta t_{(i+1)} \dot{u}^N_{(i+\frac{1}{2})}$$

where u^N is a degree of freedom (a displacement or rotation component) and the subscript i refers to the increment number in an explicit dynamics step.
The central-difference integration operator is explicit in the sense that the kinematic state is advanced using known values of and from the previous increment.
The explicit integration rule is quite simple but by itself does not provide the computational efficiency associated with the explicit dynamics procedure. The key to the computational efficiency of the explicit procedure is the use of diagonal element mass matrices because the accelerations at the beginning of the increment are computed by

$$\ddot{u}^N_{(i)} = (M^{NJ})^{-1}(P^J_{(i)} - I^J_{(i)})$$

where M^{NJ} is the mass matrix, P^J is the applied load vector, and I^J is the internal force vector. A lumped mass matrix is used because its inverse is simple to compute and because the vector multiplication of the mass inverse by the inertial force requires only n operations, where n is the number of degrees of freedom in the model. The explicit procedure requires no iterations and no tangent stiffness matrix.

The internal force vector, I^J is assembled from contributions from the individual elements such that a global stiffness matrix need not be formed. **[1]**

As it concerns the stability of the explicit procedure, the central difference operator is conditionally stable, and the stability limit for the operator (with no damping) is given in terms of the highest frequency of the system as

$$\Delta t \leq \frac{2}{\omega_{max}}$$

The time increment used in an analysis must be smaller than the stability limit of the central-difference operator. Failure to use a small enough time increment will result in an unstable solution. When the solution becomes unstable, the time history response of solution variables such as displacements will usually oscillate with increasing amplitudes. The total energy balance will also change significantly.
If the model contains only one material type, the initial time increment is directly proportional to the size of the smallest element in the mesh. If the mesh contains uniform size elements but contains multiple material descriptions, the element with the highest wave speed will determine the initial time increment. In nonlinear problems—those with large deformations and/or nonlinear material response—the highest frequency of the model will continually change, which consequently changes the stability limit. ***[12]***

Advantages of the explicit method

The use of small increments (dictated by the stability limit) is advantageous because it allows the solution to proceed without iterations and without requiring tangent stiffness matrices to be formed. It also simplifies the treatment of contact. The explicit dynamics procedure is ideally suited for analyzing high-speed dynamic events, but many of the advantages of the explicit procedure also apply to the analysis of slower (quasi-static) processes.
The results in an explicit dynamics analysis are not automatically checked for accuracy. In most cases this is not of concern because the stability condition imposes a small time increment such that the solution changes only slightly in any one time increment, which simplifies the incremental calculations. While the analysis may take an extremely large number of increments, each increment is relatively inexpensive, often resulting in an economical solution. The method is, therefore, computationally attractive for problems where the total dynamic response time that must be modeled is only a few orders of magnitude longer than the stability limit. ***[12]***

Computational cost

The computer time involved in running a simulation using explicit time integration with a given mesh is proportional to the time period of the event. The time increment based on the element-by-element stability estimate can be rewritten (ignoring damping) in the form

$$\Delta t \leq \min(L_e \sqrt{\frac{\rho}{\lambda + 2\mu}})$$

where the minimum is taken over all elements in the mesh, is a characteristic length associated with an element, ρ is the density of the material in the element, and λ and μ are the effective Lame's constants for the material in the element.
The time increment from the global stability estimate may be somewhat larger, but for this discussion we will assume that the above inequality always holds (when the inequality does not hold, the solution time will be somewhat faster).

The number of increments, n, required is n=T/Δt if Δt remains constant, where T is the time period of the event being simulated. (Even the element-by-element approximation of Δt will not remain constant in general, since element distortion will change L_e and nonlinear material response will change the effective Lame constants. But the assumption is sufficiently accurate for the purposes of this discussion.) Thus,

$$n \approx Tmax(\frac{1}{L_e}\sqrt{\frac{\lambda + 2\mu}{\rho}})$$

In a two-dimensional analysis refining the mesh by a factor of two in each direction will increase the run time in the explicit procedure by a factor of eight—four times as many elements and half the original time increment size. Similarly, in a three-dimensional analysis refining the mesh by a factor of two in each direction will increase the run time by a factor of sixteen.

In a quasi-static analysis it is expedient to reduce the computational cost by either speeding up the simulation or by scaling the mass. In either case the kinetic energy should be monitored to ensure that the ratio of kinetic energy to internal energy does not get too large—typically less than 10%. ***[12]***

Reducing the computational cost

To reduce the number of increments required, n, we can speed up the simulation compared to the time of the actual process—that is, we can artificially reduce the time period of the event, T. This will introduce two possible errors. If the simulation speed is increased too much, the increased inertia forces will change the predicted response (in an extreme case the problem will exhibit wave propagation response). The only way to avoid this error is to choose a speed-up that is not too large.
The other error is that some aspects of the problem other than inertia forces—for example, material behavior—may also be rate dependent. In this case the actual time period of the event being modeled cannot be changed. ***[12]***

2.2 Nonlinearity

General

Geometrically nonlinear static problems sometimes involve buckling or collapse behavior, where the load-displacement response shows a negative stiffness and the structure must release strain energy to remain in equilibrium. Several approaches are possible for modeling such behavior. One is to treat the buckling response dynamically, thus actually modeling the response with inertia effects included as the structure snaps.
In some simple cases displacement control can provide a solution, even when the conjugate load (the reaction force) is decreasing as the displacement increases. Another approach would be to use dashpots to stabilize the structure during a static analysis.
Alternatively, static equilibrium states during the unstable phase of the response can be found by using the “modified Riks method.” This method is used for cases where the loading is proportional; that is, where the load magnitudes are governed by a single scalar parameter. The method can provide solutions even in cases of complex, unstable response such as that shown in Figure 1.

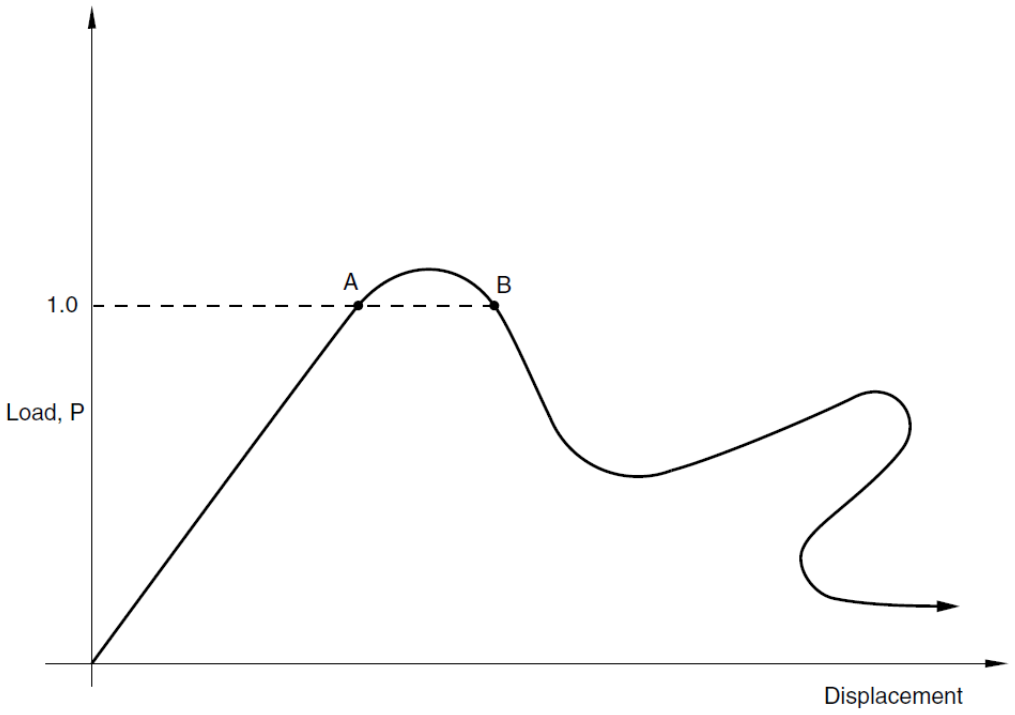

Figure 1. Proportional loading with unstable response

The Riks method is also useful for solving ill-conditioned problems such as limit load problems or almost unstable problems that exhibit softening. ***[13]*** In our case, static analysis using Newton's method as well as Riks method was conducted unsuccessfully due to the severe buckling which appeared at our models and led to unstable response. That is the reason that we solved the problems quasi-statically using dynamic explicit method. More information about the parameters of the analysis will be given in next chapters.

Sources of nonlinearity

There are three sources of nonlinearity in structural mechanics simulations:

- Material nonlinearity.
- Boundary nonlinearity.
- Geometric nonlinearity.

Material nonlinearity

It is the most common source of nonlinearity. Most of the materials have a nonlinear response after a critical value of applied stress is reached, called yield stress. After that point, the relationship between stresses and strains becomes nonlinear as shown below.

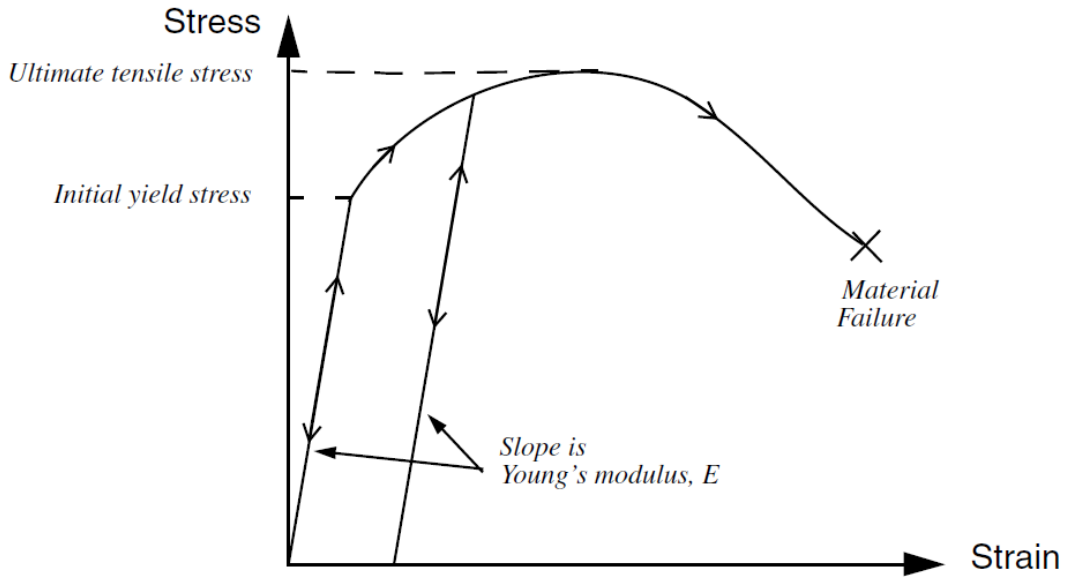

Figure 2. Stress-strain curve for an elastic-plastic material under uniaxial tension

Boundary nonlinearity

This type of nonlinearity appears when there is a change of the boundary conditions during the analysis. This can be easily understood when we consider the cantilever beam of Figure 3.

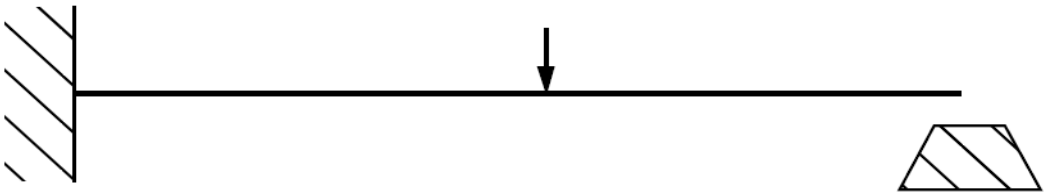

Figure 3. Cantilever beam hitting a stop

The vertical deflection of the tip is linearly related to the load (if the deflection is small) until it contacts the stop. There is then a sudden change in the boundary condition at the tip of the beam, preventing any further vertical deflection, and so the response of the beam is no longer linear.

Geometric nonlinearity

This source of nonlinearity appears when we have changes of the geometry during the analysis. This may refer to:

- Large deflections or rotations.
- “Snap through.”
- Initial stresses or load stiffening.

Explanatory figures are given below.

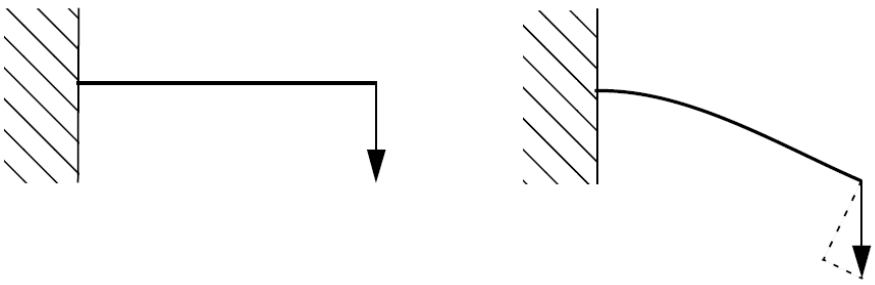

Figure 4. Large deflection of a cantilever beam

When the vertical deflections which are applied at the tip of the cantilever beam shown above become large, then the relationship between vertical loading versus vertical deflection changes to nonlinear as a portion of the total loading contributes for the vertical displacement of the cantilever beam.

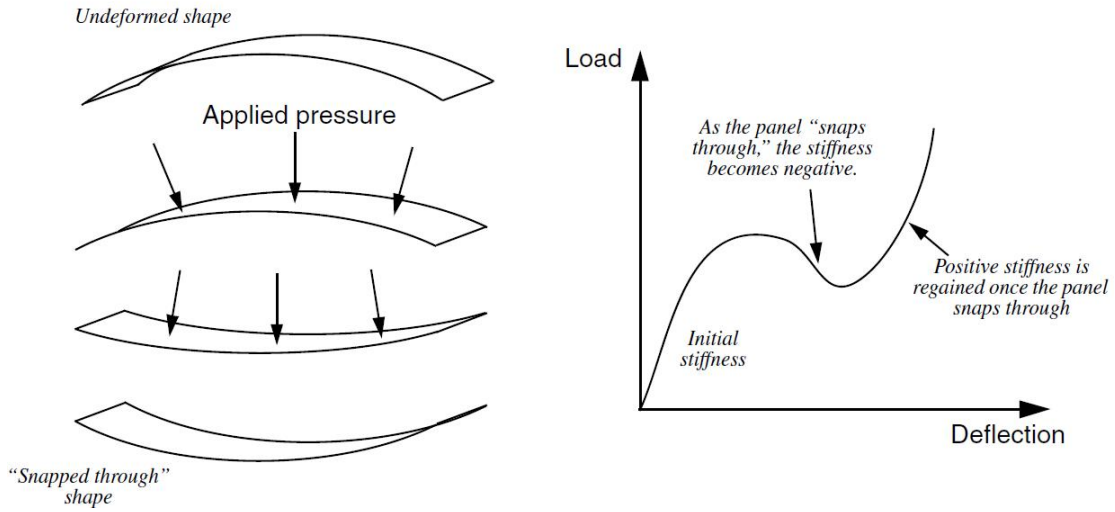

Figure 5. Snap-through of a large shallow panel

This example indicates the dramatic change of the stiffness of the panel when it snaps through. At that moment the stiffness becomes negative. Even if the displacements are small there is a considerable geometric nonlinearity.

From the sources of nonlinearity mentioned before, in our case only two of them appear; nonlinearities concerning the material properties and nonlinearities which are caused due to the large rotations applied at the ship's cross section.

2.3 Analytical methods for the evaluation of the ultimate strength of a ship-The incremental/iterative method

Among the analytical methods which are used to evaluate the ultimate strength of a ship is the Smith's method or the incremental/iterative method. In this case, the M-χ curve is derived by an incremental procedure which is summarized in Figure 6.

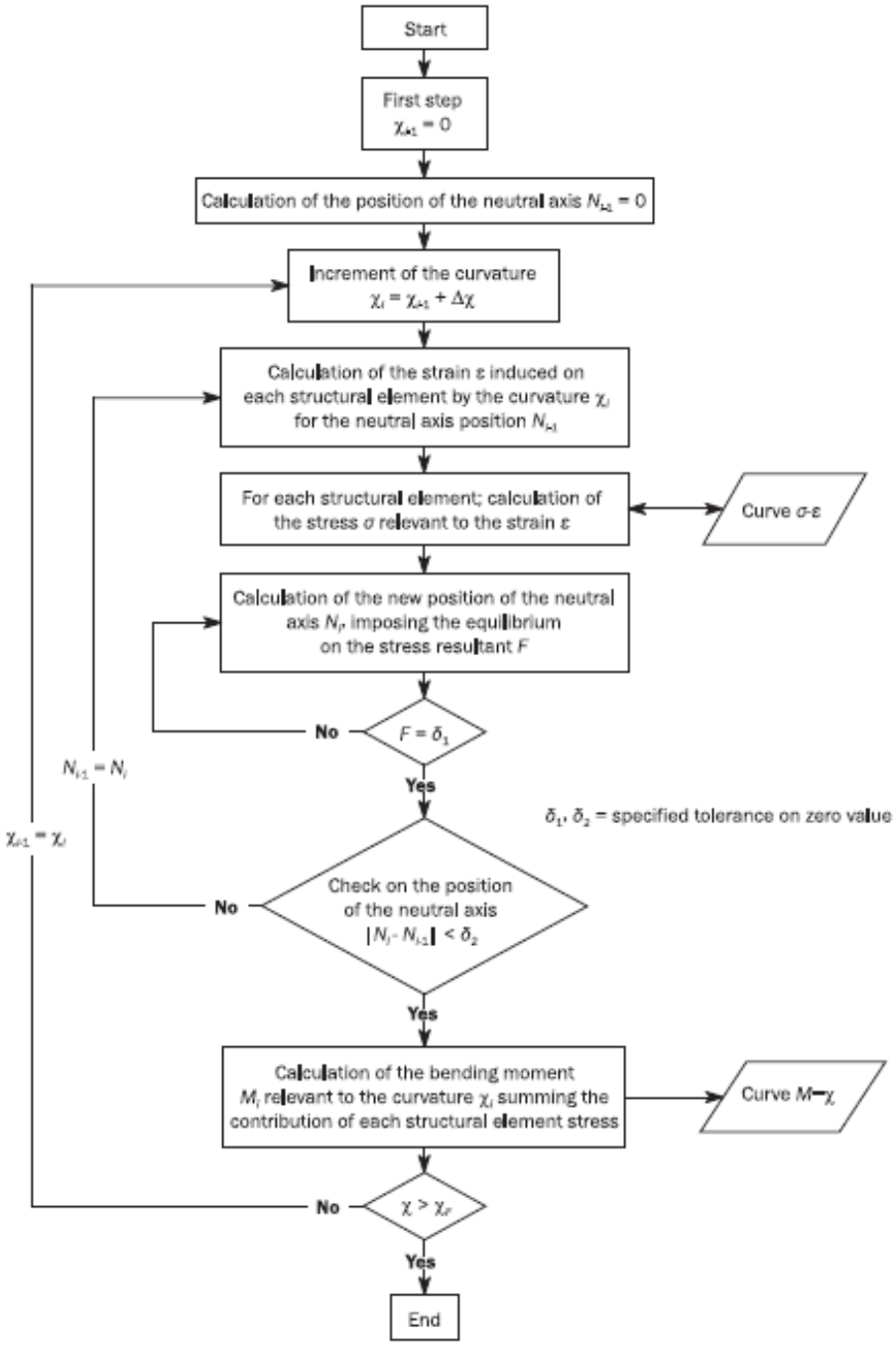

Figure 6. Flow chart displaying the incremental-iterative method

In each step of this procedure, the vertical bending moment M is calculated, which acts on the transverse section of the ship as a result of the applied curvature χ. In each step, the value of the applied curvature χ_i results from the summation of the infinite value Δχ to the curvature of the previous step. This summation Δχ is derived from an increment of the angle of rotation of the section about the horizontal neutral axis. In addition, this summation provokes normal strains ε at every structural member of the section. The value of the

normal strain ε depends on the distance of the structural member from the neutral axis. In sagging condition, which is investigated in this document, the members lying above the neutral axis are under compression, while the members below the neutral axis are under tension.

The normal stresses σ which are provoked by the normal strains, are calculated using the σ-ε relationship of the member. This relationship depends on the response of the structural member in the nonlinear, elasto-plastic region. The distribution of normal stresses along the depth of the structure determines changes of the position of the neutral axis in order to eliminate the axial forces which appear in each step of the procedure. When equilibrium of the forces is succeeded, the vertical bending moment acting on the section results from the contribution of each structural member.

The basic steps of the procedure are the following:

Step 1→ The section is separated in stiffened structural members.

Step 2→ For each structural member we determine its σ-ε relationship.

Step 3→ The curvature as well as the position of the neutral axis is initialized for the beginning of the procedure using the following equation:

$$\chi_1 = \Delta\chi = \frac{0.01\frac{R_{eH}}{E}}{Z_D - N}$$

where Z_D is the distance of the deck from the baseline of the ship.

Step 4→ For each structural member, the normal strain is calculated from the below relation:

$$\varepsilon = \chi(Z_\iota - Z_{N.A.})$$

and then, its normal stress.

Step 5→ The position of the neutral axis is calculated by applying the equilibrium of forces at the whole section.

$$\sum A\sigma_{comp} = \sum A\sigma_{tens}$$

Step 6→ The resulting moment is calculating by summing the contribution of each member.

$$M_U = \sum \sigma A \left| (Z_i - Z_{N.A._{cur}}) \right|$$

Step 7→ The calculated moment is compared to the moment of the previous step. If the slope of the M-χ curve is smaller than a fixed negative value, then the procedure stops and the value of the moment M_U is determined.

CHAPTER THREE:

MODELING ASPECTS FOR THE ESTIMATION OF A SHIP'S RESIDUAL STRENGTH USING THE F.E.M.

3. MODELING ASPECTS FOR THE ESTIMATION OF A SHIP'S RESIDUAL STRENGTH USING THE FEM

3.1 Structure of the study

The investigation of the effect of several modeling parameters including the mesh element size and type, the rate of loading application when dynamic explicit methods are applied and the material properties on the calculation of a ship's residual strength using the FE Method was founded on several models. In this document we will present the process which has been followed at two Crude Oil Carriers of similar principal dimensions. The ships' drawings are attached in the appendix. The results will also be compared with relevant published literature. Both intact and damaged conditions were studied.

3.2 Ship modeling

At first, we will present the principal particulars of the two ships.

SHIP I	
DWT	119315 tons
L_{oa}	264.68 m
L_{bp}	256.50 m
Breadth	42.50 m
Depth	22.00 m
Draft	15.00 m
Design Moment in sagging	7.732 GNm

Table 1. Principal dimensions of the studied SHIP I

SHIP II	
DWT	112700 tons
L_{oa}	250.17 m
L_{bp}	239.00 m
Breadth	44.00 m
Depth	21.00 m
Draft	14.60 m
Design Moment in sagging	6.753 GNm

Table 2. Principal dimensions of the studied SHIP II

The design moment for both ships has been calculated using the Common Structural Rules for double hull Oil Tankers ***[19]***. The minimum section modulus using the formula proposed by C.S.R. for each ship is:
$Z_{min\text{-}SHIP\ I}=29.3m^3$ and $Z_{min\ SHIP\ II}=25.59m^3$ whereas the permissible bending stress for both ships is $\sigma_{perm}=263.9$ MPa because the material used for the simulations has a yield stress of $\sigma_{yield}=355$ MPa.

The models which were created are of one (SHIP I) and three bay-long (SHIP II). The length of each bay is equal to the length between two successive web frames, that is to say, 4.00 meters for SHIP I and 3.78 meters for SHIP II.

It is considered that a model of such size can appropriately show reliable results compared to the Incremental-Iterative method providing stress and displacement distributions in larger extent. Figures 7, 8 show the studied ship models.

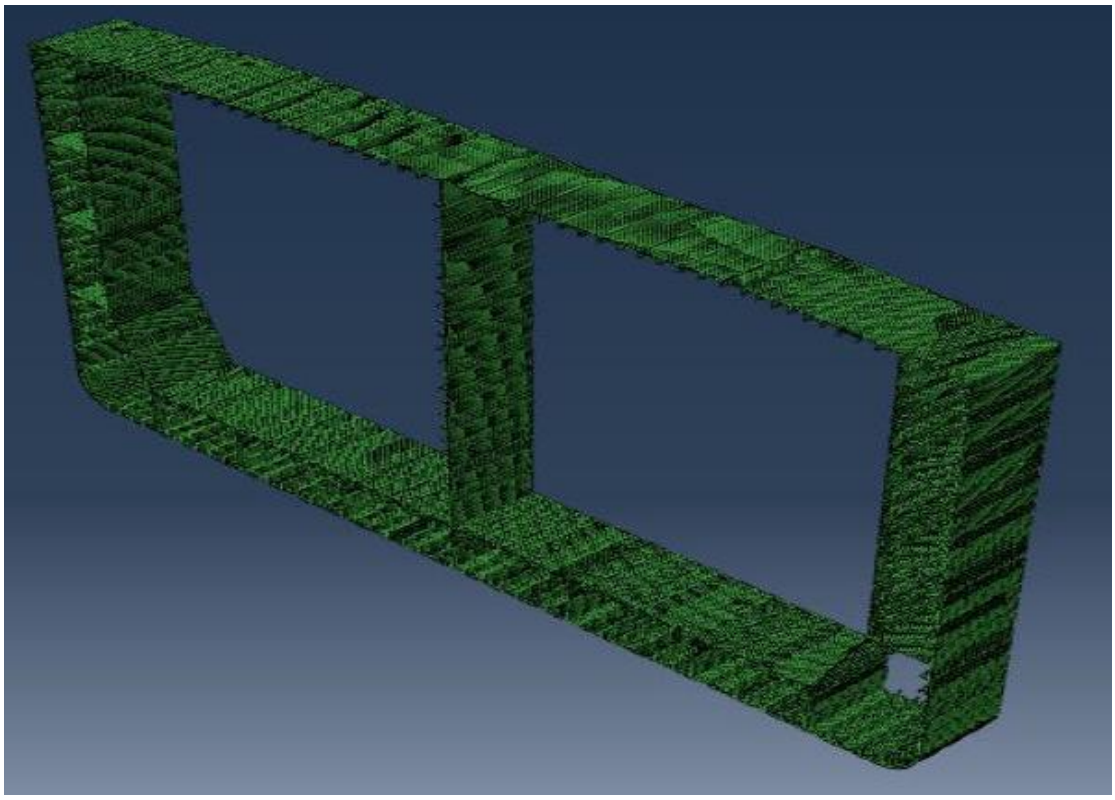

Figure 7. One bay model-SHIP I

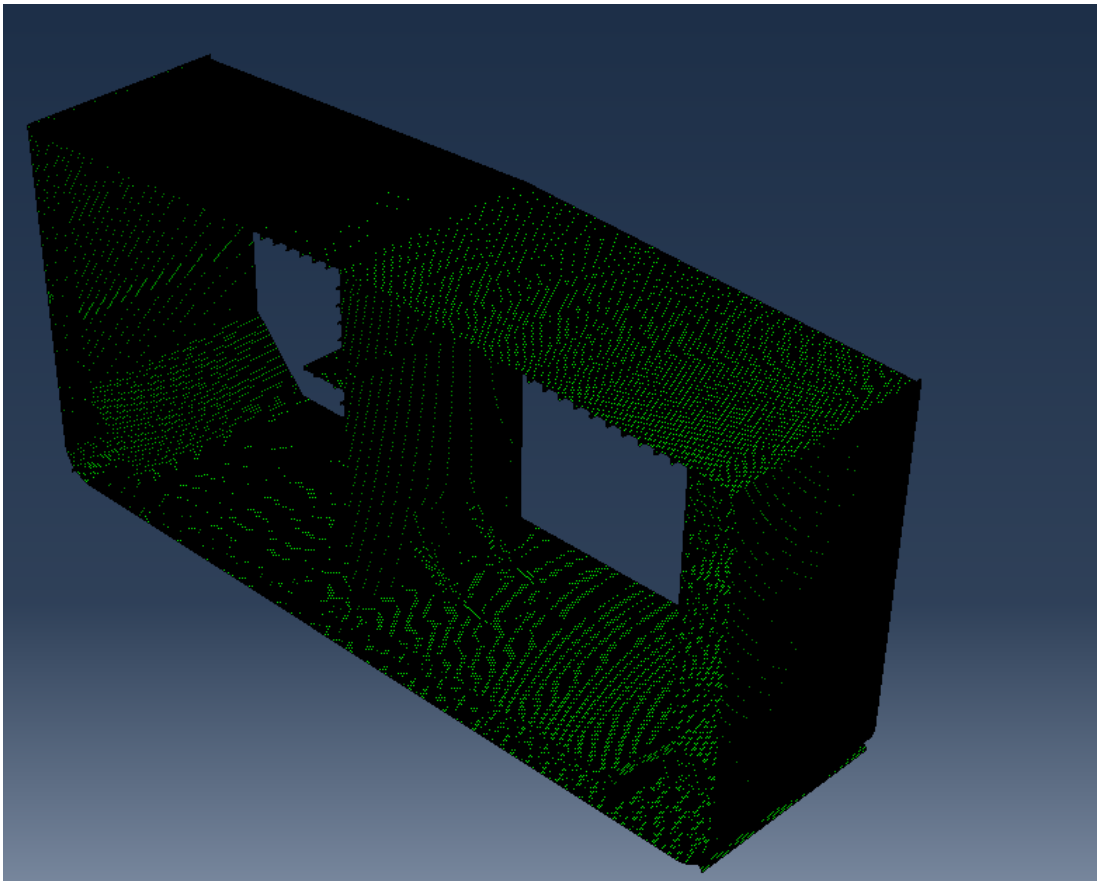

Figure 8. Three bay model-SHIP II

Apart from the intact models, we also created models having a damage as defined by IACS Harmonized Rules. The dimensions of the damage are given in the following table. The longitudinal extent of the damage is not defined in CSR, so it is considered equal to the distance of two successive web frames.

SHIP I	
Height of damage	0.60D → 13.20 m (from the upper deck)
Breadth of damage	B/16 → 2.66 m (for double hull vessels)
Length of damage (as considered by the author)	4.00 m (distance between two successive web frames)

Table 3. Dimensions of the damage for SHIP I

SHIP II	
Height of damage	0.60D → 12.60 m (from the upper deck)
Breadth of damage	B/16 → 2.75 m (for double hull vessels)
Length of damage (as considered by the author)	3.78 m (distance between two successive web frames)

Table 4. Dimensions of the damage for SHIP II

Especially, for the case of SHIP II, there were studied two possible collision cases. For the first case the damage is considered between two successive web frames (symmetrical case), while for the second case a web frame was placed between the damage (nonsymmetrical case with respect to the mid-ship section). Explanatory figures can be seen below.

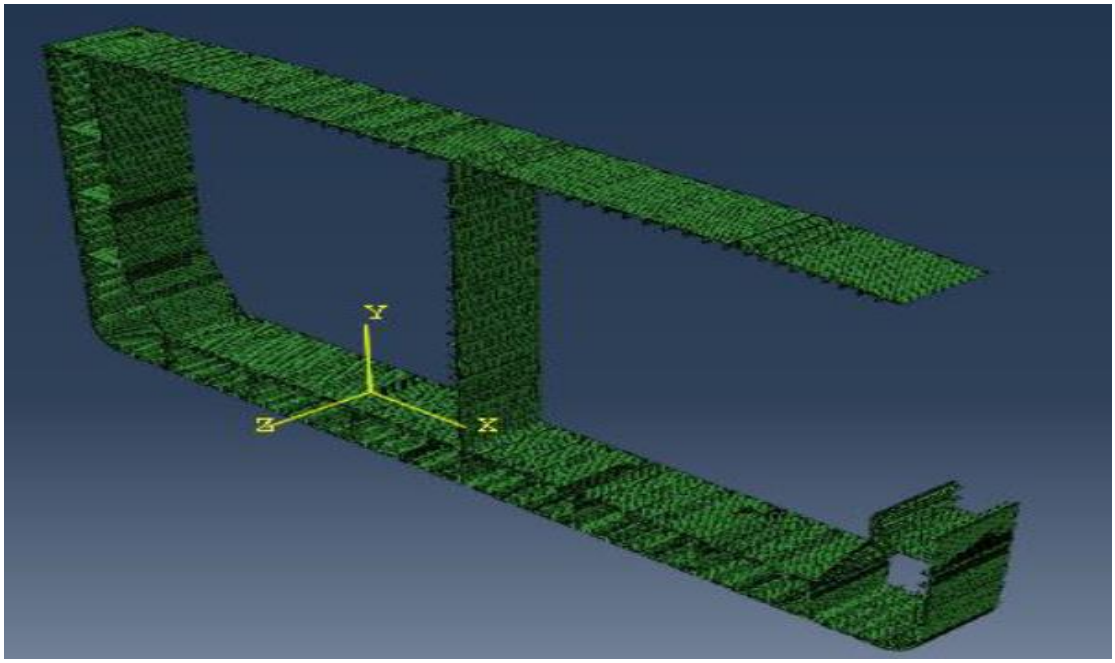

Figure 9. Model of the damaged SHIP I

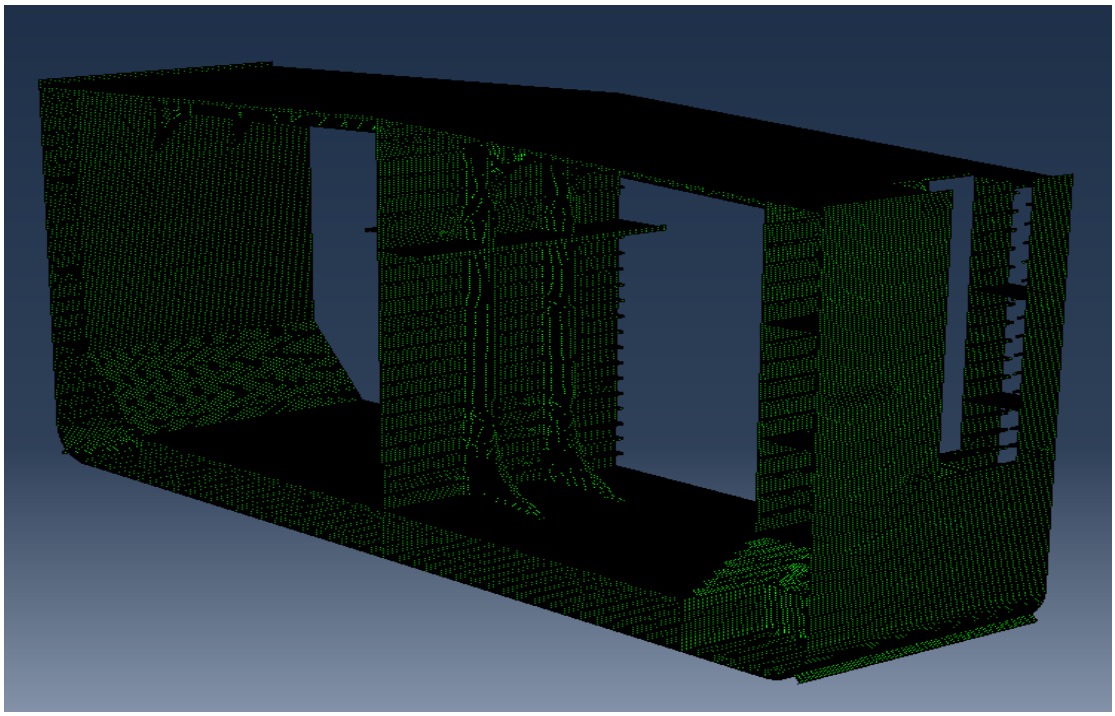

Figure 10. Model of the damaged SHIP II (scenario 1)

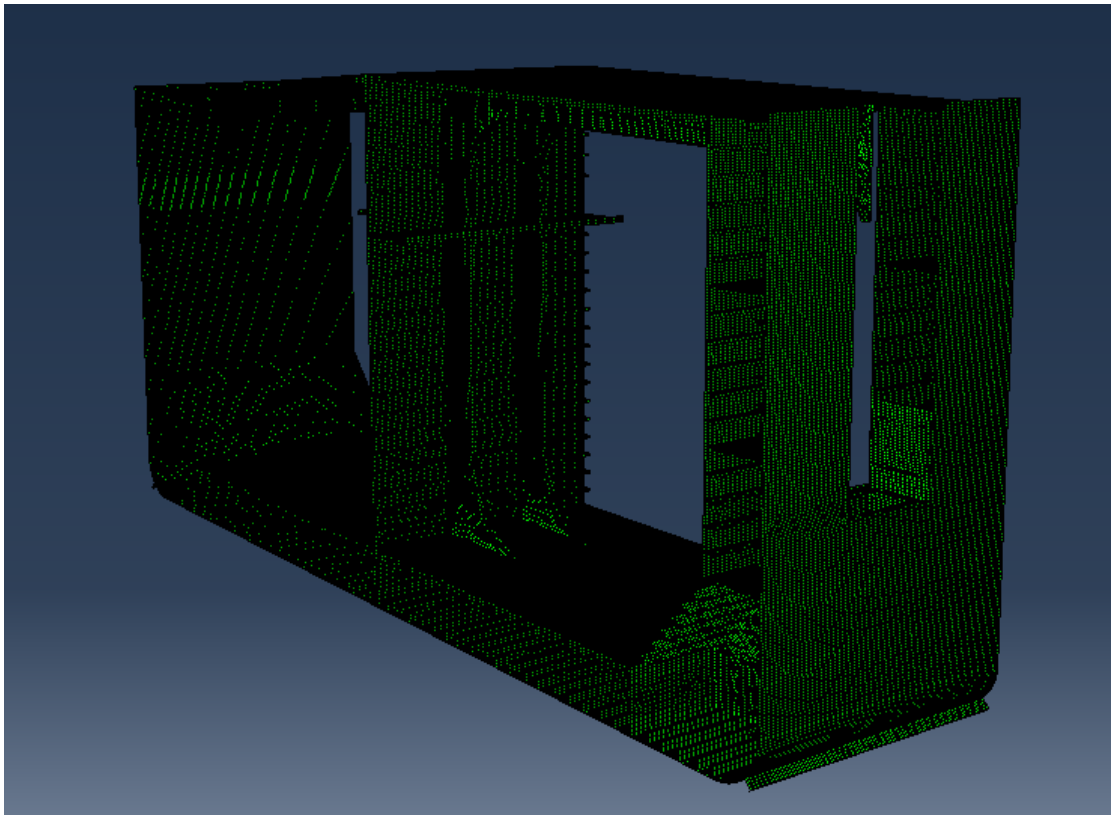

Figure 11. Model of the damaged SHIP II (scenario 2)

As the simulation of SHIP I is less demanding, due to the size of the model and the number of its elements, we conducted an integrated research on the effect of several modeling parameters and then, we used the conclusions of this research for the simulation of SHIP II in both damage cases. Our goal is, first, to develop a reliable method for the assessment of a ship's residual strength and, second, the investigation of the response of a ship when different collision scenarios are studied.

The modeling process of SHIP I is cited below.

Geometrical attributes

The model was created taking into account the given drawings which are attached to the appendix of this document. The designed length is 4.00 meters, that is to say the longitudinal span between two successive web frames.

Material Properties

The material properties used in our simulations refer to the properties of the high strength steel AH-36.

Young modulus (E)=2.07 GPa
Poisson ratio (v)=0.30

Moreover, as it concerns the response of the material after first yielding, we applied the power law ***[14]***:

$$\sigma_{eq} = \begin{cases} \sigma_y, & if \ \varepsilon_{eq} \leq \varepsilon_{plat} \\ K(\varepsilon_{eq} + \varepsilon_0)^n, otherwise \end{cases}$$

where,

- ε_{plat} is not defined in our case
- K= 750
- n= 0.20

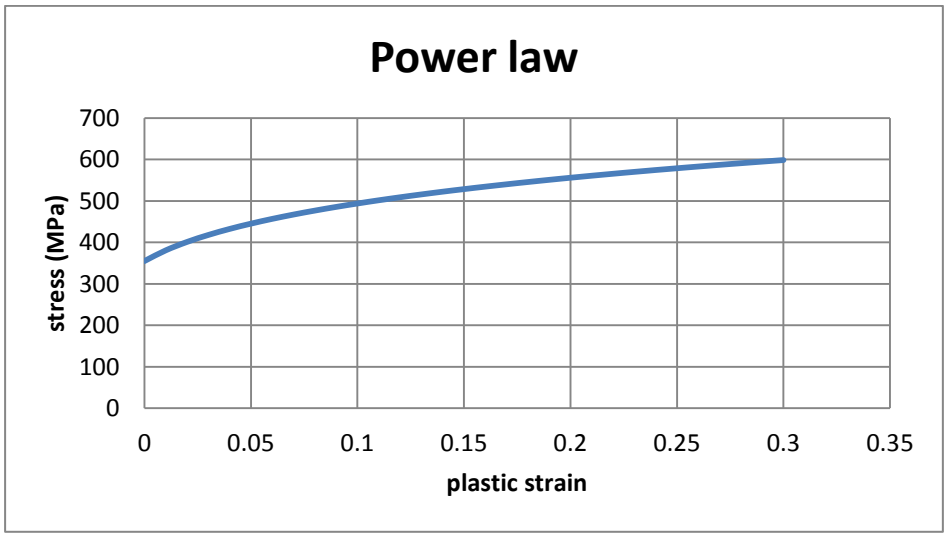

Figure 12. Stress-Strain relationship after first yielding

Element type

The element type we used is defined as S4R using the conclusions made in ***[11]*** and ***[10]***. These are general purpose, quadrilateral shell elements, appropriate for explicit analyses where large strains are considered. They are of reduced integration, meaning that such elements have only one integration point on their surface.

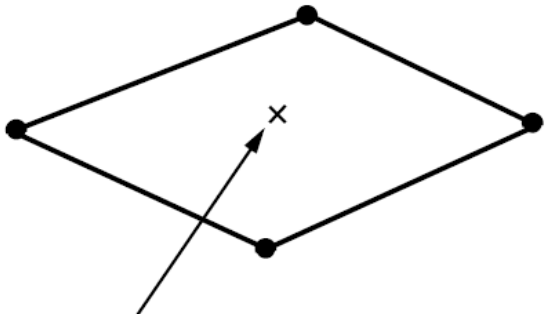

Integration point in
a S4R element

In addition, ABAQUS uses numerical integration to calculate the stresses and strains at each section point through the thickness of the element. Then, it uses linear interpolation to derive the final solution of the element.

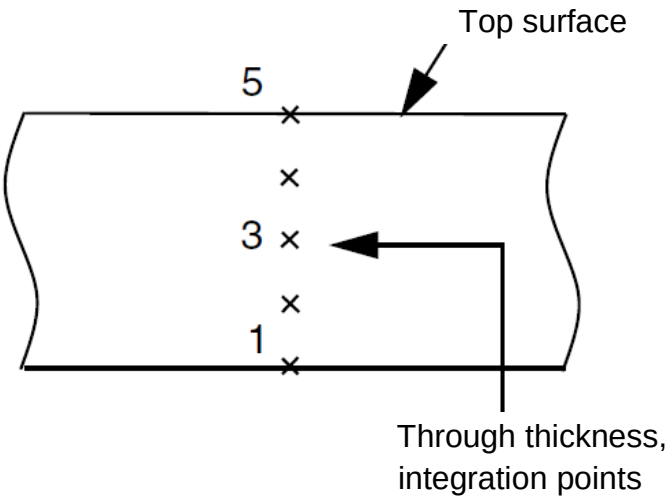

Element size

Models with several element size were created and the conclusions summarized in ***[11]***. Using these conclusions, we made our selection about the principal dimension of the mesh element that is to say, quadrilateral, square elements of 100mm side length.

Loading

The models were loaded by applying rotation at their edges. This requires the use of coupling constraint. By coupling the extreme nodes of each edge we can apply either moment or rotation.

When applying rotation, the software adjusts the suitable reaction moment which is developed similarly to the tension experiment when conducting strain control.

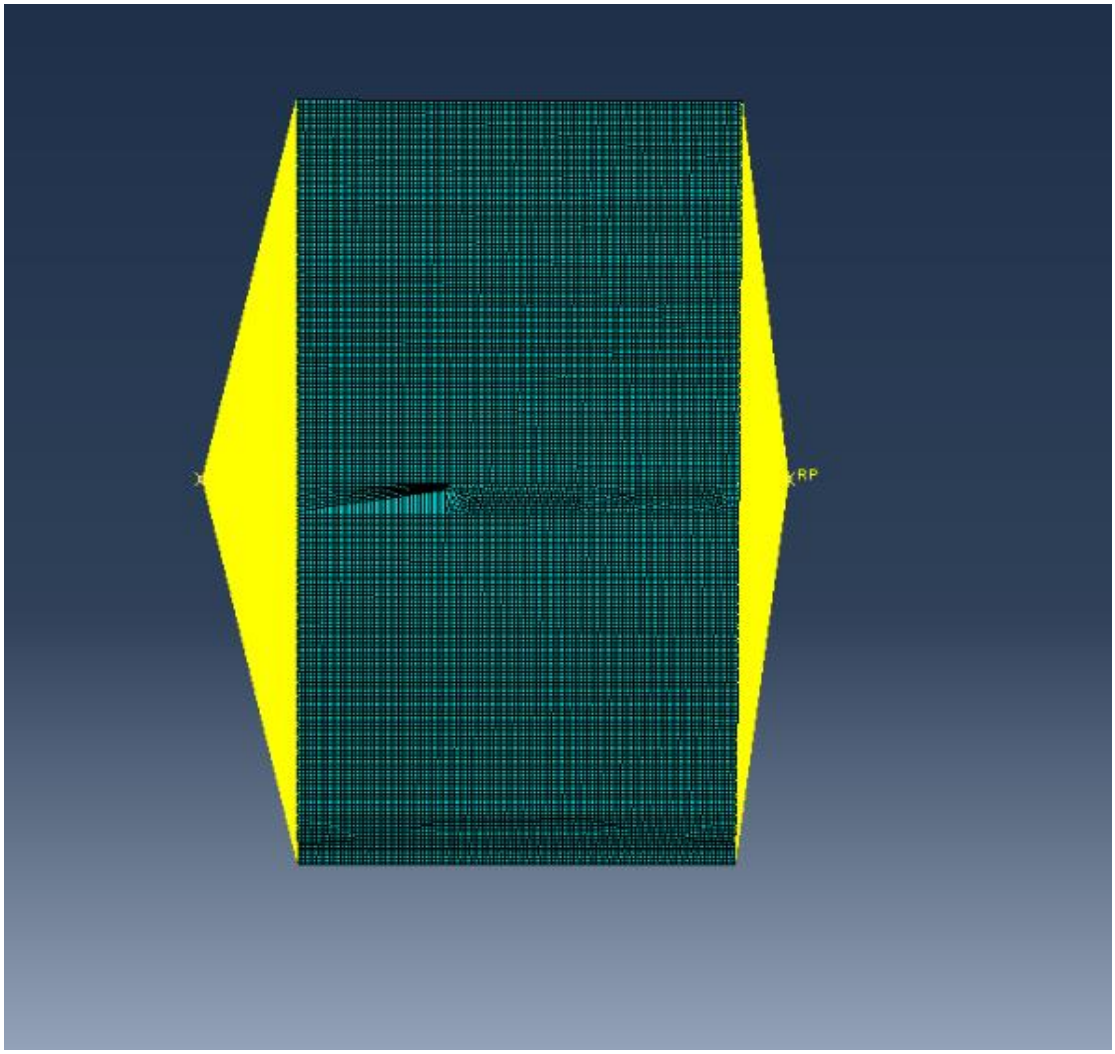

Figure 13. Application of coupling constraint in both sides of the model (SHIP II)

Boundary conditions

For the intact state our aim was to achieve pure bending condition. Therefore, the vertical bending moment should be constant through the whole span of the model and reaction forces must be eliminated. After consideration, the boundary conditions for the intact state are shown in Tables 5, 6.

Control Point 1		Control Point 2	
T_x	Fixed	T_x	Fixed
T_y	Fixed	T_y	Fixed
T_z	Free	T_z	Fixed
R_x	Kinematic	R_x	Kinematic
R_y	Fixed	R_y	Fixed
R_z	Fixed	R_z	Fixed

Table 5. Boundary conditions at control points 1, 2

Note that axis Z is the longitudinal axis. The above initial boundary conditions ensure that the only load applied in the structure is the vertical bending moment.

For the damaged condition, we conducted three analyses with different boundary conditions. These three different cases are accumulated in Table 6. In addition, we studied the result of each case concerning the value of the residual strength and the developed reaction forces and moments on the structure.

	D.O.F.	**BOUNDARY CONDITION CASE**		
		1	**2**	**3**
Control Point 1	T_x	Fixed	Free	Free
	T_y	Fixed	Free	Fixed
	T_z	Fixed	Free	Free
	R_x	Fixed	Fixed	Kinematic
	R_y	Fixed	Free	Fixed
	R_z	Fixed	Free	Free
Control Point 2	T_x	Free	Free	Free
	T_y	Free	Free	Fixed
	T_z	Free	Free	Free
	R_x	Kinematic	Kinematic	Kinematic
	R_y	Free	Free	Fixed
	R_z	Free	Free	Free

Table 6. Boundary condition cases - the red color means constrained degree of freedom. The symbol * means that rotation is applied to the d.o.f.

Rate of rotation/curvature application

When a dynamic explicit solver is used, the rate of load application plays an important role. In order to achieve quasi-static solution, we must ensure that the inertia forces are negligible. Therefore, the time period of load application should be large enough so that the dynamic solution approaches the static. For this particular simulation (SHIP I) the applied curvature rate is 0.0001216 $(m \cdot s)^{-1}$. This value was chosen because it has been observed a convergence between the static and the dynamic solution in the elastic region ***[11]***. Finally, the results of the analysis performed are of double precision.

3.3 Results-SHIP I

The diagram which depicts the moment versus curvature relationship including the intact and the damaged scenarios can be shown below.

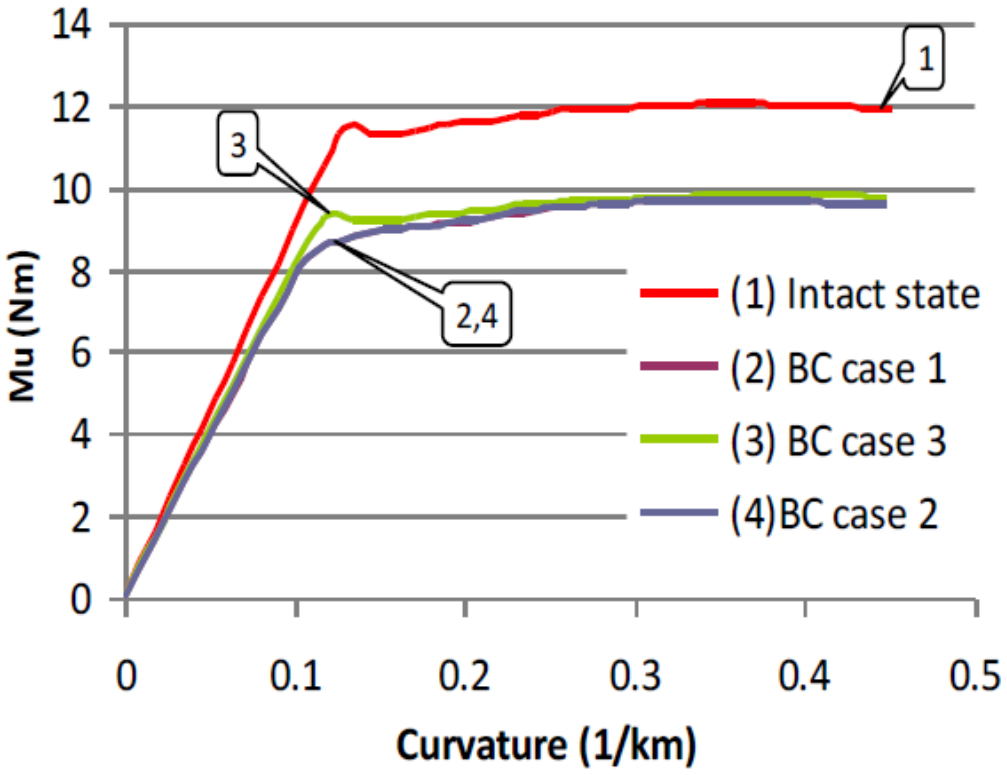

Figure 14. Curvature moment curves for the damaged one bay model of SHIP I

The values for the ultimate and residual strength for the four scenarios are:

	Intact	Damaged		
	BC case3	BC case1	BC case 2	BC case3
1Block	12.04	9.67	9.67	9.82

Table 7. Ultimate Strength for different boundary cases in GNm

As we can see from Table 8, the values of the residual strength among cases 1-2 are in accordance with each other. Moreover, there is a difference of δ=1.55% between the values for the cases 1-2 and the value of the residual strength for case 3.

Furthermore, the reduction of the ultimate strength of the vessel after collision is r_1=19.7% for the boundary cases 1-2 and r_2=18.5% for the boundary case 3.

3.4 Conclusions

For the SHIP I case, we could reach the following conclusions:

1. A mesh size of 100x100 mm seems to be appropriate for the investigation of the ultimate and the residual strength of ship models as it demands less computational cost and accurate results as it will be shown in Chapters 4 and 5. In addition, there is no significant difference between results taken when using S4 or S4R elements, which were used for the modeling of ship hull structures as shown in ***[10], [11]***. Therefore, we prefer to use S4R elements which, as mentioned before, reduce the computational cost.
2. Restriction of the rotation about the transverse horizontal axis of the first control node and rotation application about the transverse horizontal axis of the second control node leads to almost the same results with the cantilever support, and is considered to be more suitable for damage problems modeling, as it introduces negligible reaction forces to the model. Restriction of bending about the vertical axis results to a somewhat different curvature - moment curve and it is not suggested for modeling problems of damaged hulls.
3. As it concerns the appropriate value of the time increment, it seems that a value between 1E-06 and 3E-06 is more appropriate as it is also depicted in ***[11]***, because we can always consider the increased computational cost when greater accuracy is needed and vice versa.

We will then try to verify the above-mentioned conclusions by applying the same modeling parameters using the SHIP II model. Final conclusions of the study can be seen in the end of the chapter.

3.5 Results-SHIP II

In this section we present the results of the simulation when SHIP II was used As it is mentioned above (see pg.21), apart from the intact state, two damage scenarios have been investigated, where a different position of the damage has been considered.

A. Intact state

In order to succeed constant vertical bending moment along the span of the model, boundary conditions of Tables 5 & 6 were considered not appropriate because shear forces could have been developed due to the asymmetry of the hull . For this reason, the vertical displacement (U2) at the front end of the model was released. In that way, the effect of shear forces becomes negligible.

The applied loading is a symmetric rotation about the horizontal axis and its attributes are described in Table 8.

Angle of rotation	0.0028 rad
Time of loading application	4 seconds
Rate of curvature application	0.000123 $(m \cdot sec)^{-1}$

Table 8. Loading attributes of SHIP II

Meshing of the model was created using the same element size and type as defined before (see pg 23-24). Also in the case of SHIP II, S4R square elements of 100mm side length were used as proposed by ***[11]***.

Figure 15 shows the vertical bending moment versus the applied angle of rotation.

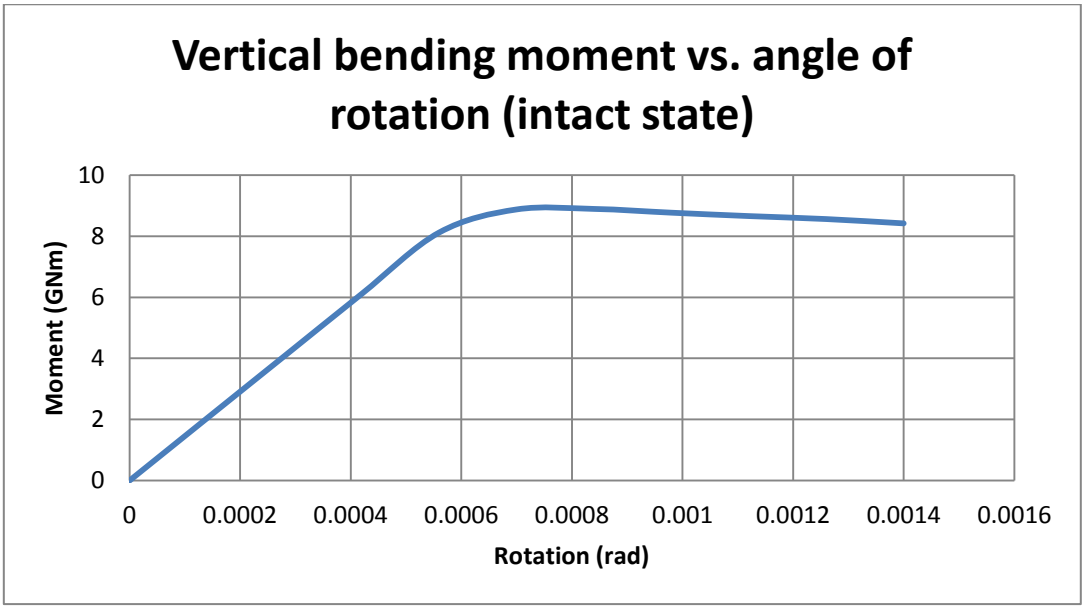

Figure 15. Vertical bending moment vs. Angle of rotation (intact state)

The maximum value of vertical bending moment, as well as, the angle of its appearance is:

Maximum value of vertical bending moment	8.891 GNm
Angle of maximum vertical bending moment	0.00168 rad

Table 9. Maximum value of vertical bending moment (intact state)

Figures 16,17 &18 depict the deformed model.

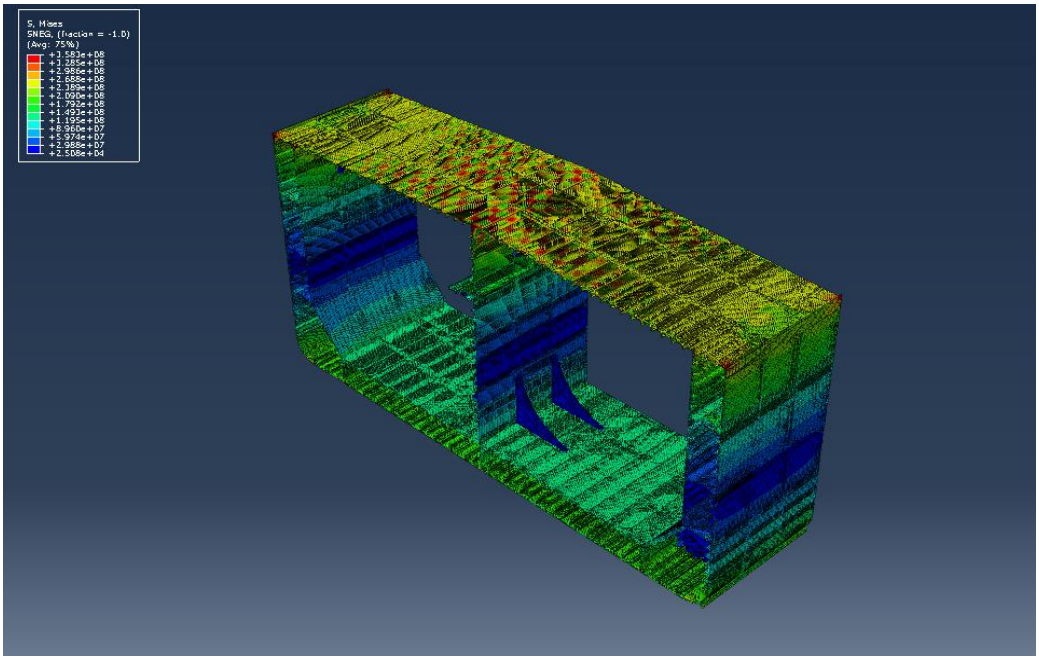

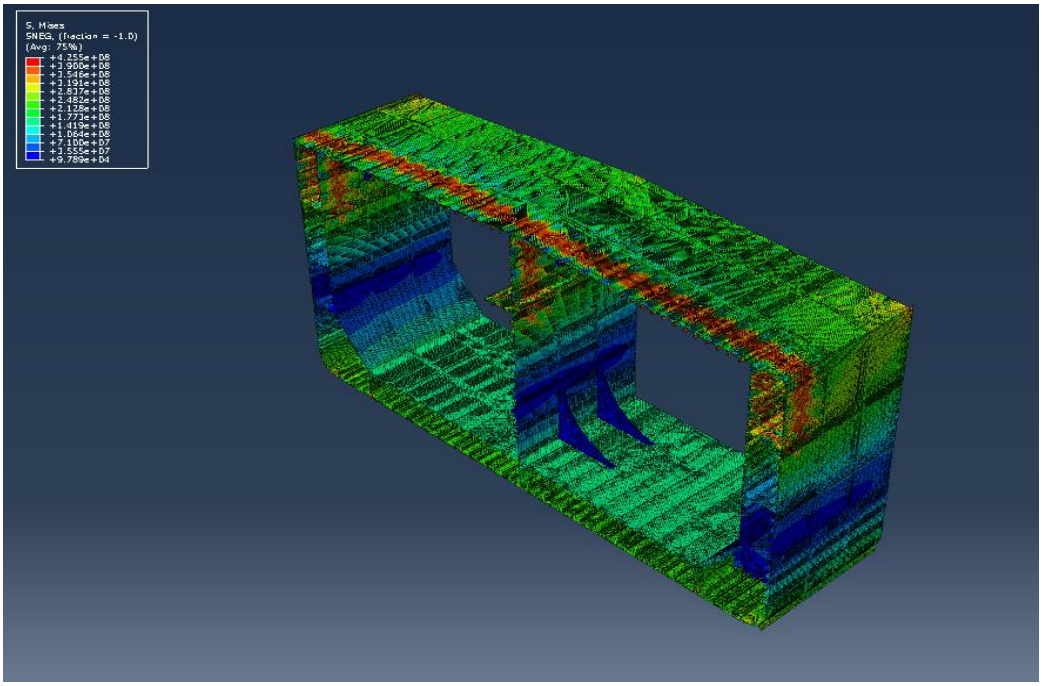

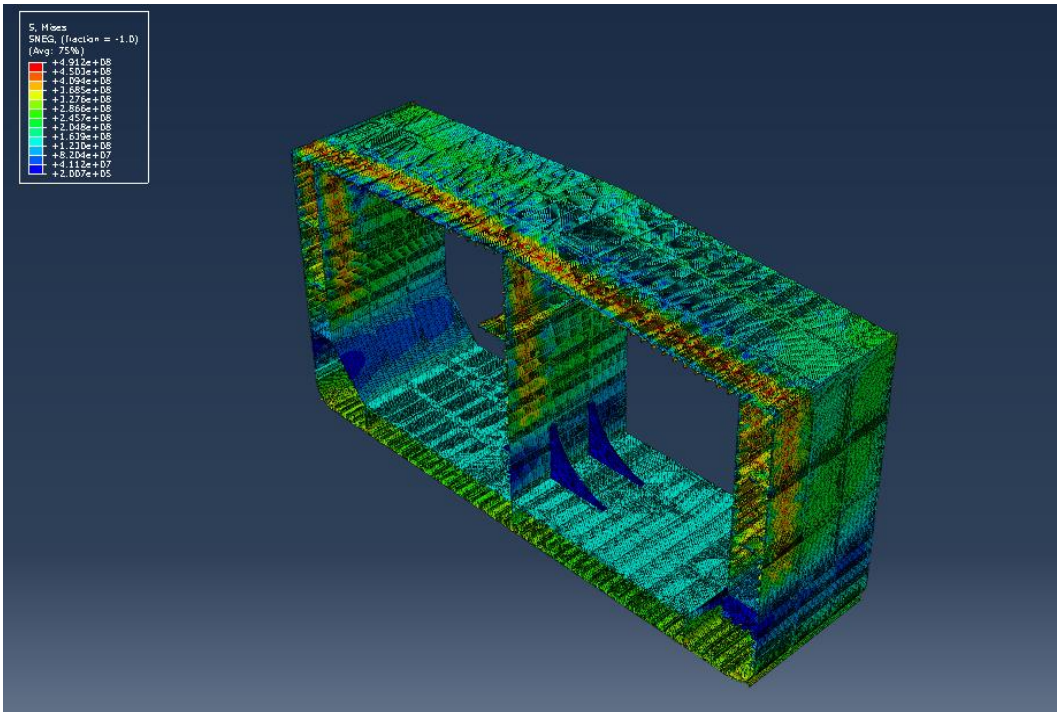

Figures 16, 17, 18. Stages of hull's Von Mises stresses when 20, 30 and 50% of the loading is applied

The simulation was ended at the 50% of the total angle of rotation in order to reduce the computational cost, as the maximum moment was achieved at the 30% of it. As we can see from the above Figures, when 20% of the total angle of rotation has been applied, large stresses at the deck appear of maximum value 350MPa approximately. When 30% of the total of rotation has been applied, maximum stress of approximately 430MPa can be observed at the first bay. At the end of the run (50% of the total angle of rotation) just a small region at the first bay is highly stressed and at the same time, stresses reduce as we move towards the third bay of the model.

Figure 7 depicts the final distribution of vertical displacements at the central path of the deck.

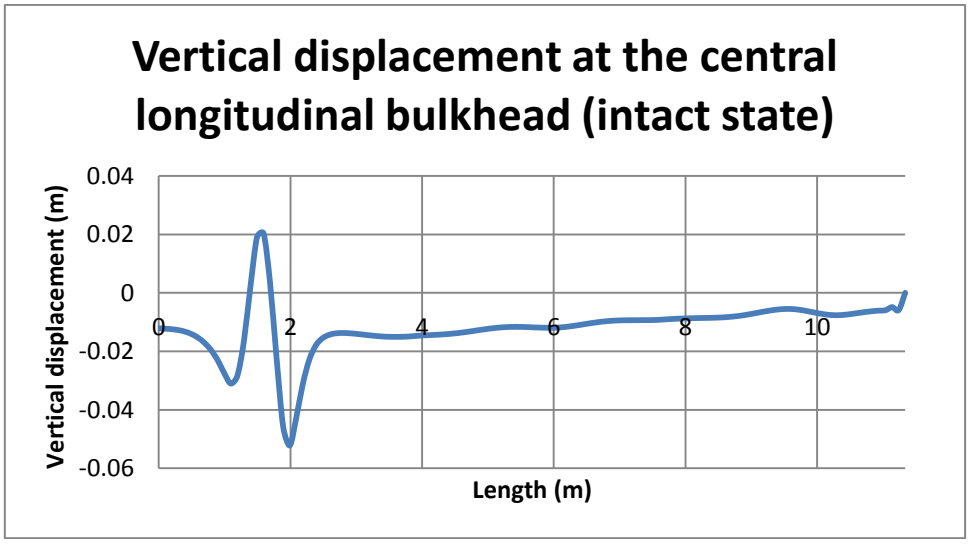

Figure 19. Vertical displacement at the central path of the deck (intact state)

It can be easily observed from Figure 19 that the structure mainly collapsed at the first bay, where maximum stresses had appeared.

The position of the neutral axis of the structure at certain time frames can be seen in Figure 20. The initial position of the undeformed hull is $Y_{N.A.}$=9.22m.

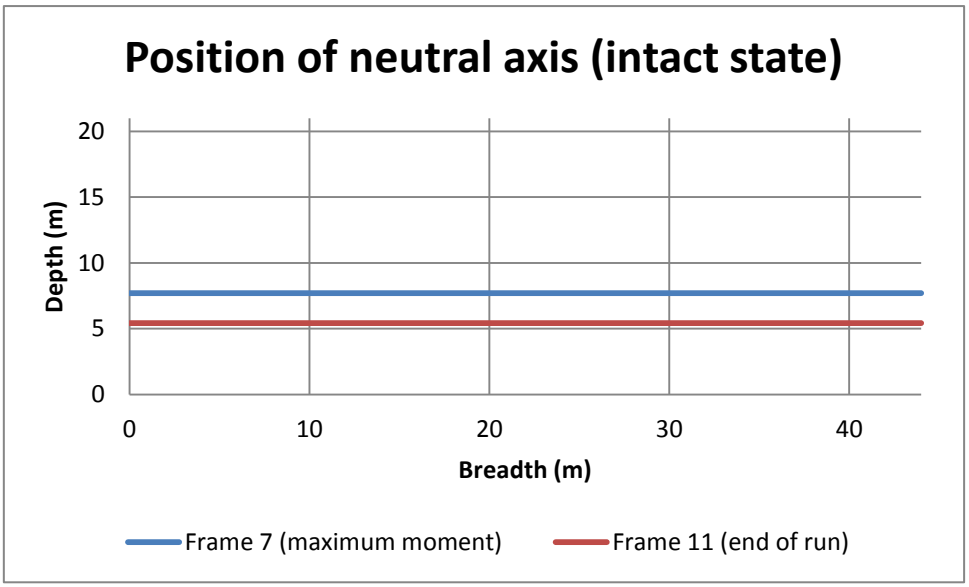

Figure 20. Position of the neutral axis at two different time frames (intact state)

B. Damage scenario-1 (nonsymmetrical)

In this case, the damage extends at the both sides of a web frame (also see Figure 9), and it is nonsymmetrical with respect to the mid-ship section. The dimensions of the damaged area are given in Table 4. Three sets of boundary conditions were applied according to Table 7. Each case will be presented separately and they will be compared.

i. **BC_1**

As we can see from Table 7, BC_1 refers to the cantilever support case, where the rear nodes are totally constrained and rotation is applied at the front nodes of the model. The magnitude of the loading and the time period of its application can be seen in Table 9.

Figure 19 shows the vertical bending moment versus the applied rotation about the horizontal axis.

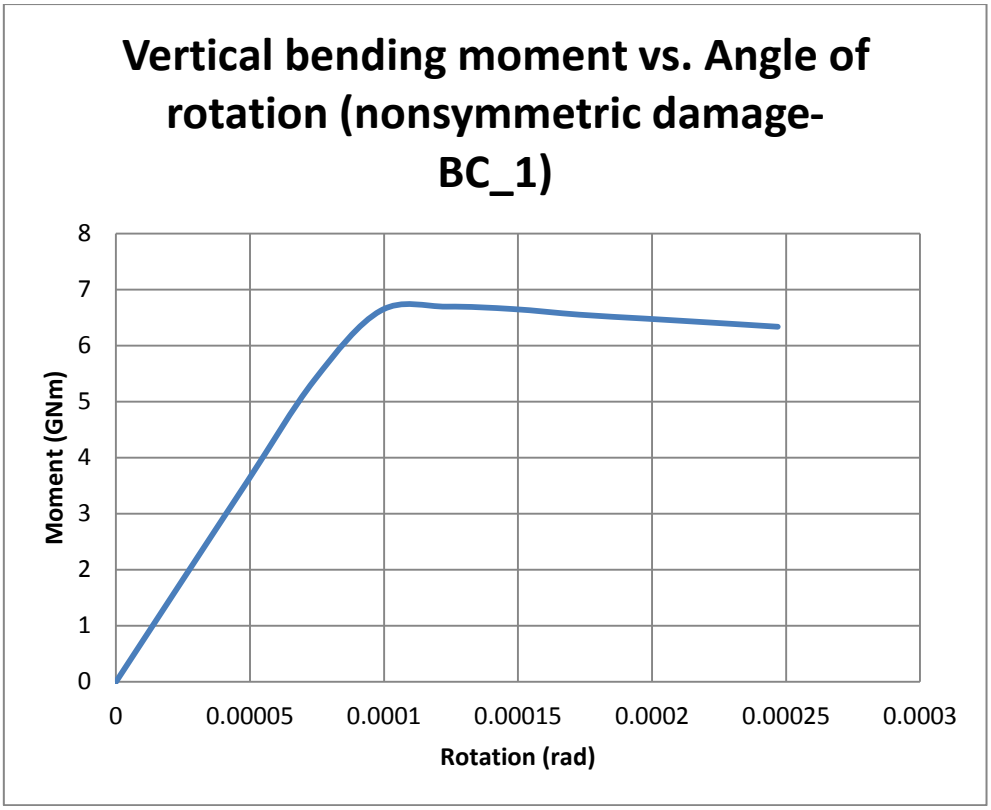

Figure 21.Vertical bending moment vs. Curvature (nonsymmetric damafe-BC_1)

The maximum value of vertical bending moment for BC_1 case is given in the Table below.

Maximum value of vertical bending moment	6.695GNm
Angle of maximum vertical bending moment	0.0014rad

Table 11. Maximum value of vertical bending moment (nonsymmetrical damage-BC_1)

Figures of the damaged model are shown below.

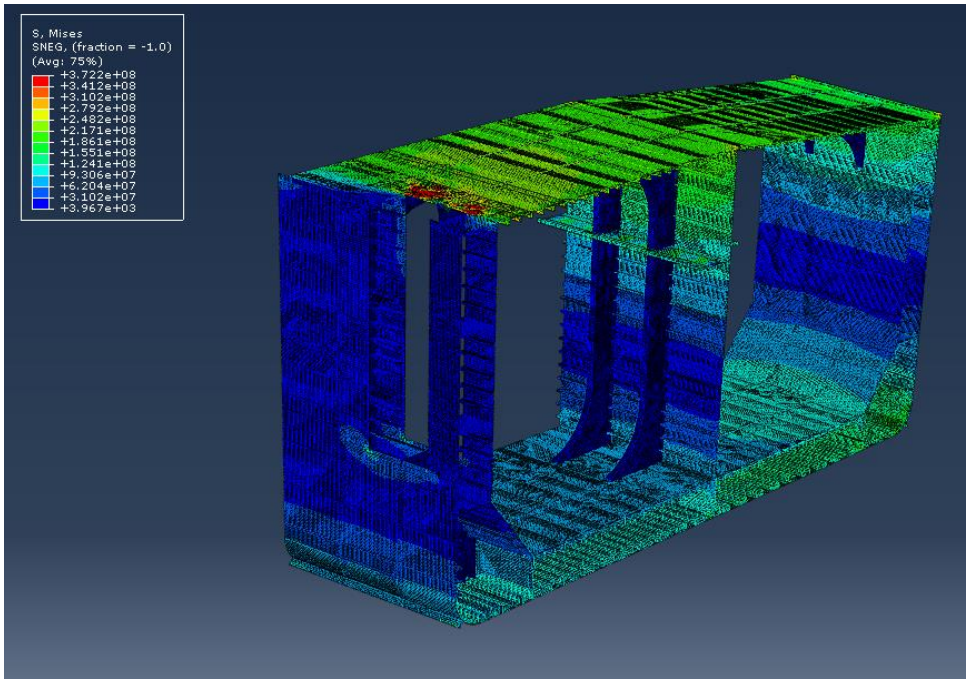
S, Mises
SNEG, (fraction = -1.0)
(Avg: 75%)
+3.722e+08
+3.412e+08
+3.102e+08
+2.792e+08
+2.482e+08
+2.171e+08
+1.861e+08
+1.551e+08
+1.241e+08
+9.306e+07
+6.204e+07
+3.102e+07
+3.967e+03

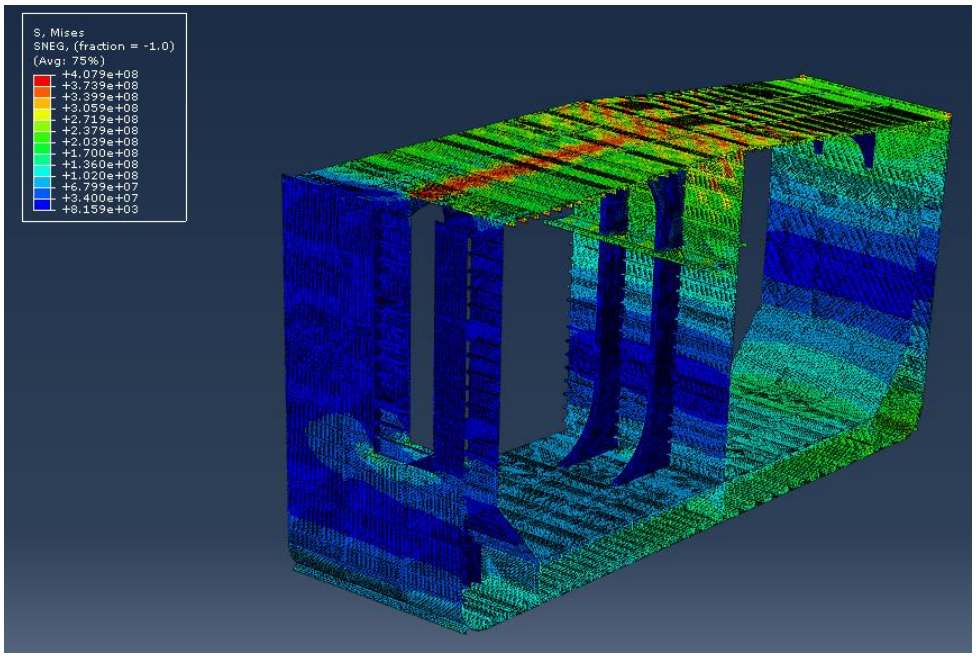
S, Mises
SNEG, (fraction = -1.0)
(Avg: 75%)
+4.079e+08
+3.739e+08
+3.399e+08
+3.059e+08
+2.719e+08
+2.379e+08
+2.039e+08
+1.700e+08
+1.360e+08
+1.020e+08
+6.799e+07
+3.400e+07
+8.159e+03

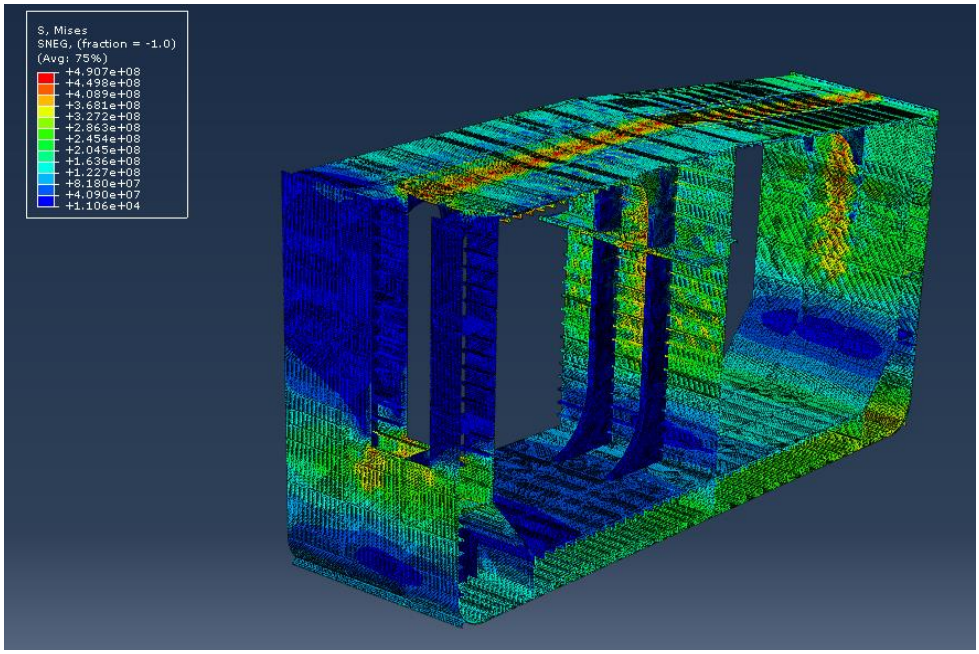

Figures 22, 23, 24. Stages of hull's Von Mises stresses when 15, 20 and 50% of the loading is applied

As we can see from Figures 22, 23 & 24 when 15% of the total angle of rotation is applied, there is a stress concentration of approximately 370MPa at the edges of the damaged area which is the first area that enters the elasto-plastic region. Afterwards, a region of maximum stress is formulated at the center of the deck and mostly at the left side, having a value of approximately 410MPa. Finally, when 50% of the total angle of rotation is applied, the whole central region of the deck buckles and therefore, the structure collapses.

Because of the ship's hull asymmetry, due to the existence of the damaged area, there is also horizontal bending moment which acts on the structure. Its maximum value is M_{hor}=3.82MNm, more than one thousand times smaller than the vertical bending moment, and appears when the angle of rotation about the vertical axis is θ=0,000233rad. Buckling and tripping of the stiffeners at deck plating is also observed.

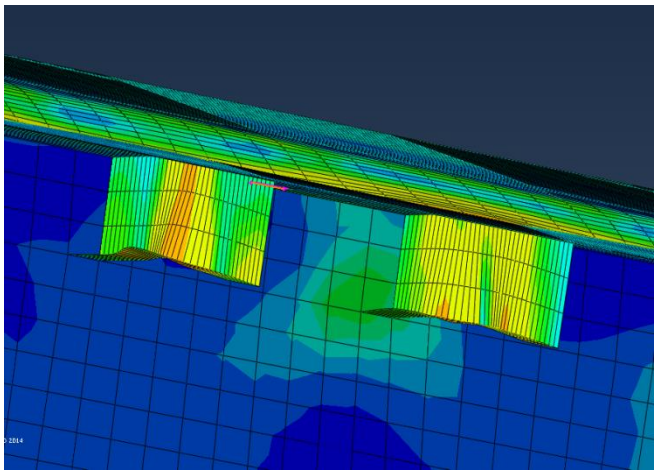

Figure 25. Stiffeners at deck plating suffering from buckling and tripping

In Figure 26, the vertical displacement at the deck due to the applied bending moment is presented.

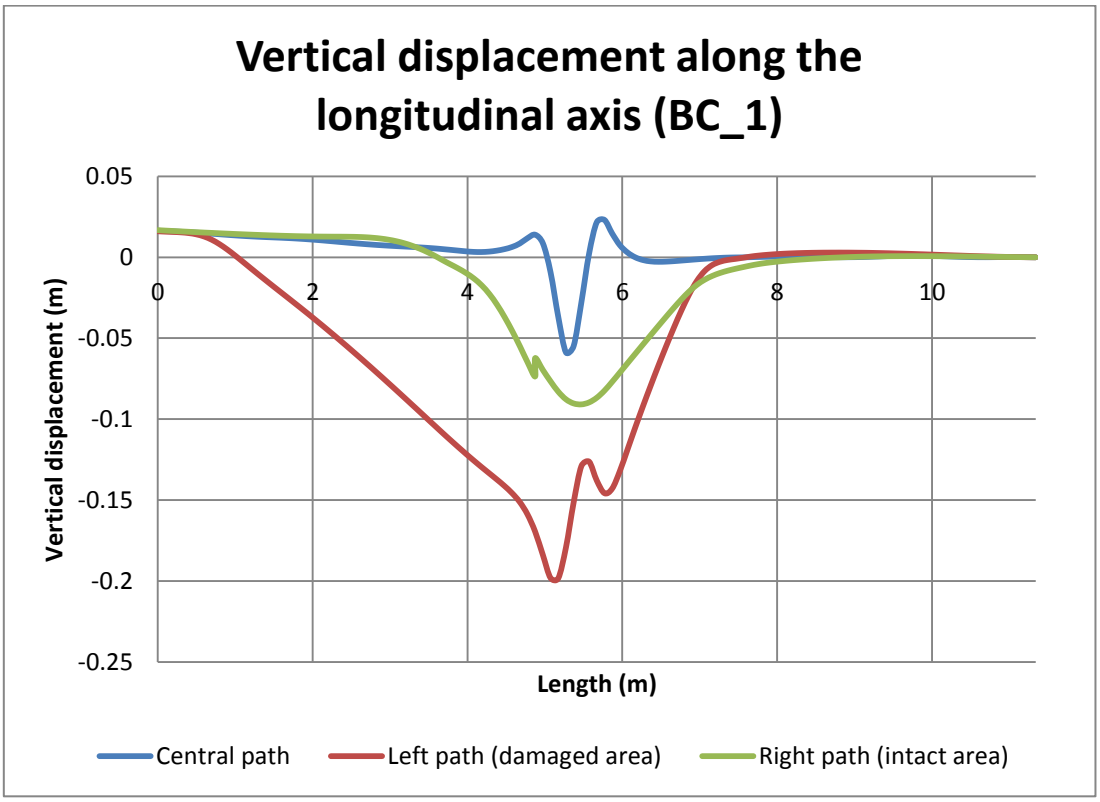

Figure 26. Vertical displacements at three different longitudinal paths at the deck

The central path refers to the nodes of the deck at the center line of the ship, while the left and the right path at the nodes placed r=±14.45m from the center line. As it can be seen, the maximum value of vertical displacement is observed at the left side of the center line where the damaged area occurs. Furthermore, there are two regions of buckling along this path which also prove the severe collapse at the left side of the structure. The minimum value of vertical displacement can be seen at the central path, where the stiffness of the structure is larger due to the longitudinal bulkhead.

It is also interesting to see the position of the neutral axis of the structure in two separate time frames. The first refers to the moment of maximum bending load and the second to the end of the run. When the section is not symmetric, the neutral axis is not only translated but also rotated in order to reach the equilibrium of the forces acting at the structure.

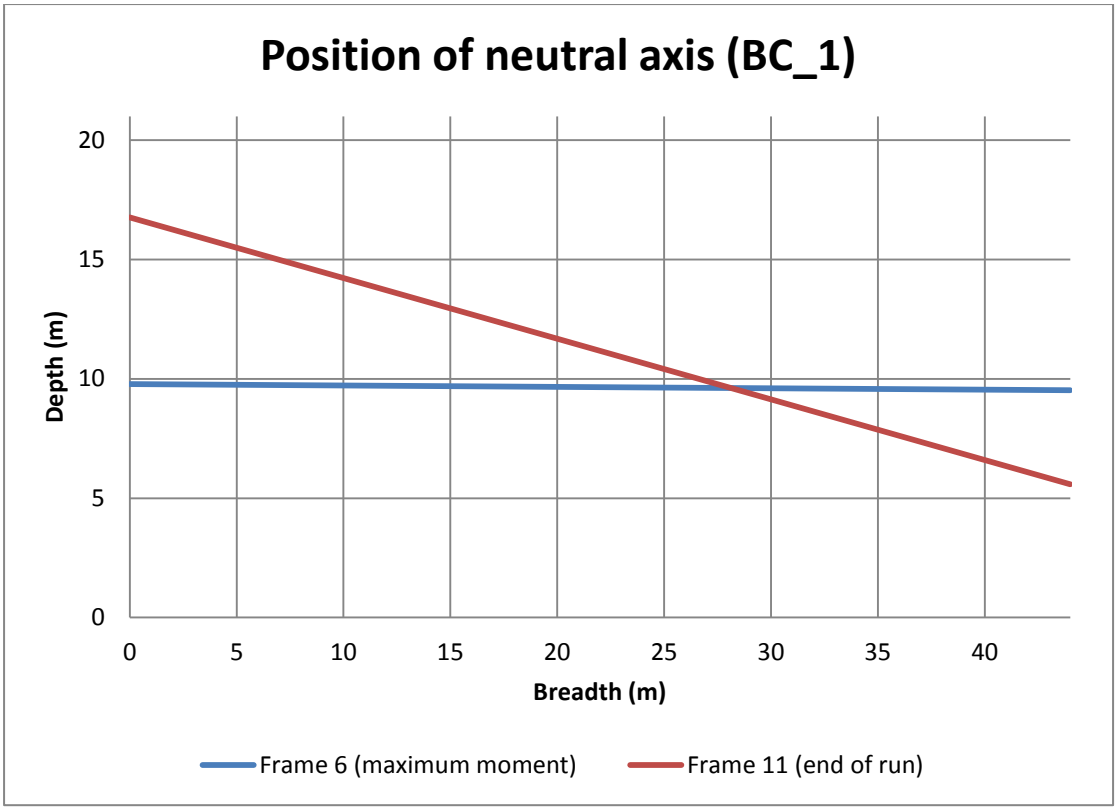

Figure 27. Position of the neutral axis at two different time frames

As it can be seen in Figure 27, the neutral axis of the extreme cross section, the closest to the damage, is almost a straight line when maximum bending moment is applied. At the end of the run, when most of the section has entered the plastic region, the neutral axis is translated to the top and rotated clockwise $\delta\theta$=-14,26^{o}.

ii. **BC_2**

Table 7 shows that BC_2 is a case similar to the cantilever support case. The difference is that the rear nodes of the model are not totally constrained apart from the rotation about the horizontal axis which is fixed. Figure 28 shows the vertical bending moment versus the rotation about the horizontal axis.

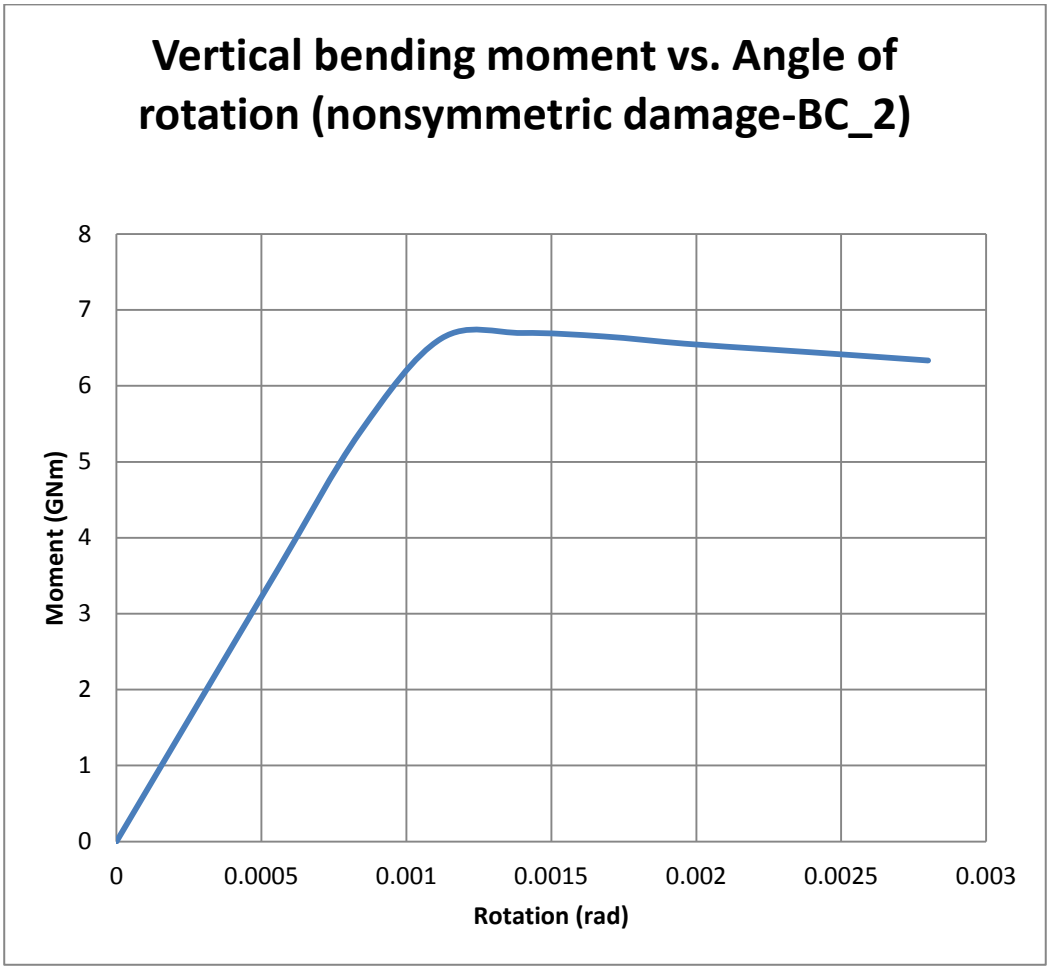

Figure 28. Vertical bending moment vs. Curvature (nonsymmetrical damafe-BC_2)

The maximum value of vertical bending moment for BC_2 case is given in the Table 12.

Maximum value of vertical bending moment	6.697GNm
Angle of maximum vertical bending moment	0.0014rad

Table 12. Maximum value of vertical bending moment (nonsymmetrical damage-BC_2)

As the figures of the deformed hull are similar to those cited above (Figures 22-24), only the figures of the vertical displacements and the position of the neutral axis will be given.

As there are no constraints to the rotations of the model, there are also no horizontal and torsional bending moments as well as reaction forces in this case. The latter means that only vertical bending moment is applied at the hull.

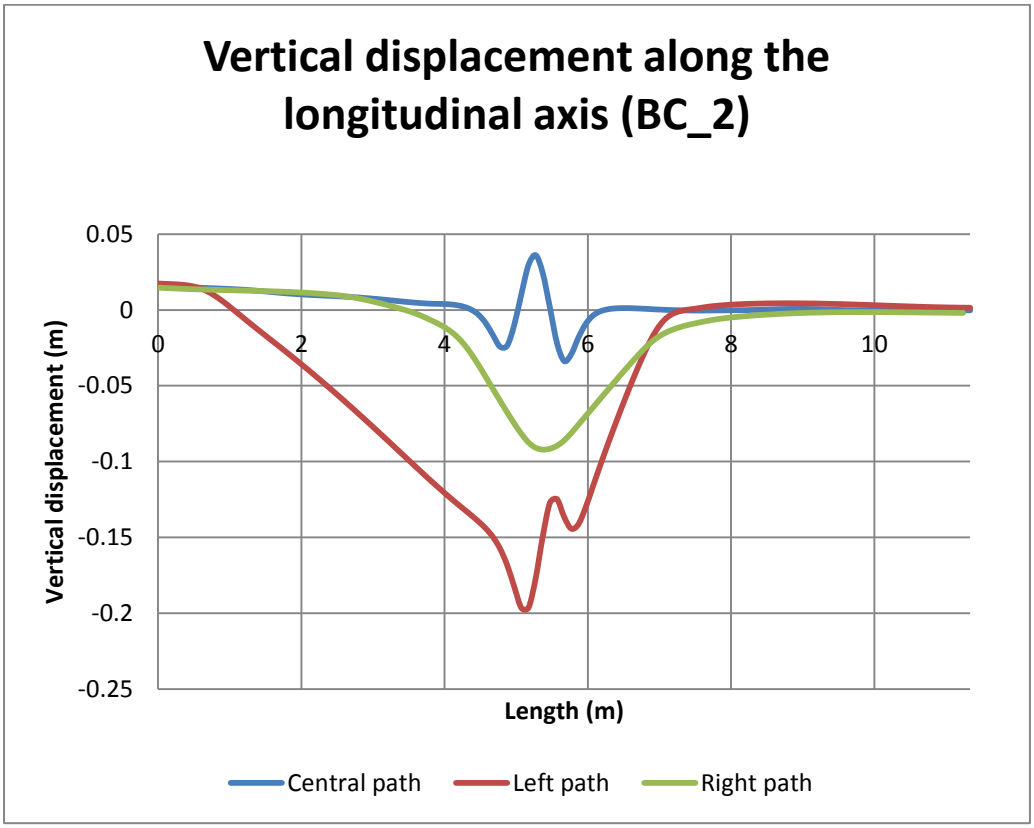

Figure 29. Vertical displacements at three different longitudinal paths at the deck

Figure 29 shows that the values and the shapes of vertical displacements along the deck at same regions are almost the same. There is also a difference in relation to the shape of the vertical displacements concerning the central path. In this case, there are more buckling regions and moreover, the maximum vertical displacement is positive.

As it concerns the position of the neutral axis, it is more or less the same as we discussed above.

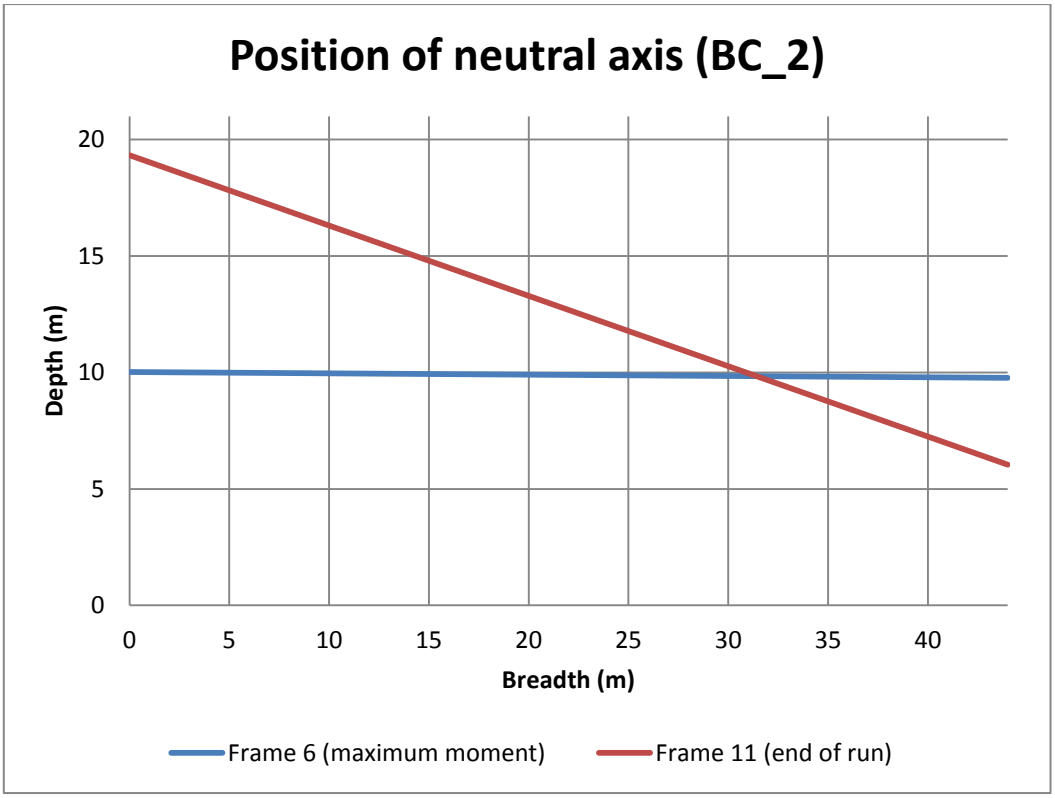

Figure 30. Position of the neutral axis at two different time frames

The position of the neutral axis of the extreme cross section, the closest to the damage, is almost the same as it can be seen from BC_1. The rotation of the neutral axis in this case at the end of the run is $\delta\theta$=-16.8^{o} close to the value measured for case BC_1.

iii. BC_3

As it is shown in Table 7, this boundary condition refers to the simple support case. Symmetric loading has been applied with value θ=0,0028rad in T=4sec. Figure 31 that shows the vertical bending moment versus the rotation angle.

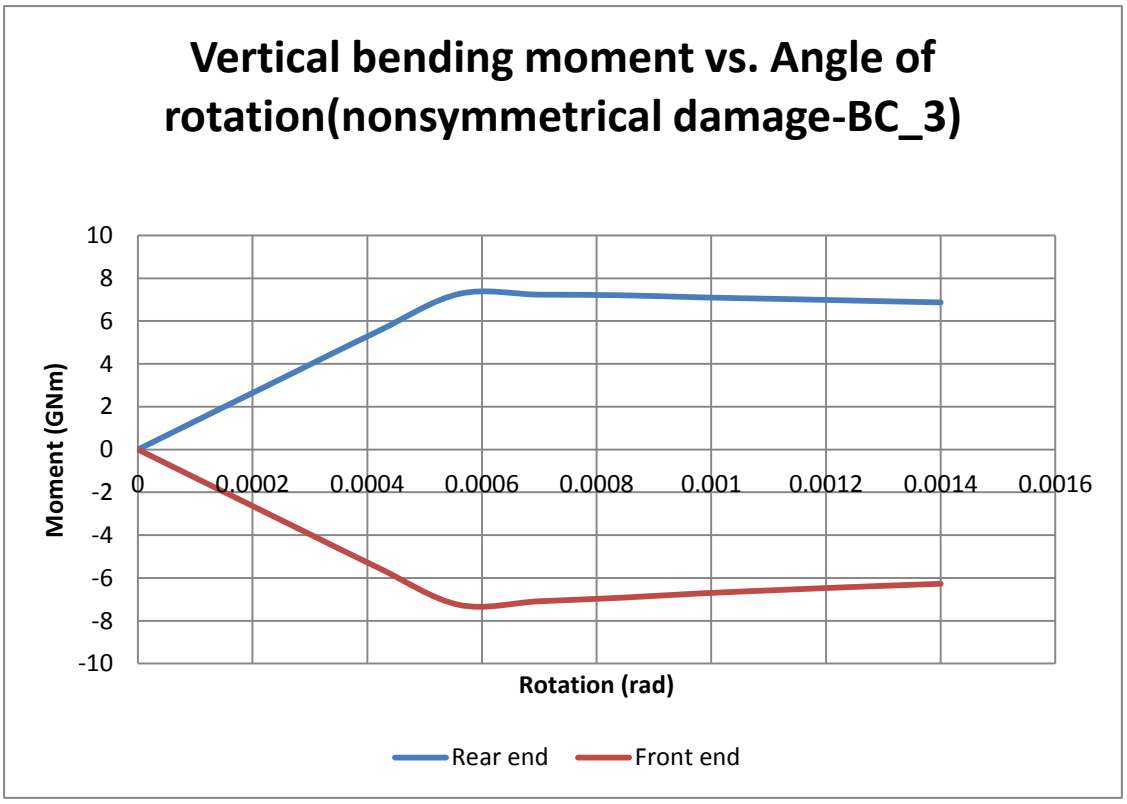

Figure 31. Vertical bending moment vs. Angle of rotation (nonsymmetrical damafe-BC_3)

In case of the symmetric boundary condition of simple support the vertical bending moment does not remain constant along the span of the model. That means that shear forces appear that lead to additional moment added to the existing one.

The maximum value of vertical bending moment for BC_3 case is given in the Table below.

Maximum value of vertical bending moment	7.2696GNm
Angle of maximum vertical bending moment	0.00112rad

Table 13. Maximum value of vertical bending moment (nonsymmetrical damage-BC_3)

Figures 32, 33, 34 show the Von Misses stress field in different frames of the simulation.

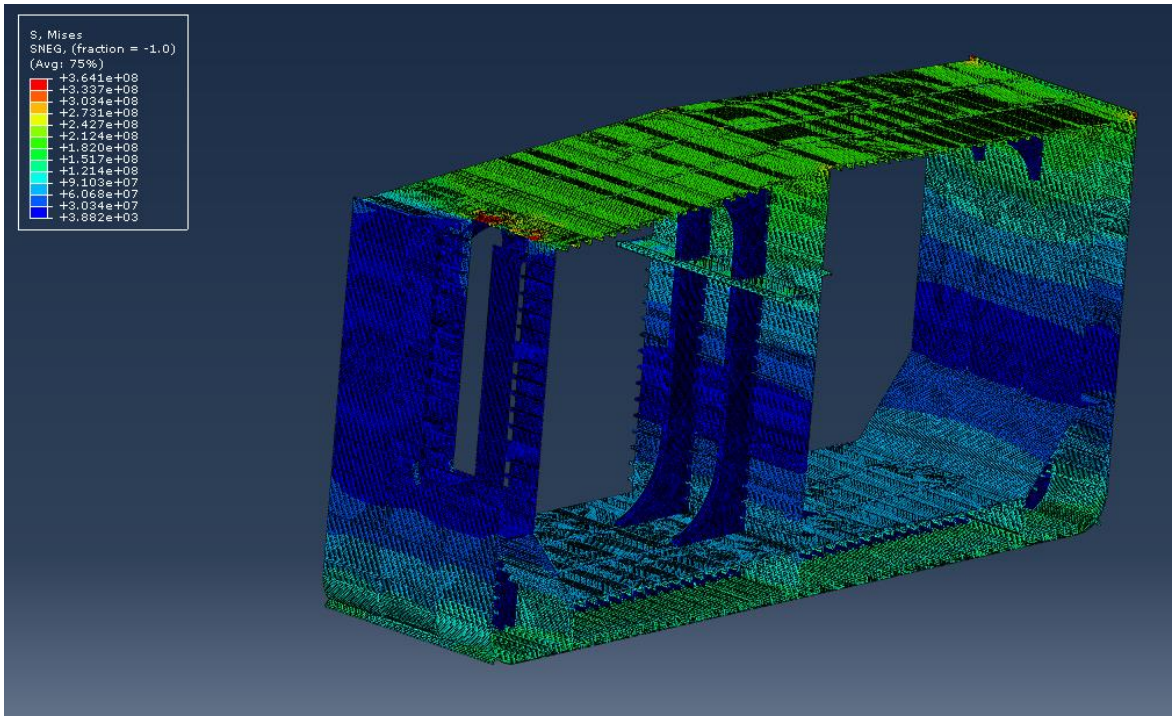
S, Mises
SNEG, (fraction = -1.0)
(Avg: 75%)
+3.641e+08
+3.337e+08
+3.034e+08
+2.731e+08
+2.427e+08
+2.124e+08
+1.820e+08
+1.517e+08
+1.214e+08
+9.103e+07
+6.068e+07
+3.034e+07
+3.882e+03

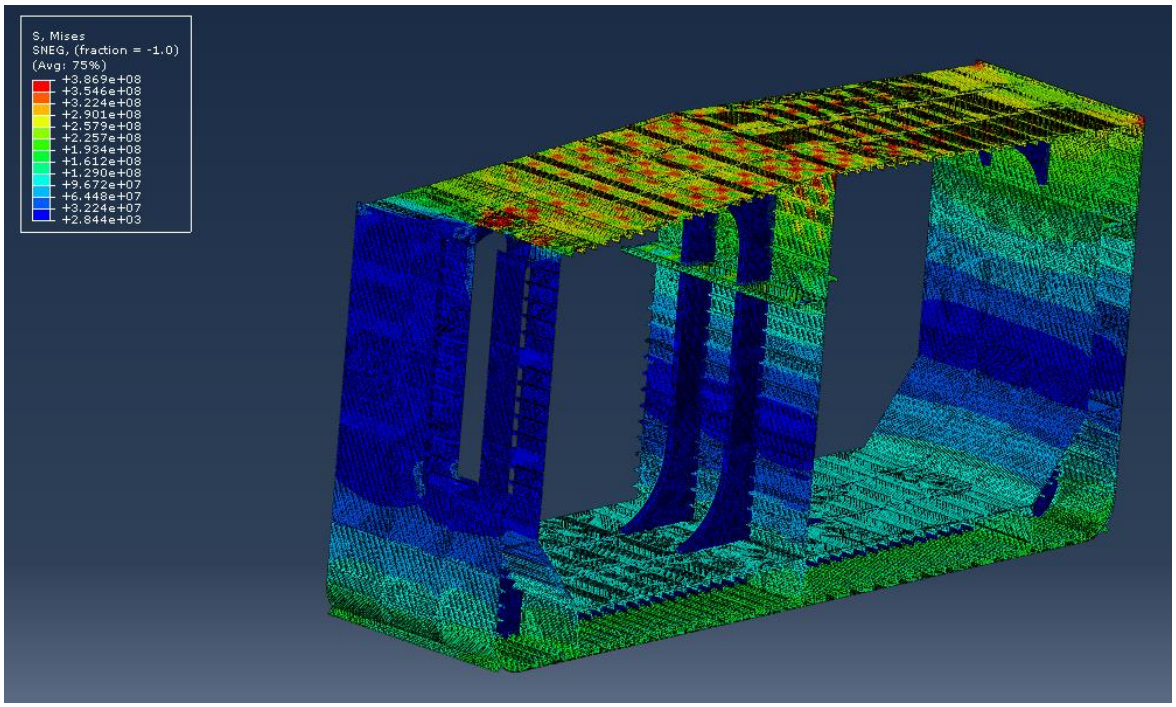
S, Mises
SNEG, (fraction = -1.0)
(Avg: 75%)
+3.869e+08
+3.546e+08
+3.224e+08
+2.901e+08
+2.579e+08
+2.257e+08
+1.934e+08
+1.612e+08
+1.290e+08
+9.672e+07
+6.448e+07
+3.224e+07
+2.844e+03

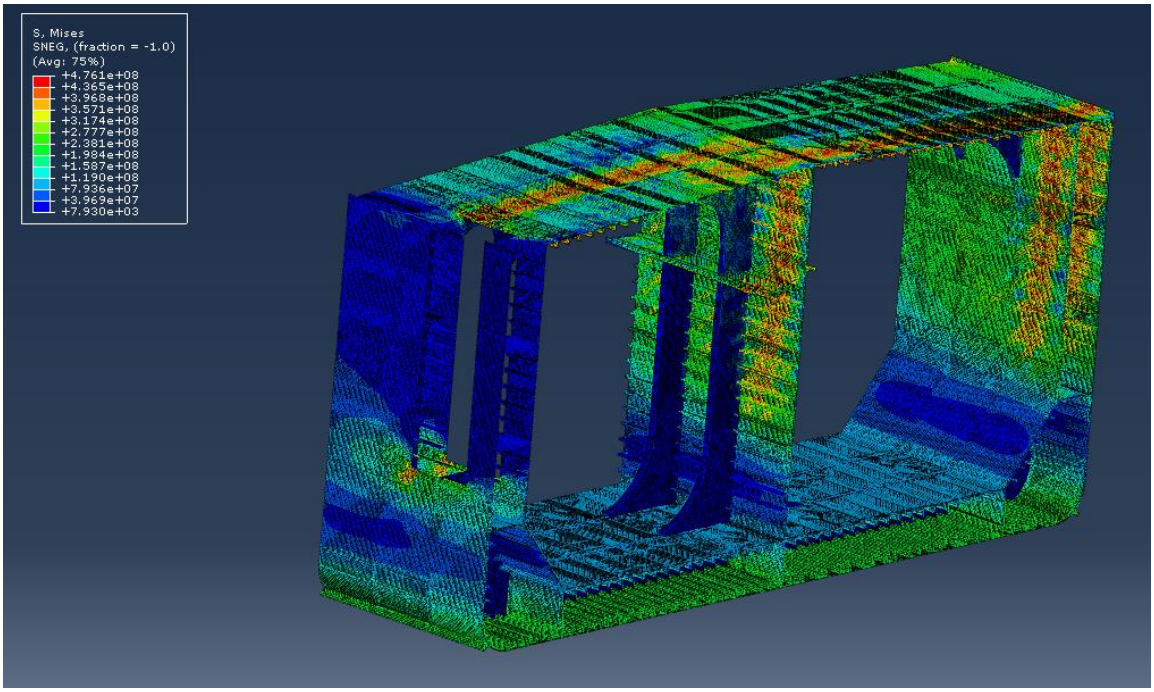

Figures 32, 33, 34. Stages of hull's Von Mises stresses when 15, 20 and 50% of the loading is applied

As it can be seen from Figures 32, 33, 34 when 15% of the total angle of rotation is applied there is stress concentration at the edges of the damaged area having a value of approximately 364MPa. When 30% of the total angle of rotation is applied, the stress concentration area becomes larger and several regions at the deck of the structure have a maximum stress of approximately 386MPa and finally, when 50% of the total angle of rotation is applied, two nonsymmetrical regions of maximum stress are formulated having a maximum stress of 476MPa.

Apart from the vertical bending moment, also horizontal bending moment is applied in the model having a maximum value of M_{hor}=3.11GNm that is to say, approximately 1000 times larger than the horizontal bending moment in case of BC_1.

Figure 35 shows the vertical displacements at the deck in case BC_3.

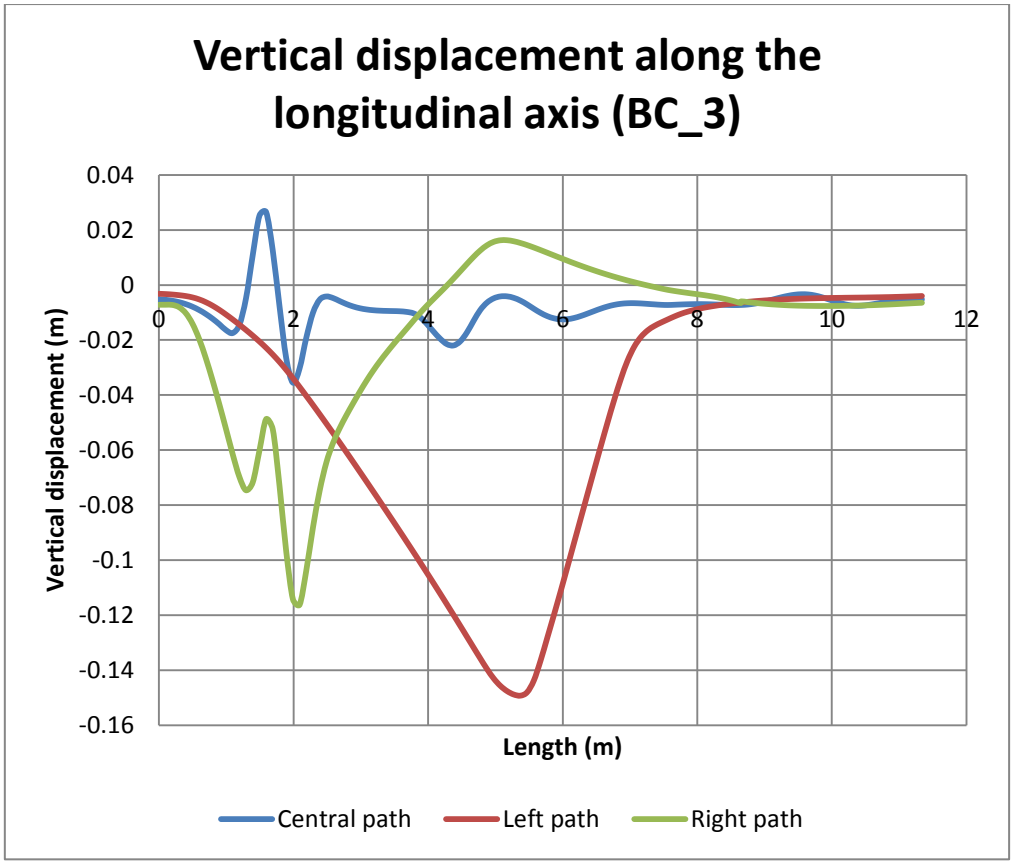

Figure 35. Vertical displacements at three different longitudinal paths at the deck

Figure 35, which depicts the vertical displacements at three different paths at the deck of the hull, has a different shape than figures 26, 28. Herein, the maximum negative displacement appears approximately at the middle of the longitudinal span of the model at the left side, and more buckling points appear at the central path. Moreover, vertical displacements at the right path also take positive values which probably are due to the symmetric constraints which have been applied in the model resulting in larger vertical reaction forces. In addition, it shall be noted that there is a negative vertical displacements of the model of approximately U_2=-0.005m at the front and rear nodes.

Finally, the position of the neutral axis at the same two time frames of the simulation which have been also investigated in Figures 27, 30 is presented below.

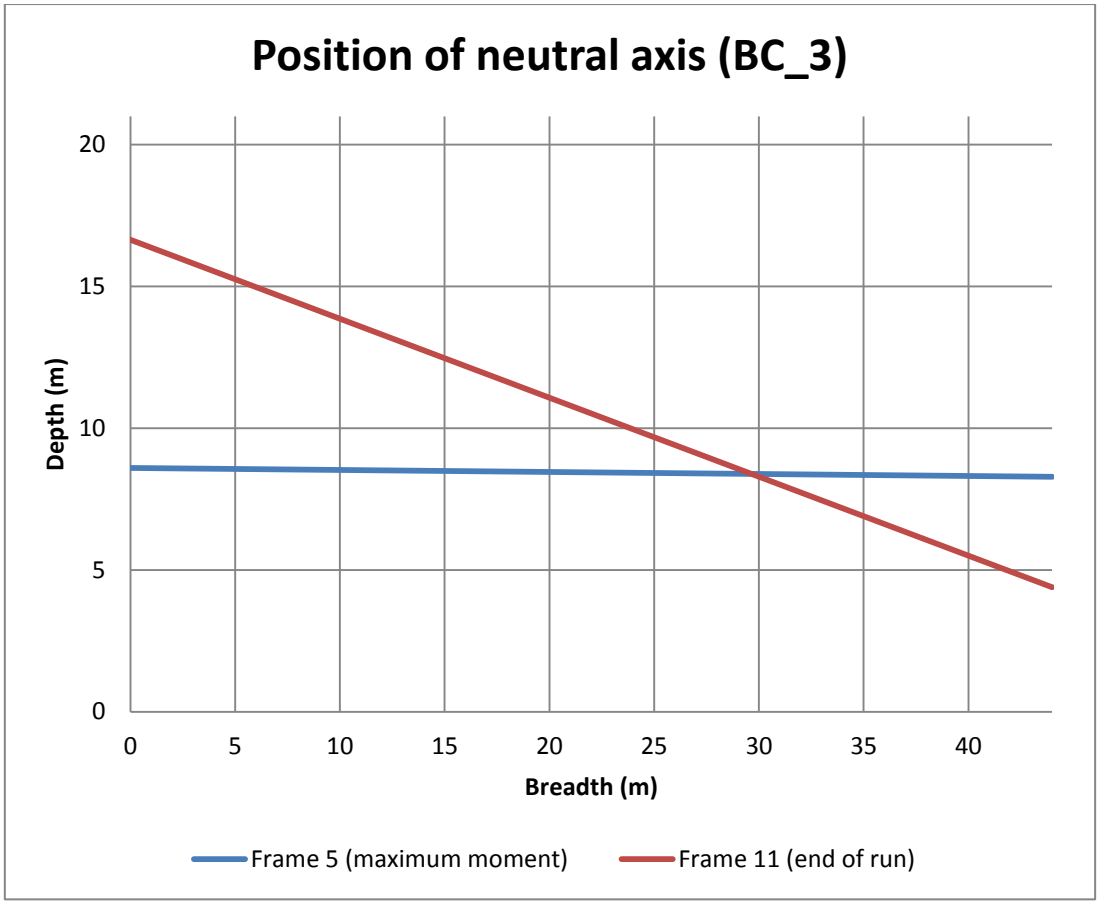

Figure 34. Position of the neutral axis at two different time frames

The position of the neutral axis of the exterme cross section, the closest to the damage, is almost the same as it can be seen from BC_1 and BC_2. The rotation of the neutral axis in this case at the end of the run is $\delta\theta$=-15.6^{o}, close to the value measured for case BC_1 and BC_2.

C. Damage scenario-2 (symmetrical)

In this case, the damage extends between two successive web frames (also see Figure 11). The dimensions of the damaged area are given in Table 4. Three sets of boundary conditions were also applied according to Table 7. Each case will be presented separately and finally they will be compared as in the case scenario 1.

i. **BC_1**

This boundary condition set refers to the cantilever support case as it has been shown above. The magnitude of the loading and the time period of its application are the same as it can be seen from Table 9.

The figure which shows the vertical bending moment versus the applied rotation about the horizontal axis is presented below.

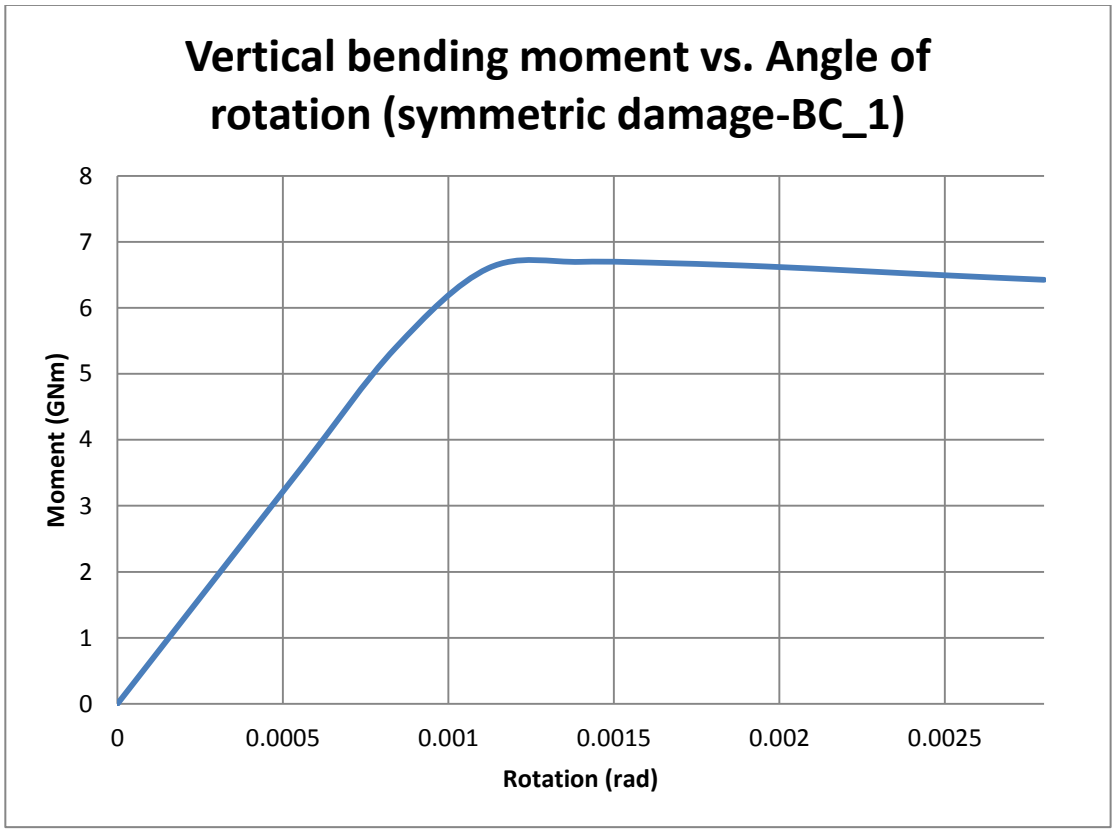

Figure 35.Vertical bending moment vs. Curvature (symmetrical damafe-BC_1)

The maximum value of vertical bending moment can be seen in Table 14.

Maximum value of vertical bending moment	6.697GNm
Angle of maximum vertical bending moment	0.0014rad

Table 14. Maximum value of vertical bending moment (symmetrical damage-BC_1)

Figures 36, 37 of the damaged model can be seen below.

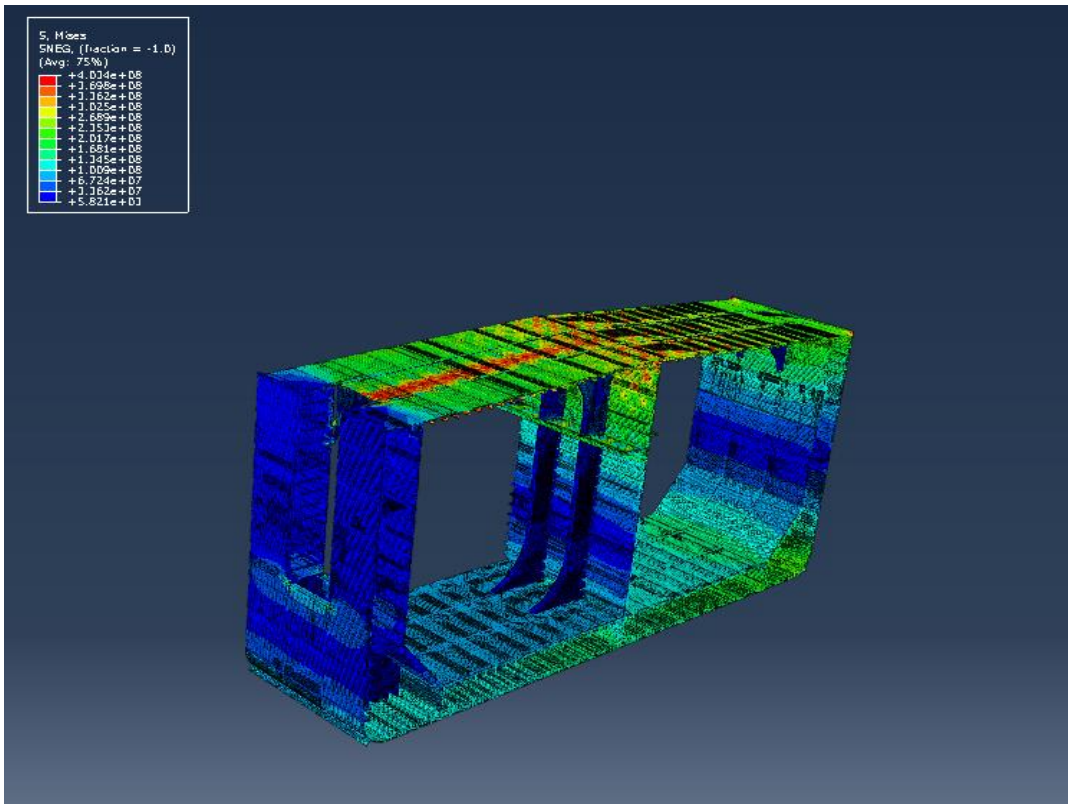

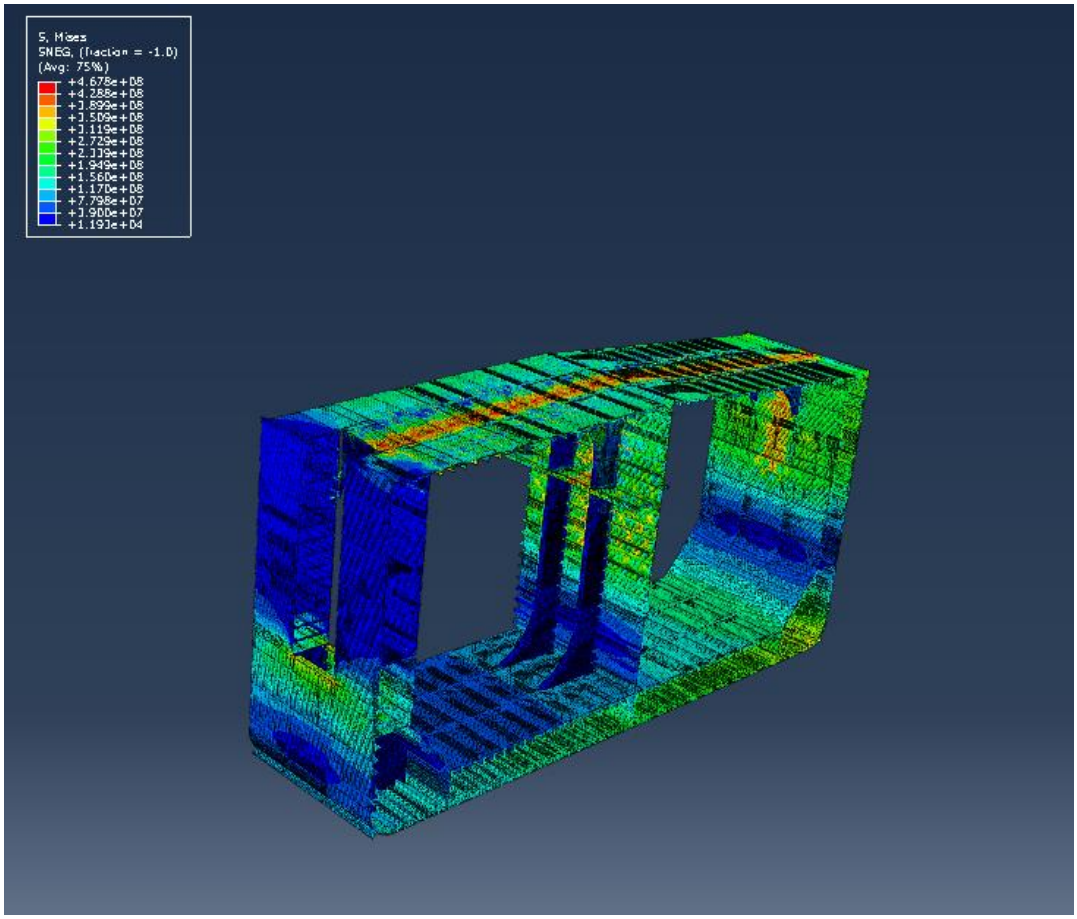

Figures 36, 37. Stages of hull's Von Mises stresses when 20% and 40% of the loading is applied

As we can see from Figures 36, 37 high stresses appear when 20% of the total angle of rotation is applied. There was no stress concentration before. Afterwards, when 40% of the total angle of rotation is applied, we notice a region of maximum stresses along the breadth of the model and at the mid-span having a value of 467MPa. In addition, the width of the region of maximum stresses has decreased, meaning that after the appearance of the maximum moment, there is a stress relaxation at the deck as the structure cannot sustain larger loading.

The horizontal bending moment which also appears due to the asymmetry of the hull has a maximum value of M_{hor}=1.71MNm when the angle of rotation about the vertical axis is θ=0.000238rad. In this case, tripping of the stiffeners is not observed.

As it was done before, figures of vertical displacements at three different longitudinal paths at the deck and also figures of the position of neutral axis will be presented. The transverse position of the longitudinal paths is the same as it was defined above (see pg. 38).

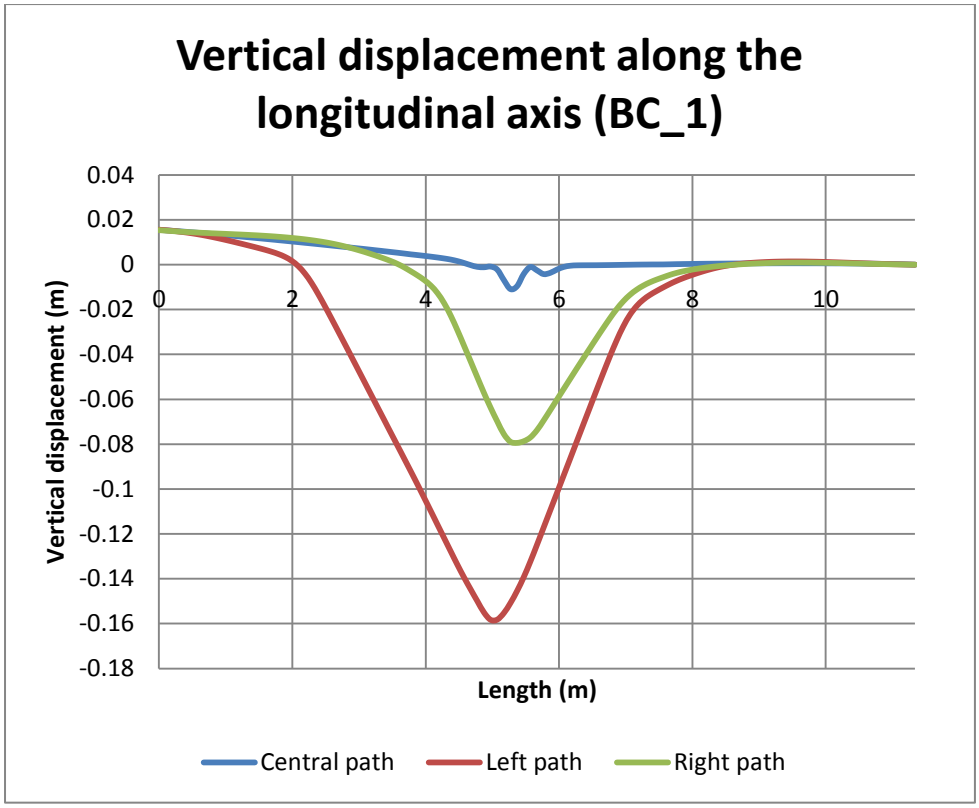

Figure 38. Vertical displacements at three different longitudinal paths at the deck

As we can see, vertical displacements are larger at the left path where the damage exists. There is only one buckling point as well as at the right path. Vertical displacements at the central path can be considered as negligible.

The position of the neutral axis of the extreme cross section at two different time frames can be seen below.

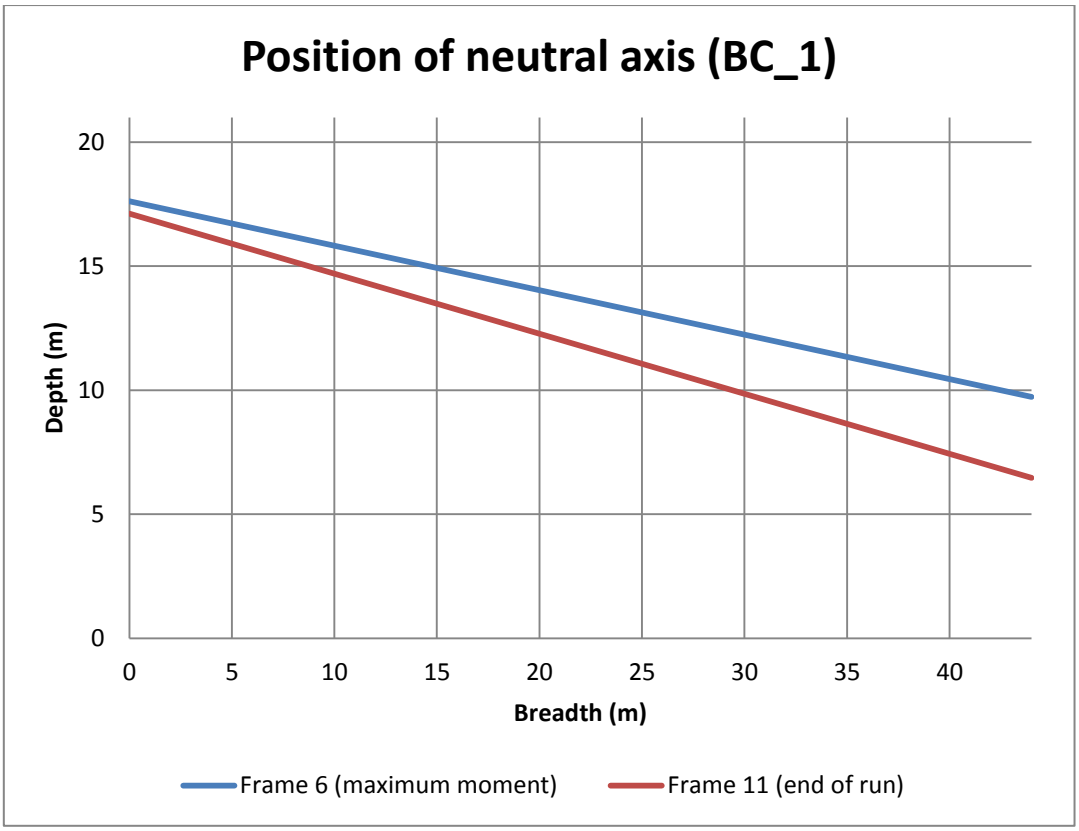

Figure 39. Position of the neutral axis at two different time frames

It can be seen from Figure 39, that neutral axis has been translated and rotated due to the asymmetry of the ship's hull. The angle of rotation is θ_1=-10,16^o when maximum moment is applied and θ_2=-13,61^o at the end of the run.

ii. BC_2

Same as it was mentioned for the nonsymmetrical case, this boundary condition set is similar to the cantilever support case.

The figure which shows the vertical bending moment versus the applied angle of rotation can be seen in Figure 40.

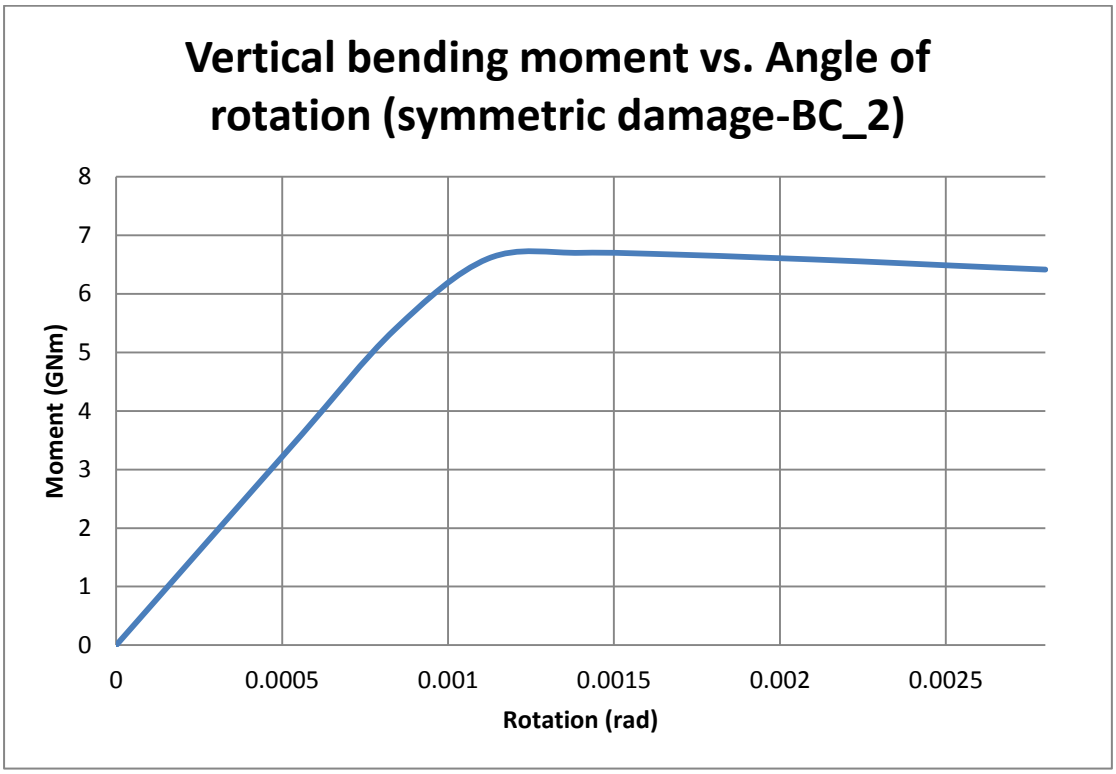

Figure 40.Vertical bending moment vs. Curvature (symmetric damafe-BC_2)

The maximum value of vertical bending moment as well as the angle of rotation where it appears can be seen below.

Maximum value of vertical bending moment	6.699GNm
Angle of maximum vertical bending moment	0.0014rad

Table 15. Maximum value of vertical bending moment (symmetrical damage-BC_2)

Figures of the damaged model where Von Misses stress is shown as well as its maximum value are almost the same as we discussed in the previous case, so it is decided not to be shown. Moreover, due to the applied boundary conditions, there is not horizontal bending moment.

The vertical displacements of the deck at this case can be seen in Figure 41.

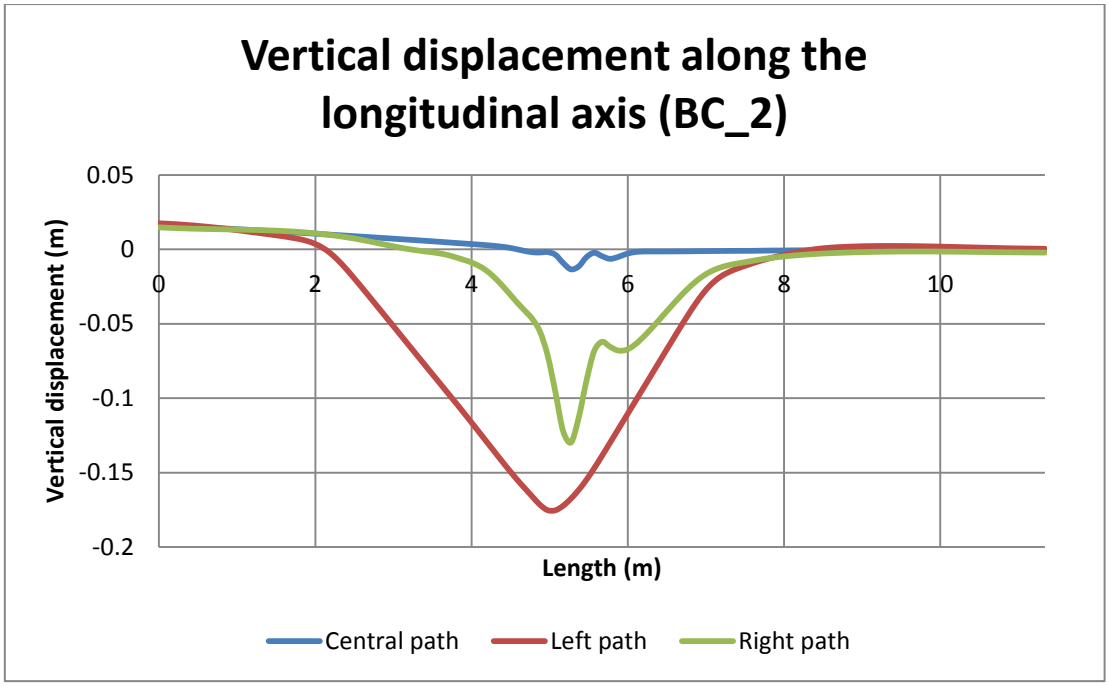

Figure 41. Vertical displacements at three different longitudinal paths at the deck

As it can be noticed, maximum vertical displacements occur at the left path where the damage exists. Furthermore, there are two buckling points at the right path while at the central path vertical displacements are negligible.

The position of the neutral axis of the extreme cross section of the structure at two separate time frames is shown in the Figure 42.

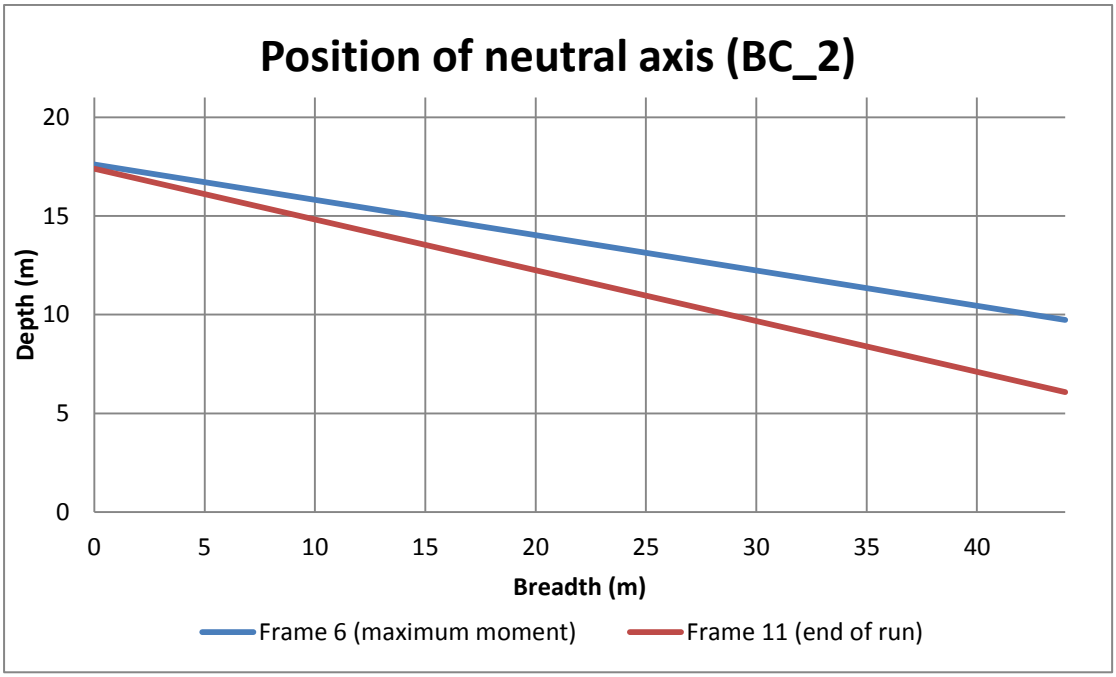

Figure 42. Position of the neutral axis at two different time frames

It can be seen that also in this case the neutral axis is translated and rotated due to the asymmetry of the section. The angles of rotation are θ_1=-10,15rad when maximum moment is applied and θ_2=-14.42rad at the end of the run. These values are similar to the angles of rotation in BC_1.

iii. BC_3

Similarly to the nonsymmetrical case, BC_3 refers to the simple support case. The magnitude of the loading and the time period where it was applied are the same as in nonsymmetrical case.

Figure 43 shows the vertical bending moment versus the applied angle of rotation.

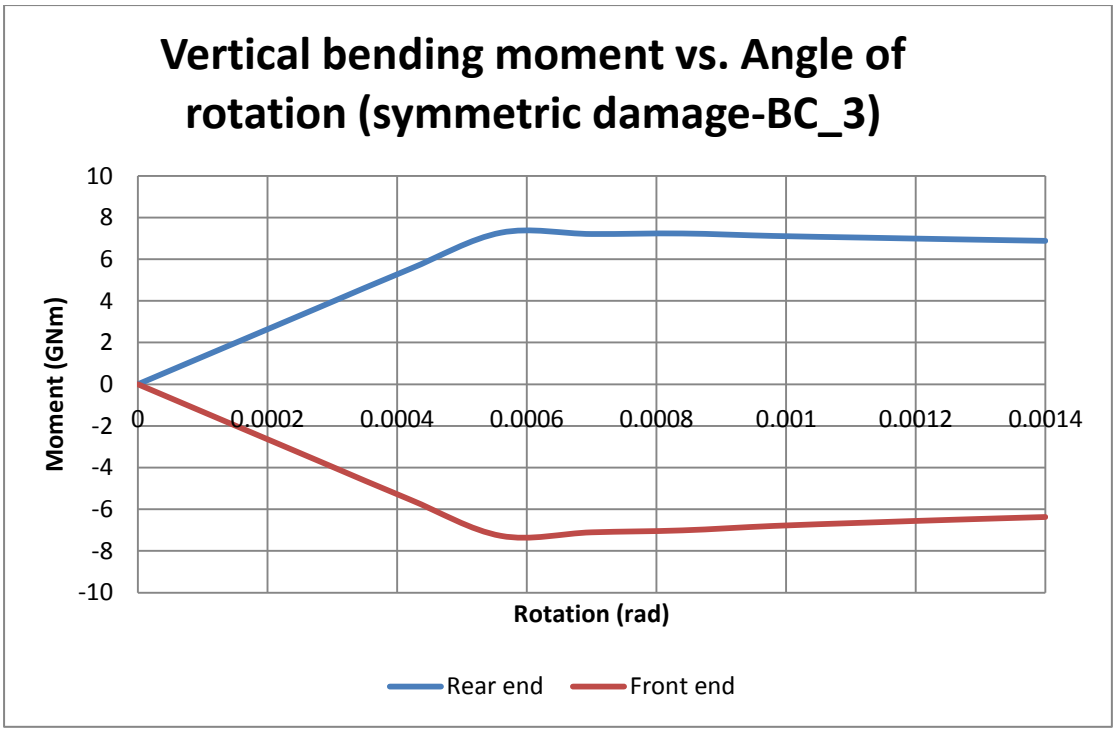

Figure 43.Vertical bending moment vs. Angle of rotation (symmetrical damafe-BC_3) at both sides of the model

As we can see, vertical bending moment is not constant along the span of the model. That means that shear forces are developed at both ends of the structure which then produce a moment which affects the final bending moment applied in the structure.

The maximum vertical bending moment as well as the angle of rotation where it appeared can be seen at the table which follows.

Maximum value of vertical bending moment	7.275GNm
Angle of maximum vertical bending moment	0.00112rad

Table 16. Maximum value of vertical bending moment (symmetrical damage-BC_3)

Figures of the damaged model can be seen below.

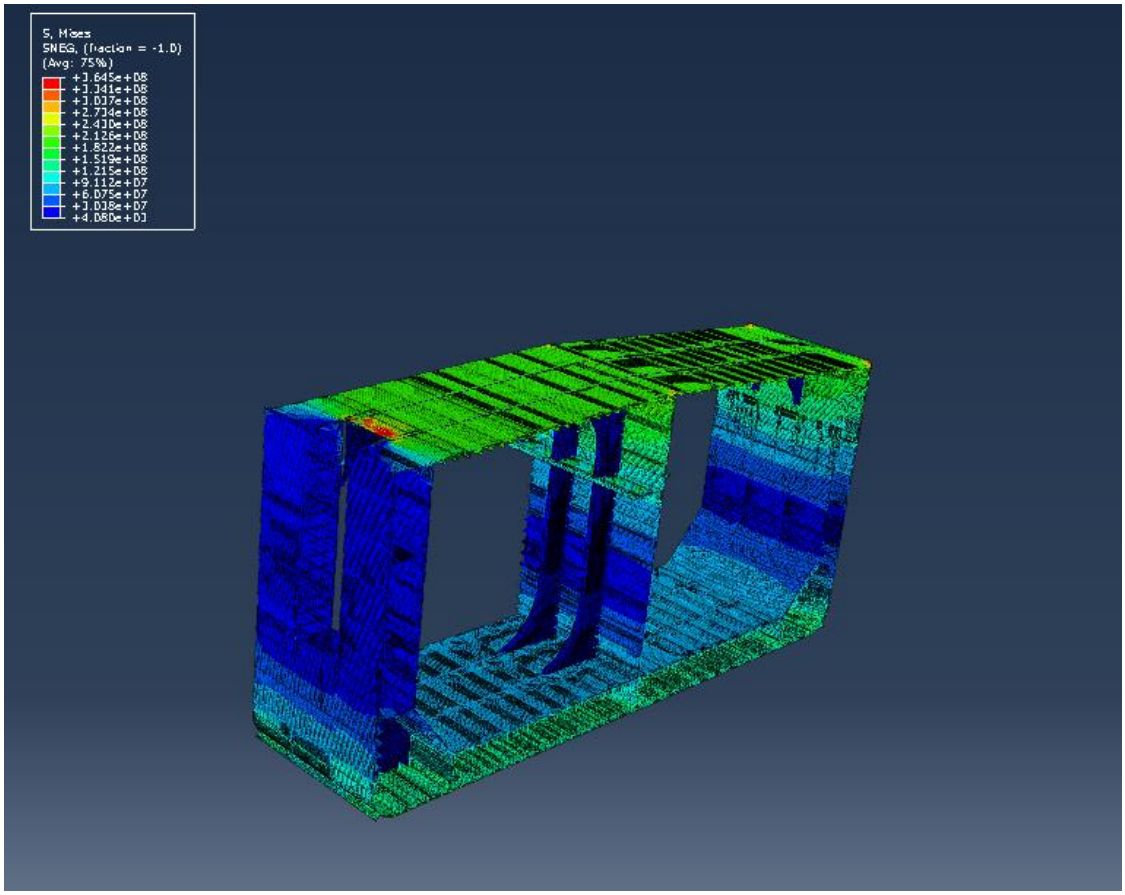
S, Mises
SNEG, (fraction = -1.0)
(Avg: 75%)
+3.645e+08
+3.241e+08
+2.837e+08
+2.434e+08
+2.030e+08
+1.626e+08
+1.222e+08
+8.186e+07
+4.148e+07

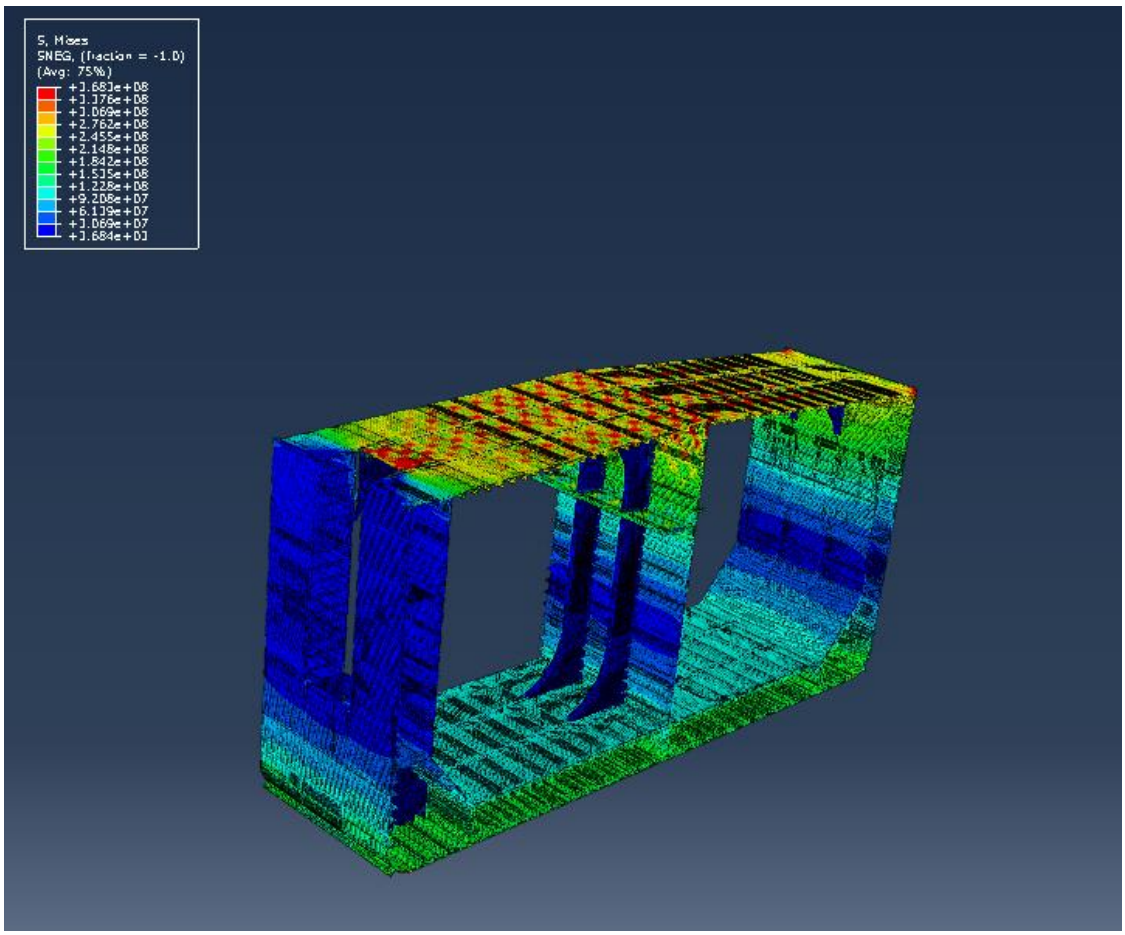
S, Mises
SNEG, (fraction = -1.0)
(Avg: 75%)
+3.681e+08
+3.276e+08
+2.869e+08
+2.462e+08
+2.055e+08
+1.648e+08
+1.242e+08
+8.350e+07
+4.284e+07

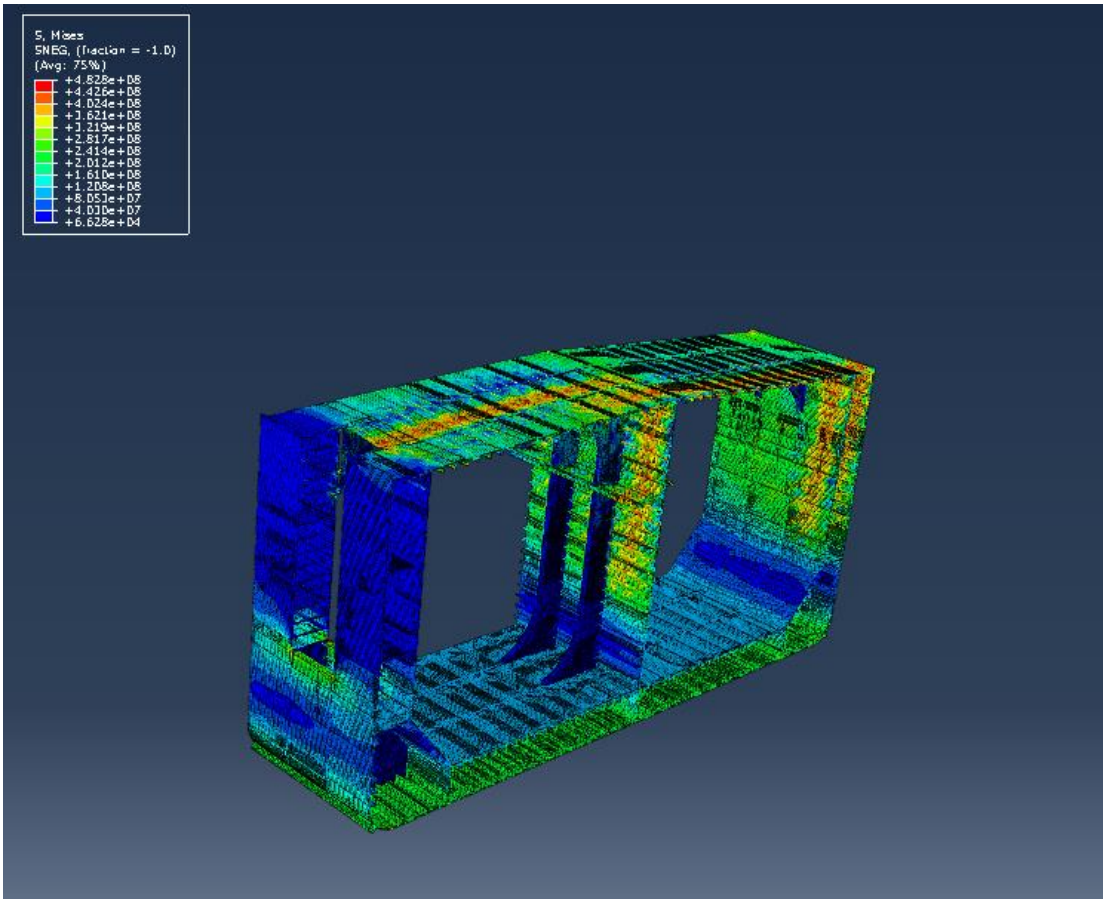

Figures 44, 45, 46. Stages of hull's Von Mises stresses when 15, 20 and 50% of the loading is applied

It can be seen from Figures 44, 45 and 46 that in this case there is stress concentration at the area of the damage having a maximum value of approximately 360Mpa. Afterwards, regions of maximum stress can be found at the deck having a maximum value of approximately 370MPa and in the end of the run, two nonsymmetrical regions of maximum stress can be noticed.

The maximum horizontal bending moment acting on the structure is M_{hor}=3.18GNm, approximately one thousand times larger than the horizontal moment acting on the structure in case BC_1.

The vertical displacements appeared at the deck can be seen in Figure 47.

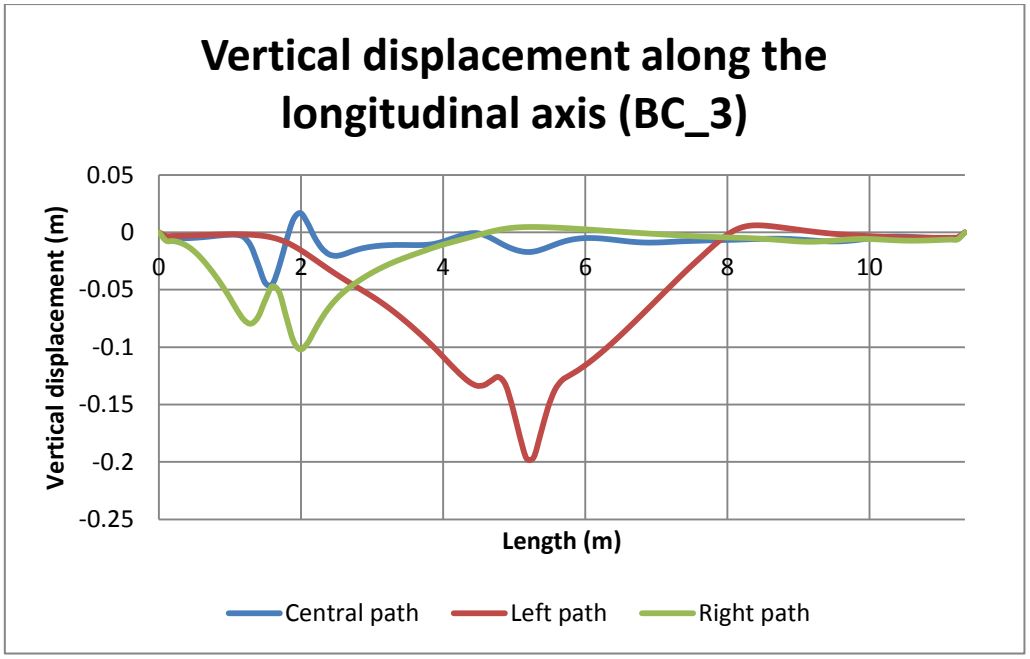

Figure 47. Vertical displacements at three different longitudinal paths at the deck

As we can see, vertical displacements are bigger than the previously discussed cases. In addition, the central and the right side of the hull has collapsed in more points and also closer to the front side. We also notice that displacements at the left path are twice than the displacements at the right path, whereas at the central path can be considered negligible.

In this case, the position of the neutral axis can be seen in the following figure.

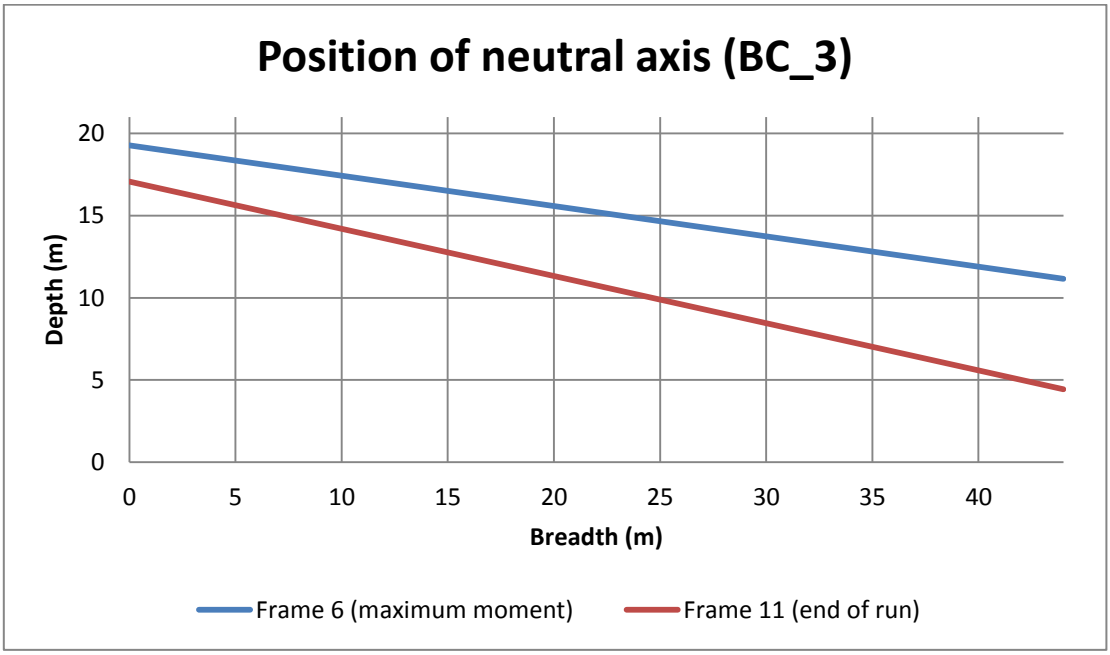

Figure 48. Position of the neutral axis at two different time frames

It can also be seen that, in this case, the neutral axis is translated and rotated due to the asymmetry of the section. The angle of rotation is θ_1=-10,45rad when maximum moment is applied and θ_2=-16.02rad at the end of the run. The value of the angle when maximum moment is applied is similar to the angles of rotation in BC_1 and BC_2 while the angle of rotation at the end of the run is larger in BC_3.

3.6 Conclusions of Chapter II

As far as it concerns the first damage scenario (nonsymmetrical), the common figure of vertical bending moments versus the applied curvature can be seen below. Curvature is now used as the independent variable so that the results can be easily compared.

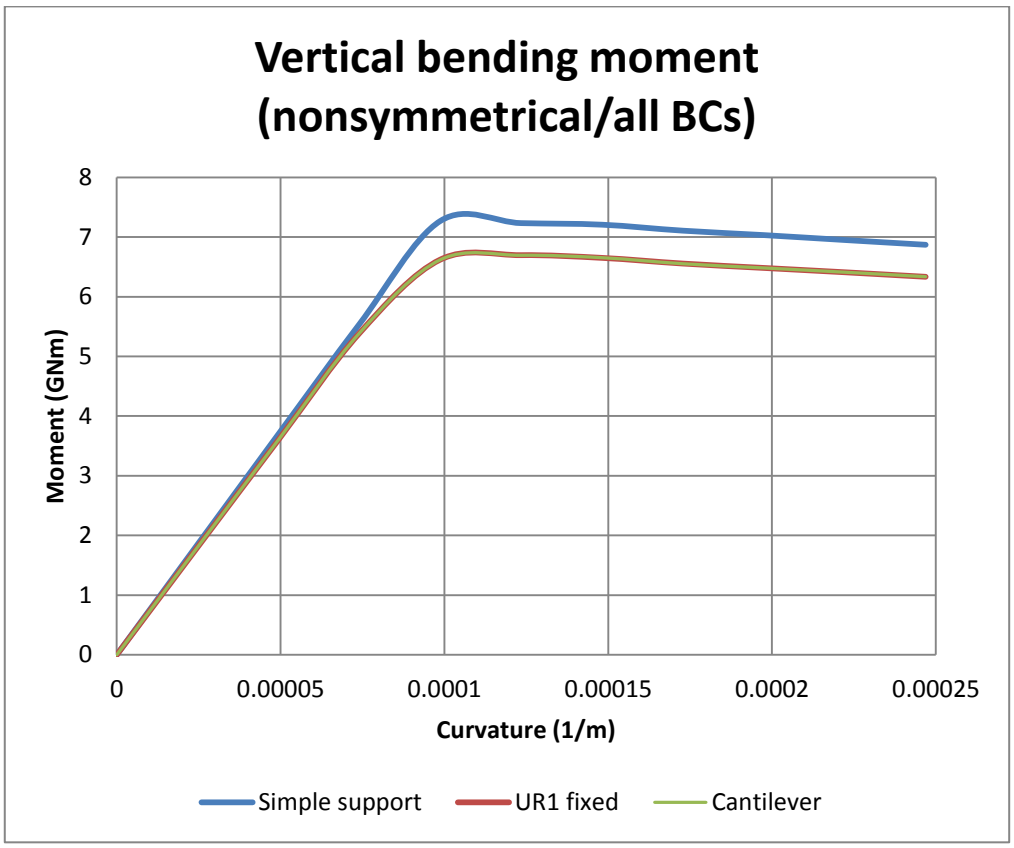

Figure 49.Vertical bending moment vs. Curvature (nonsymmetrical damage-all BCs)

It can be easily noticed that Figure 49 is similar to Figure 11 as far as it concerns the curves for the damaged cases. Simple support boundary condition increases the stiffness of the model resulting in larger value of maximum bending moment. The other two boundary conditions provide the same result. Moreover, different boundary conditions result in different distributions of vertical displacements at the deck of the hull as we saw in figures 26, 29 and 35. It seems that symmetrical boundary conditions lead to large shear forces at both ends of the structure that affect vertical displacements which get maximized close to the boundary conditions. Cantilever boundary condition as well as boundary condition where only the rear rotation about the horizontal axis is constrained, provide almost the same distribution of vertical displacements with a difference lying on the central path where cantilever support seems to provide more rational results as it can be

seen from Figures 26, 29 for the nonsymmetrical case and Figures 38, 41 for the symmetrical one.

The corresponding figure for the second damage scenario is the following.

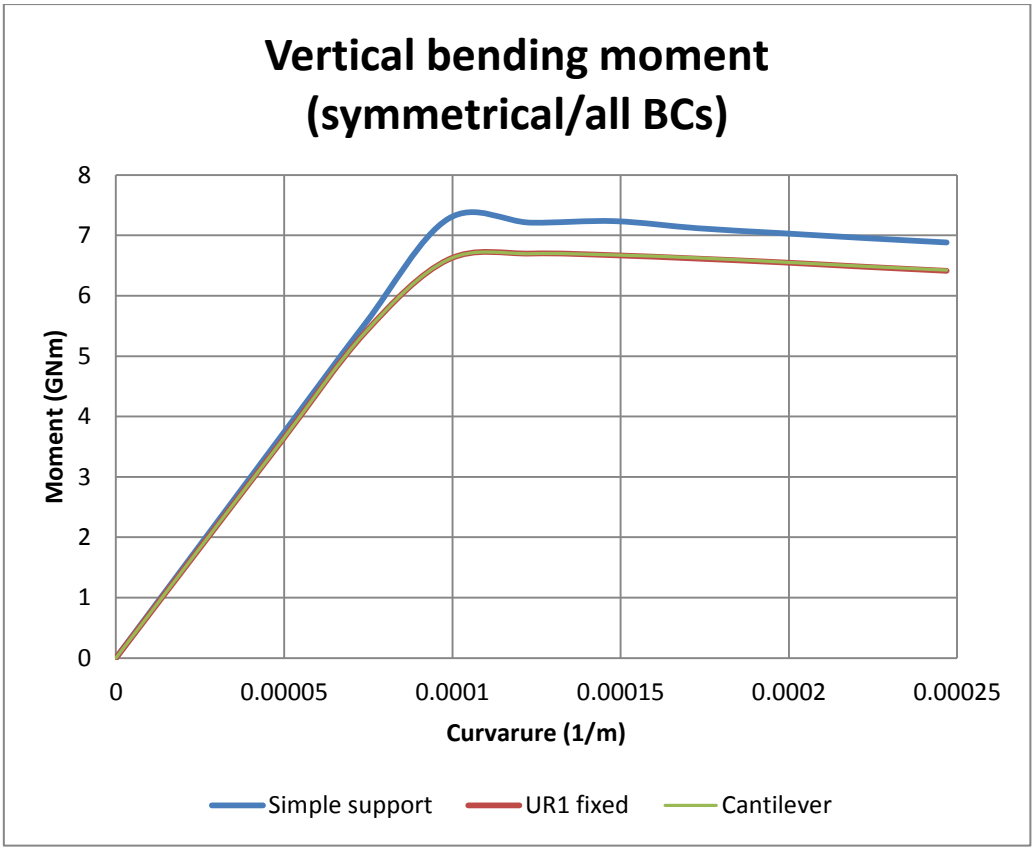

Figure 50.Vertical bending moment vs. Curvature (symmetrical damage-all BCs)

Also in this case, simple support boundary condition provides larger results than the other two boundary condition cases. Cantilever boundary condition and the boundary condition where only rotation about horizontal axis is fixed result in the same curve concerning the vertical bending moment. For the vertical displacements at the deck we can reach the same conclusions as before. In addition, results taken from the two similar boundary conditions are almost the same, which is probably because the damage is symmetrical.

Table 17 shows the results of vertical bending moment for better understanding.

	Damage scenario 1 (nonsymmetrical)	Damage scenario 2 (symmetrical)
Cantilever	6.695 GNm	6.697 GNm
UR1 fixed (rear)	6.697 GNm	6.699 GNm
Simple support	7.27 GNm	7.28 GNm

Table 17.Results in GNm for the two damage scenarios (all BCs)

It can be easily seen that the results for both damage scenarios are more or less the same. That means that the place of the damage does not play an important role for the ship's integrity in sagging condition. Furthermore, results of the intact and damaged cases should be compared in order to assess ship's residual strength after such collision cases.

	Damage scenario 1 (nonsymmetrical)	Damage scenario 2 (symmetrical)	Intact	Damage scenario1/ Intact	Damage scenario1/ Intact
	6.695 GNm	6.697 GNm	8.891 GNm	0.753	0.753
	6.697 GNm	6.699 GNm		0.753	0.753
	7.27 GNm	7.28 GNm		0.818	0.819

Table 18.Comparison of results with the intact state

As we can see the reduction of the ship's strength ranges between 18.2%÷24.7%. If we compare these results with the results obtained from SHIP I simulation, we realize that our simulations converge.
Results of the residual strength for both ships are shown in Table 19.

	SHIP I	**SHIP II**	
		Damage scenario 1/ Intact	Damage scenario 2/ Intact
BC_1	0.803	0.753	0.753
BC_2	0.803	0.753	0.753
BC_3	0.816	0.818	0.819

Table 19.Comparison of results for both ships

CHAPTER FOUR:

ANALYTICAL CALCULATION OF A SHIP'S ULTIMATE STRENGTH

4. ANALYTICAL CALCULATION OF A SHIP'S ULTIMATE STRENGTH

4.1 Description of the scope

In this chapter we implemented the incremental-iterative method for the SHIP II cross section. The moment versus curvature relationship which was derived will be compared to this derived using the Finite Element Method, as well as, the position of the neutral axis. This will provide data to investigate if the two methods res9ult in comparable results or not.

4.2 Incremental-iterative method (intact case)

Theoretical aspects of this method were given in section 2.3. Taking into account these basic aspects of the method we discretized the cross section In 128 members of stiffened plates, 27 hard corner elements and 19 attached plates. In Tables 19, 20 & 21 someone can see the discretization of the cross section.

STIFFENER ELEMENTS														
		s (m)	tp (cm)	bp (cm)	tw (cm)	bw (cm)	tf (cm)	bf (cm)	A (cm^2)	rehs (MPa)	rehp (Mpa)	l (m)	z (m)	Is (cm^4)
	1	0.85	1.65	85	1.1	42.5	1.8	15	214	355	355	3.78	0.112272488	59509.212
	2	0.85	1.65	85	1.1	42.5	1.8	15	214	355	355	3.78	0.112272488	59509.212
	3	0.85	1.65	85	1.1	42.5	1.8	15	214	355	355	3.78	0.112272488	59509.212
	4	0.85	1.65	85	1.1	42.5	1.8	15	214	355	355	3.78	0.112272488	59509.212
	5	0.85	1.65	85	1.1	42.5	1.8	15	214	355	355	3.78	0.112272488	59509.212
	6	0.85	1.65	85	1.1	42.5	1.8	15	214	355	355	3.78	0.112272488	59509.212
	7	0.85	1.65	85	1.1	42.5	1.8	15	214	355	355	3.78	0.112272488	59509.212
	8	0.85	1.65	85	1.1	42.5	1.8	15	214	355	355	3.78	0.112272488	59509.212
	9	0.85	1.65	85	1.1	42.5	1.8	15	214	355	355	3.78	0.112272488	59509.212
	10	0.85	1.7	85	1.1	42.5	1.8	15	218.25	355	355	3.78	0.110581329	60036.84
BOTTOM	11	0.85	1.7	85	1.1	42.5	1.8	15	218.25	355	355	3.78	0.110581329	60036.84
	12	0.85	1.7	85	1.1	42.5	1.8	15	218.25	355	355	3.78	0.110581329	60036.84
	13	0.85	1.7	85	1.1	42.5	1.8	15	218.25	355	355	3.78	0.110581329	60036.84
	14	0.85	1.7	85	1.1	42.5	1.8	15	218.25	355	355	3.78	0.110581329	60036.84
	15	0.85	1.75	85	1.1	42.5	1.8	15	222.5	355	355	3.78	0.108964326	60548.921
	16	0.85	1.75	85	1.1	42.5	1.8	15	222.5	355	355	3.78	0.108964326	60548.921
	17	0.85	1.75	85	1.1	42.5	1.8	15	222.5	355	355	3.78	0.108964326	60548.921
	18	0.84	1.75	84	1.1	42.5	1.8	15	220.75	355	355	3.78	0.109758777	60371.331
	19	0.79	1.8	79	1.1	42.5	1.8	15	215.95	355	355	3.78	0.112339315	59945.034
	20	0.79	1.8	79	1.1	42.5	1.8	15	215.95	355	355	3.78	0.112339315	59945.034
	21	0.79	1.8	79	1.1	42.5	1.8	15	215.95	355	355	3.78	0.112339315	59945.034
	22	0.79	1.8	79	1.1	42.5	1.8	15	215.95	355	355	3.78	0.112339315	59945.034
	23	0.7	1.8	70	1.1	42.5	1.8	15	199.75	355	355	3.78	0.120720275	58070.355

INNER BOTTOM	1	0.85	1.65	85	1.1	42.5	1.8	15	214	355	355	3.78	2.387727512	59509.212
	2	0.85	1.65	85	1.1	42.5	1.8	15	214	355	355	3.78	2.387727512	59509.212
	3	0.85	1.65	85	1.1	42.5	1.8	15	214	355	355	3.78	2.387727512	59509.212
	4	0.85	1.65	85	1.1	42.5	1.8	15	214	355	355	3.78	2.387727512	59509.212
	5	0.85	1.65	85	1.1	42.5	1.8	15	214	355	355	3.78	2.387727512	59509.212
	6	0.85	1.65	85	1.1	42.5	1.8	15	214	355	355	3.78	2.387727512	59509.212
	7	0.85	1.65	85	1.1	42.5	1.8	15	214	355	355	3.78	2.387727512	59509.212
	8	0.85	1.65	85	1.1	42.5	1.8	15	214	355	355	3.78	2.387727512	59509.212
	9	0.85	1.65	85	1.1	42.5	1.8	15	214	355	355	3.78	2.387727512	59509.212
	10	0.85	1.7	85	1.1	42.5	1.8	15	218.25	355	355	3.78	2.389418671	60036.84
	11	0.85	1.7	85	1.1	42.5	1.8	15	218.25	355	355	3.78	2.389418671	60036.84
	12	0.85	1.7	85	1.1	42.5	1.8	15	218.25	355	355	3.78	2.389418671	60036.84
	13	0.85	1.7	85	1.1	42.5	1.8	15	218.25	355	355	3.78	2.389418671	60036.84
	14	0.85	1.7	85	1.1	42.5	1.8	15	218.25	355	355	3.78	2.389418671	60036.84
	15	0.85	1.75	85	1.1	42.5	1.8	15	222.5	355	355	3.78	2.391035674	60548.921
	16	0.85	1.75	85	1.1	42.5	1.8	15	222.5	355	355	3.78	2.391035674	60548.921
	17	0.85	1.75	85	1.1	42.5	1.8	15	222.5	355	355	3.78	2.391035674	60548.921
	18	0.84	1.75	84	1.1	42.5	1.8	15	220.75	355	355	3.78	2.390241223	60371.331
UPPER DECK	1	0.85	1.7	85	1.1	30	1.6	9	191.9	355	355	3.78	20.94053869	20221.733
	2	0.85	1.7	85	1.1	30	1.6	9	191.9	355	355	3.78	20.94053869	20221.733
	3	0.85	1.7	85	1.1	30	1.6	9	191.9	355	355	3.78	20.94053869	20221.733
	4	0.85	1.7	85	1.1	30	1.6	9	191.9	355	355	3.78	20.94053869	20221.733
	5	0.85	1.7	85	1.1	30	1.6	9	191.9	355	355	3.78	20.94053869	20221.733
	6	0.85	1.7	85	1.1	30	1.6	9	191.9	355	355	3.78	20.94053869	20221.733
	7	0.85	1.7	85	1.1	30	1.6	9	191.9	355	355	3.78	20.94053869	20221.733
	8	0.85	1.7	85	1.1	30	1.6	9	191.9	355	355	3.78	20.94053869	20221.733
	9	0.85	1.7	85	1.1	30	1.6	9	191.9	355	355	3.78	20.94053869	20221.733
	10	0.85	1.7	85	1.1	30	1.6	9	191.9	355	355	3.78	20.94053869	20221.733
	11	0.85	1.7	85	1.1	30	1.6	9	191.9	355	355	3.78	20.94053869	20221.733
	12	0.85	1.7	85	1.1	30	1.6	9	191.9	355	355	3.78	20.94053869	20221.733
	13	0.85	1.7	85	1.1	30	1.6	9	191.9	355	355	3.78	20.94053869	20221.733
	14	0.85	1.7	85	1.1	30	1.6	9	191.9	355	355	3.78	20.94053869	20221.733
	15	0.85	1.7	85	1.1	30	1.6	9	191.9	355	355	3.78	20.94053869	20221.733
	16	0.85	1.7	85	1.1	30	1.6	9	191.9	355	355	3.78	20.94053869	20221.733
	17	0.85	1.7	85	1.1	30	1.6	9	191.9	355	355	3.78	20.94053869	20221.733
	18	0.85	1.7	85	1.1	30	1.6	9	191.9	355	355	3.78	20.94053869	20221.733
	19	0.84	1.7	84	1.1	30	1.6	9	190.2	355	355	3.78	20.9400831	20176.702
	20	0.84	1.7	84	1.1	30	1.6	9	190.2	355	355	3.78	20.9400831	20176.702
	21	0.84	1.7	84	1.1	30	1.6	9	190.2	355	355	3.78	20.9400831	20176.702
	22	0.84	1.7	84	1.1	30	1.6	9	190.2	355	355	3.78	20.9400831	20176.702
	23	0.84	1.7	84	1.1	30	1.6	9	190.2	355	355	3.78	20.9400831	20176.702
	24	**0.84**	**1.7**	**84**	**1.1**	**30**	**1.6**	**9**	**190.2**	**355**	**355**	**3.78**	**20.9400831**	**20176.702**
	25	**0.84**	**1.7**	**84**	**1.1**	**30**	**1.6**	**9**	**190.2**	**355**	**355**	**3.78**	**20.9400831**	**20176.702**

SIDE SHELL	1	0.7	1.8	70	1.1	42.5	1.8	15	199.75	355	355	3.78	1.55	51960.964
	2	0.75	1.8	75	1.1	42.5	1.8	15	208.75	355	355	3.78	2.25	63792.214
	3	0.75	1.8	75	1.1	42.5	1.8	15	208.75	355	355	3.78	3	63792.214
	4	0.75	1.8	75	1.1	42.5	1.6	15	205.75	355	355	3.78	3.75	63735.964
	5	0.75	1.8	75	1.1	42.5	1.6	15	205.75	355	355	3.78	4.5	63735.964
	6	0.75	1.8	75	1.1	42.5	1.6	15	205.75	355	355	3.78	5.25	63735.964
	7	0.85	1.7	85	1.1	38.5	1.5	12.5	205.6	355	355	3.78	6.85	87249.453
	8	0.85	1.7	85	1.1	38.5	1.5	12.5	205.6	355	355	3.78	7.7	87249.453
	9	**0.85**	**1.7**	**85**	**1.1**	**38.5**	**1.5**	**12.5**	**205.6**	**355**	**355**	**3.78**	**8.55**	**87249.453**
	10	**0.85**	**1.7**	**85**	**1.2**	**35**	**1.7**	**10**	**203.5**	**355**	**355**	**3.78**	**9.35**	**87147.748**
	11	**0.85**	**1.5**	**85**	**1.2**	**35**	**1.7**	**10**	**186.5**	**355**	**355**	**3.78**	**11.05**	**76912.332**
	12	**0.85**	**1.5**	**85**	**1.2**	**35**	**1.7**	**10**	**186.5**	**355**	**355**	**3.78**	**11.9**	**76912.332**
	13	**0.85**	**1.5**	**85**	**1.2**	**35**	**1.7**	**10**	**186.5**	**355**	**355**	**3.78**	**12.75**	**76912.332**
	14	**0.85**	**1.5**	**85**	**1.2**	**35**	**1.7**	**10**	**186.5**	**355**	**355**	**3.78**	**13.6**	**76912.332**
	15	**0.85**	**1.5**	**85**	**1.2**	**35**	**1.7**	**10**	**186.5**	**355**	**355**	**3.78**	**14.45**	**76912.332**
	16	**0.85**	**1.5**	**85**	**1.2**	**25**	**1.6**	**9**	**171.9**	**355**	**355**	**3.78**	**16.15**	**76866.425**
	17	**0.85**	**1.5**	**85**	**1.2**	**25**	**1.6**	**9**	**171.9**	**355**	**355**	**3.78**	**17**	**76866.425**
	18	**0.85**	**1.5**	**85**	**1.1**	**25**	**1.6**	**9**	**169.4**	**355**	**355**	**3.78**	**17.9**	**76865.598**
	19	**0.85**	**1.7**	**85**	**1.1**	**25**	**1.6**	**9**	**186.4**	**355**	**355**	**3.78**	**18.75**	**87101.015**
	20	**0.85**	**1.7**	**85**	**1.1**	**25**	**1.6**	**9**	**186.4**	**355**	**355**	**3.78**	**19.6**	**87101.015**
INNER SIDE SHELL	1	0.85	1.7	85	1.1	38.5	1.8	12.5	209.35	355	355	3.78	6.85	87298.281
	2	0.85	1.7	85	1.1	38.5	1.8	12.5	209.35	355	355	3.78	7.7	87298.281
	3	**0.85**	**1.7**	**85**	**1.1**	**38.5**	**1.8**	**12.5**	**209.35**	**355**	**355**	**3.78**	**8.55**	**87298.281**
	4	**0.85**	**1.7**	**85**	**1.1**	**38.5**	**1.8**	**12.5**	**209.35**	**355**	**355**	**3.78**	**9.4**	**87298.281**
	5	**0.85**	**1.5**	**85**	**1.1**	**38.5**	**1.5**	**12.5**	**188.6**	**355**	**355**	**3.78**	**11.1**	**77014.036**
	6	**0.85**	**1.5**	**85**	**1.1**	**38.5**	**1.5**	**12.5**	**188.6**	**355**	**355**	**3.78**	**11.95**	**77014.036**
	7	**0.85**	**1.5**	**85**	**1.2**	**35**	**1.7**	**10**	**186.5**	**355**	**355**	**3.78**	**12.75**	**76912.332**
	8	**0.85**	**1.5**	**85**	**1.2**	**35**	**1.7**	**10**	**186.5**	**355**	**355**	**3.78**	**13.6**	**76912.332**
	9	**0.85**	**1.5**	**85**	**1.2**	**35**	**1.7**	**10**	**186.5**	**355**	**355**	**3.78**	**14.45**	**76912.332**
	10	**0.85**	**1.5**	**85**	**1.3**	**30**	**1.7**	**9**	**181.8**	**355**	**355**	**3.78**	**16.1**	**76874.393**
	11	**0.85**	**1.5**	**85**	**1.3**	**30**	**1.7**	**9**	**181.8**	**355**	**355**	**3.78**	**16.95**	**76874.393**
	12	**0.85**	**1.7**	**85**	**1.2**	**25**	**1.6**	**9**	**188.9**	**355**	**355**	**3.78**	**17.85**	**87101.842**
	13	**0.85**	**1.7**	**85**	**1.2**	**25**	**1.6**	**9**	**188.9**	**355**	**355**	**3.78**	**19.935**	**87101.842**
	14	**0.85**	**1.7**	**85**	**1.4**	**68**	**1.4**	**15**	**260.7**	**355**	**355**	**3.78**	**18.985**	**87410.341**

CENTRELINE	1	0.81	0.75	81	1.15	40	1.5	10	121.75	355	355	3.78	3.319089836	33684.812
	2	0.81	0.75	81	1.15	40	1.5	10	121.75	355	355	3.78	4.129089836	33684.812
	3	0.81	0.75	81	1.15	40	1.5	10	121.75	355	355	3.78	4.939089836	33684.812
	4	0.81	0.75	81	1.2	35	1.7	10	119.75	355	355	3.78	5.748151879	33735.086
	5	0.81	0.75	81	1.2	35	1.7	10	119.75	355	355	3.78	6.558151879	33735.086
	6	0.81	0.75	81	1.2	35	1.7	10	119.75	355	355	3.78	7.368151879	33735.086
	7	0.81	0.75	81	1.2	35	1.7	10	119.75	355	355	3.78	8.178151879	33735.086
	8	0.81	0.75	81	1.2	35	1.7	10	119.75	355	355	3.78	8.988151879	33735.086
	9	0.81	0.75	81	1.2	35	1.7	10	119.75	355	355	3.78	9.798151879	33735.086
	10	0.81	0.75	81	1.2	35	1.7	10	119.75	355	355	3.78	10.60815188	33735.086
	11	0.81	0.75	81	1.2	35	1.7	10	119.75	355	355	3.78	11.41815188	33735.086
	12	0.81	0.75	81	1.2	35	1.7	10	119.75	355	355	3.78	12.22815188	33735.086
	13	0.81	0.75	81	1.2	30	1.6	9	111.15	355	355	3.78	13.03942004	33579.156
	14	0.81	0.75	81	1.2	30	1.6	9	111.15	355	355	3.78	13.84942004	33579.156
	15	0.81	0.75	81	1.2	30	1.6	9	111.15	355	355	3.78	14.65942004	33579.156
	16	0.81	0.75	81	1.2	30	1.6	9	111.15	355	355	3.78	15.46942004	33579.156
	17	0.81	0.75	81	1.2	30	1.6	9	111.15	355	355	3.78	16.27942004	33579.156
	18	0.81	0.75	81	1.2	25	1.6	9	105.15	355	355	3.78	17.08908738	33574.623
	19	0.81	0.75	81	1.2	25	1.6	9	105.15	355	355	3.78	17.89908738	33574.623
	20	0.81	0.75	81	1.2	25	1.6	9	105.15	355	355	3.78	18.70908738	33574.623
	21	0.81	0.75	81	1.1	30	1.6	9	108.15	355	355	3.78	19.51925832	33576.289
	22	0.81	0.75	81	1.1	30	1.6	9	108.15	355	355	3.78	20.32925832	33576.289
HOPPER	1	0.75	1.9	75	1.1	42.5	1.6	15	213.25	355	355	3.78	2.82744967	10815.072
	2	0.75	1.9	75	1.1	42.5	1.6	15	213.25	355	355	3.78	3.404928219	10815.072
	3	0.75	1.9	75	1.1	42.5	1.6	15	213.25	355	355	3.78	3.982406768	10815.072
	4	0.75	1.9	75	1.1	42.5	1.6	15	213.25	355	355	3.78	4.559885318	10815.072
	5	0.75	1.9	75	1.1	42.5	1.6	15	213.25	355	355	3.78	5.137363867	10815.072
	6	0.75	1.8	75	1.1	42.5	1.6	15	205.75	355	355	3.78	5.715633803	10732.57

Table 20. Stiffener elements

hard corners					
	bp (mm)	tp (mm)	z (m)	Rehp (MPa)	A (cm^2)
1	360	18	6.124	355	6480
2	2500	18	6.541	355	45000
3	340	17	6.73	355	5780
4	420	17.5	2.49125	355	7350
5	360	18	2.789	355	6480
6	350	17.5	2.3075	355	6125
7	**420**	**17**	**20.9915**	**355**	**7140**
8	**420**	**17**	**20.9915**	**355**	**7140**
9	**340**	**17**	**20.813**	**355**	**5780**
10	**415**	**17**	**20.9915**	**355**	**7055**
11	**340**	**17**	**20.813**	**355**	**5780**
12	**2500**	**15**	**15.8925**	**355**	**37500**
13	**1200**	**15**	**15.8925**	**355**	**18000**
14	**2500**	**17**	**10.7915**	**355**	**42500**
15	**1360**	**17**	**10.7915**	**355**	**23120**
16	720	18	6.541	355	12960
17	425	17	22.1415	355	7225
18	330	8.25	21.968	355	2722.5
19	1000	18	0.009	355	18000
20	360	18	0.18	355	6480
21	420	17.5	0.00875	355	7350
22	395	18	0.009	355	7110
23	425	18.5	2.49075	355	7862.5
24	350	8.75	2.3065	355	3062.5
25	300	7.5	2.65	355	2250
26	425	12.5	0.00625	355	5312.5
27	350	8.75	0.1875	355	3062.5

Table 21. Hard corner elements

attached plates							
	tp (cm)	bp (mm)	s (m)	bp (m)	z (m)	A (mm^2)	Rehp (Mpa)
1	1.25	175	0.85	0.175	0.00625	2187.5	355
2	1.75	420	0.84	0.42	2.49125	7350	355
3	1.25	420	0.84	0.42	0.00625	5250	355
4	1.25	395	0.79	0.395	0.00625	4937.5	355
5	1.8	365	0.75	0.365	6.409573	6570	355
6	1.7	85	0.85	0.085	6.5925	1445	355
7	**1.7**	**85**	**0.85**	**0.085**	**10.7575**	**1445**	**355**
8	**1.5**	**85**	**0.85**	**0.085**	**10.7575**	**1275**	**355**
9	**1.5**	**125**	**0.85**	**0.125**	**10.8625**	**1875**	**355**
10	**1.5**	**125**	**0.85**	**0.125**	**10.8625**	**1875**	**355**
11	1.5	250	0.85	0.25	15.8375	3750	355
12	**1.5**	**250**	**0.85**	**0.25**	**15.9625**	**3750**	**355**
13	1.7	40	0.898	0.04	20.98	680	355
14	**1.7**	**85**	**0.85**	**0.085**	**20.9575**	**1445**	**355**
15	**1.7**	**75**	**0.84**	**0.075**	**20.9915**	**1275**	**355**
16	1.7	160	0.84	0.16	20.9915	2720	355
17	0.825	120	0.9	0.12	22.09	990	355
18	1.7	85	0.85	0.085	22.1415	1445	355
19	1.8	1000	0.7	1	0.009	18000	355

Table 22. Attached plate elements

Input constant variables for the algorithm apart from the elastic material properties, is the initial position of the neutral axis. For this particular occasion of SHIP II the initial position of the neutral axis is:

$$y_{N.A.} = 9.05\text{m}$$

We notice that this value slightly differs from the value evaluated by using ABAQUS software (see pg. 34). This might occurred due to differences during the creation of the numerical and the analytical model.

After using the algorithm written in Fortran95, we derived the following results concerning the Ultimate Strength of the intact SHIP II.

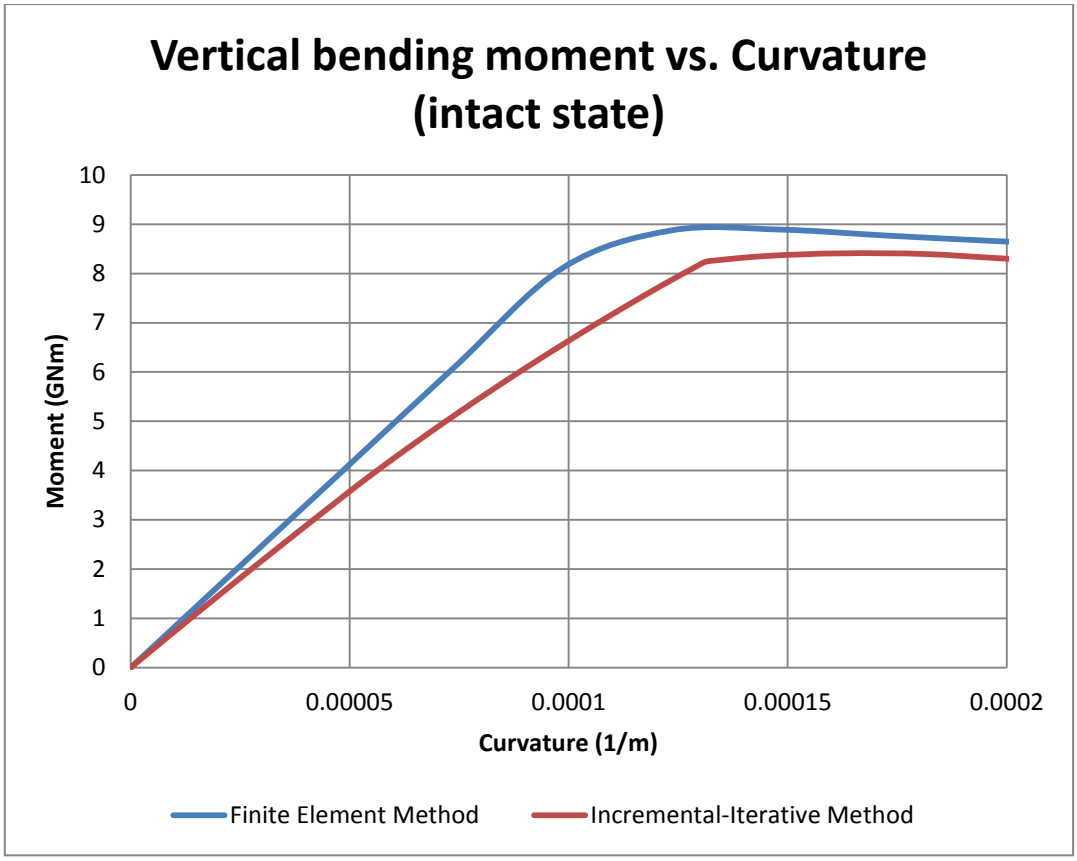

Figure 51. Common diagram for the ultimate strength of SHIP II using two different methods

The maximum value of the Ultimate Strength derived from the incremental-iterative method is shown in Table 22.

Maximum value of vertical bending moment	8.414GNm
Curvature of maximum vertical bending moment	0.001896

Table 23. Maximum value of vertical bending moment for the intact state (incremental-iterative method)

As it concerns the position of the neutral axis when maximum bending moment was succeeded, we added Figure 52 below where differences between the analytical and the numerical solutions can be observed.

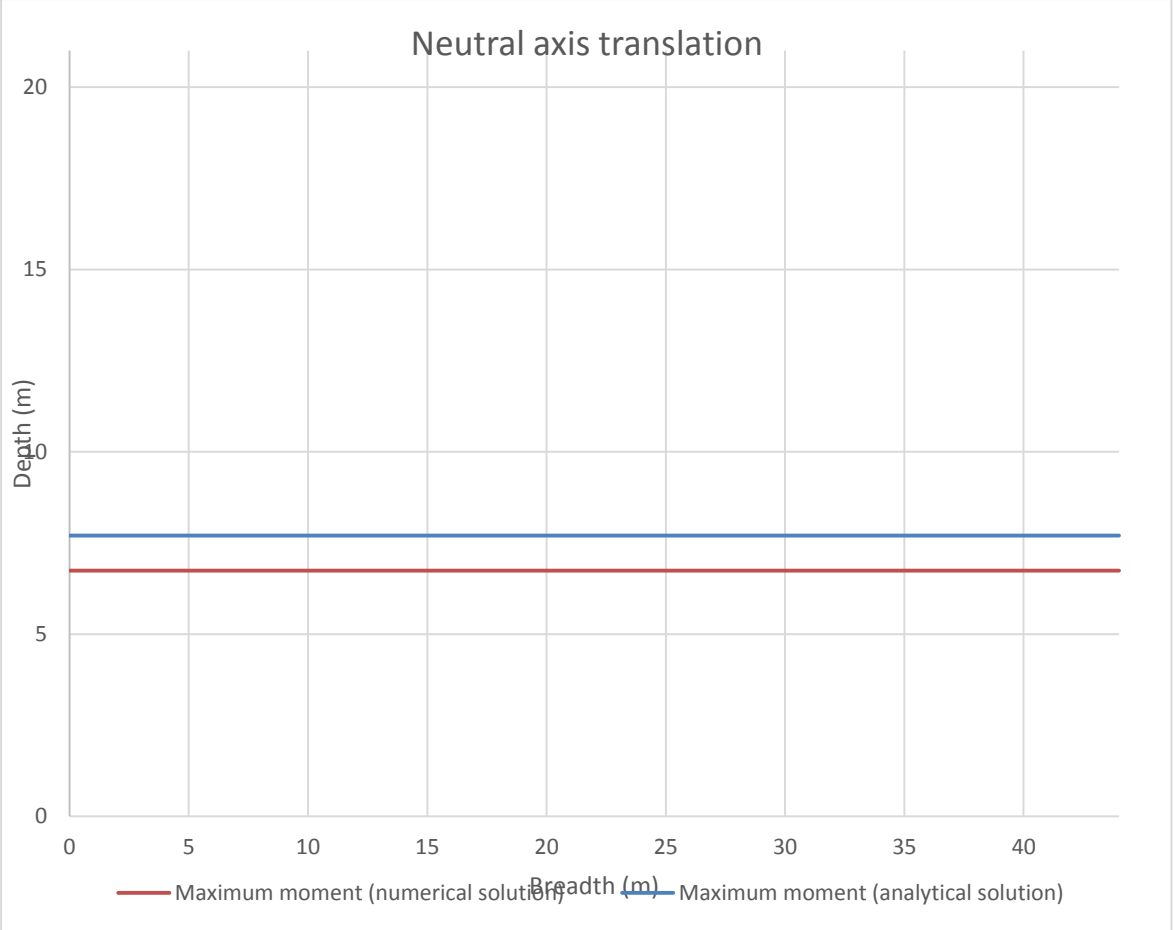

Figure 52. Position of the neutral axis when maximum bending moment is succeeded (analytical & numerical solutions)

4.3 Incremental-iterative method (damaged case)

When a part of the ship's cross section is missing due to a collision, bending takes place about a new neutral axis which, apart from being translated, also rotates about an axis vertical to the section's X-Y plane. The value of this angle is given by the following expression,

$$tan\varphi = \frac{I_x}{I_{xy}}$$

where I_x is the section's moment of inertia with regards to X-axis and

$I_{xy}=\int(x^2+y^2)dm$ is the product of inertia, which is non-zero for an asymmetric section. For an intact section I_{xy} is zero because for every positive contribution of (xydm) there is always a negative one to the opposite side of the symmetry plane.

The initial angle of rotation as well as the initial position of the neutral axis for the damaged section can be seen below. Note that in this case, structural elements included in Tables 19, 20, and 21 were used for the calculations, except for those indicated, which consist of the damaged region. Suffice it is to say that the dimensions of the damage are equal to those considered in the case of Finite Element Analysis.

$$y_{N.A.} = 8.99\text{m}$$

$$x_{N.A.} = -6.3697\text{m}$$

$$\varphi = -0.001004^{o}$$

For the development of the numerical tool for the evaluation of the residual strength of a damaged ship, the theory of asymmetric bending of beams was implemented. It has been chosen that a repetition of the theory would not be helpful as someone can easily backdate to a vast amount of relevant scientific papers and books. ***[15]***

Nevertheless, it is really important to mention that there has been made a modification to the software used before (see section *4.2)*, because in the damaged case the criterion of zero axial forces is not sufficient. When bending moment is imposed on an asymmetric section, its vector can be decomposed in two components, parallel to the principle axes. Therefore, two equilibria have to be satisfied. The first corresponds to the equilibrium of axial forces and the second to the equilibrium of the forces induced by the M_y component of the moment. Consequently, the solution for each step of the simulation is obtained in two phases.

- At first, the equilibrium of axial forces is satisfied by simply translating the neutral axis.
- After the equilibrium of axial forces has been satisfied, rotation was implemented to the neutral axis until the M_y component of the bending moment is bounded between *-1000Nm< M_y <1000Nm* so that the induced stresses remain at a low level, approximately zero.

Elements missing from the section due to the collided area are defined as having transverse center of mass greater than *b=20.625m* (measured from the centerline) and vertical center of mass greater than *d=8.4m* (measured from the baseline). These structural elements are indicated in Tables 19, 20, 21 in bold.

Figure 53 depicts the vertical bending moment in the damaged case versus the applied curvature when using both the Incremental-Iterative Method and the Finite Element Method.

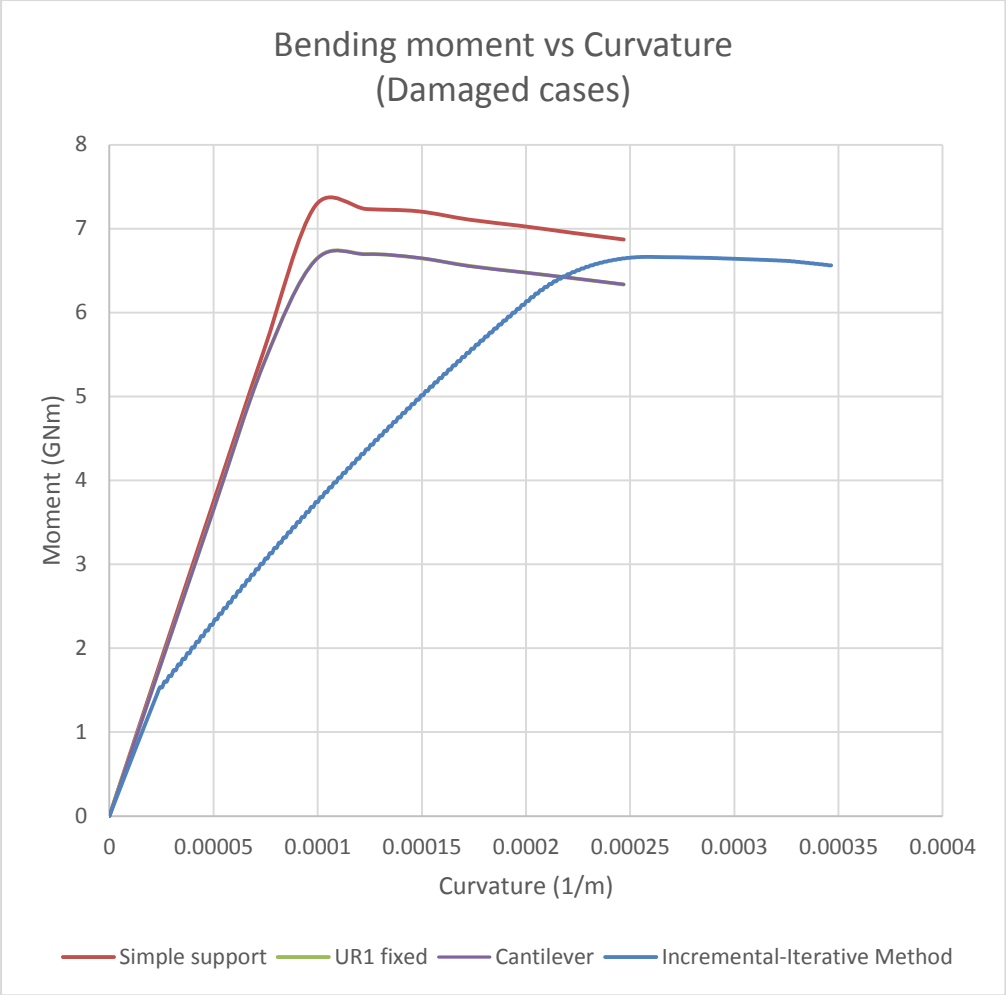

Figure 53. Residual strength (SHIP II) using both the Finite Element Method and the Incremental-Iterative Method

The maximum value of the residual strength obtained when using the Incremental-Iterative Method can be seen in Table 23.

Maximum value of vertical bending moment	6.663GNm
Curvature of maximum vertical bending moment	0.0002596

Table 24. Maximum value of vertical bending moment for the damaged state (incremental-iterative method)

The position of the neutral axis when maximum residual strength has been succeeded is given by the following values:

$$y_{N.A.} = 7.198\text{m}$$

$$x_{N.A.} = -6.3697\text{m}$$

$$\varphi = -5.676^{o}$$

4.4 Discussion

By comparing the maximum values of bending moments in Tables 23, 24 with the maximum values in Tables 17, 18 respectively we notice a relatively acceptable difference as it concerns the value of the ultimate and the residual strength. In the case where intact cross section was considered, the difference between the values obtained by the Finite Element Method and the Incremental-Iterative method differ by $\delta_{intact}=5.36\%$, whereas in the case of the damaged section the difference is much smaller $\delta_{damage\_1}=0.48\%$ for the cantilever and "quasi-cantilever" boundary conditions for both damage scenarios approximately, and $\delta_{damage\_2}=8.3\%$ for the symmetrical-simple support boundary condition for both damage scenarios approximately.

Furthermore, in Figure 51 we notice that the maximum bending moment for the intact case is satisfied in a lower value of curvature when using the Finite Element Method rather than in the case where the Incremental-Iterative Method has been applied. This fact can be explained if we consider that we conducted a dynamic explicit analysis and consequently, there are inertia forces that make the model stiffer and cannot be totally eliminated. The same effect can be observed in the damaged case, where the maximum value of the residual strength when using the Finite Element Method is satisfied far in advance compared to the case where the Incremental-Iterative Method was applied. However, application of cantilever or "quasi-cantilever" boundary conditions in this case provide less stiffness to the model, therefore the results between the methods are almost equal.

Finally, as it concerns the position of the neutral axes in both intact and damaged cases, differences between the two methods can be observed. At first, in the intact case there is a difference of approximately one meter between the vertical positions of the section's neutral axis. Moreover, in the damaged case, the angle of rotation of the neutral axis is half the angle of rotation when symmetrical damage is considered. As we can see from Figures 27, 30, 34 the angle of rotation of the neutral axis in the nonsymmetrical case is approximately zero for the studied section however, f9urther investigation 0is needed to explain the differences.

CHAPTER FIVE:

CONCLUSIONS AND ISSUES FOR FUTURE RESEARCH

5. CONCLUSIONS AND ISSUES FOR FUTURE RESEARCH

5.1 Conclusions

The following conclusions can be derived from the present work.

1. As we can see from Tables 8, 18, 19, 23, 24 the percentage of ship's ultimate strength reduction after the considered damage occurred is:
   SHIP I → 19.7% (only FEA conducted)
   SHIP II → 24.7% (when FEA conducted) and
   → 20.8 (when the Incremental-Iterative Method applied)
   From the aforementioned results it can be considered that the damage proposed by the CSR and modeled here, results in a reduction of a ship' ultimate strength between 20-25%.

2. Differences between the design moments shown in Tables 1, 2 and the calculated using the FEM and the Incremental-Iterative method can be explained because the CSR proposed method for the calculation of a ship's design moment takes into account the corrosion addition.

3. The modeling parameters proposed for the simulation of a ship under sagging bending moment are:
   Mesh element size → Quadrilateral square elements of 100mm side length.
   Mesh element type → Reduced integration (S4R) elements having one integration point along thickness.
   Rate of loading application → A rate of curvature application approximately 0.00012 $(ms)^{-1}$ seems to represent satisfactory a quasi-static phenomenon when dynamic explicit analysis is conducted.
   Boundary Conditions → For the intact case, the proposed unconstrained boundary conditions are the rotation about the transverse axis and the translation along the longitudinal axis so that no axial forces appear. For the damaged cases, using also the results taken from the Incremental-Iterative Method, we suggest that cantilever or "quasi-cantilever" boundary conditions are used as they do not make our model stiffer.

4. The method developed here for the numerical modeling of a ship's hull under extreme bending loading using the FEM can be considered relatively reliable for the estimation of her bending capacity as we have noticed good agreement when also Smith's method has been applied.

5.2 Proposals for future research

Some interesting proposals for future research which arise from the present work are added below.

1. Further investigation is needed to explain the difference between the values of the ultimate and residual strength of a ship's hull when the FEM and the Incremental-Iterative method are applied.

2. Implementation of other material models when using the Finite Element Method that refer to real conditions.

3. Modeling of other hulls, both symmetrical and asymmetrical, so that the present conclusions become more legible.

4. In order to conduct a purely static analysis, initial imperfection can be introduced at a part of the main deck. In this way, the mode of collapse can be more predictive.

5. Application of the implicit algorithm.

REFERENCES-BIBLIOGRAPHY

1. Bryan G.H. 1890. On the stability of a Plane Plate under Thrusts in its own Plane, with application to the “Buckling” of the Sides of a Ship. *Jornal de Sciencias Mathematicas e Astronomicas, Vol. ix No. 6*
2. Caldwell, J.B. 1965. Ultimate longitudinal strength. *RINA Transactions 107, 411-430*
3. Turner J.L., Clough R.W., Martin H.G., Topp L.J. 1956. Stiffness and deflection analysis of complex structures. *J. aero. Sci, 23, pp. 805-825*
4. Paik, J.K., Kim, D.K., Park, D.H., Kim, H.B., Kim, M.S. 2012. A new method for assessing the safety of ships damaged by grounding. *RINA Transactions 154, Part A1, International Journal of Maritime Engineering, Jan-Mar 2012*
5. Paik J.K., Kim D.K., Park D.H., Kim H.B., Mansour, H.B., Caldwell, J.B. 2011. Modified Paik-Mansour formula for ultimate strength calculations of ship hulls. *Proceedings of MARSTRUCT 2011 Conference, 28-30 March, Hamburg, Germany*
6. ALPS/HULL 2006. A computer program for progressive collapse analysis of ship hulls. *Advanced Technology Center, USA*
7. Villavicencio R., Guedes Soares C., Liu Z., Amdhal J. 2011. Influence of the neutral axis displacement on the residual strength of a damaged tanker double bottom structure. *Proceedings of MARSTRUCT 2011 Conference, 28-30 March, Hamburg, Germany*
8. Notaro G., Kippenes, J., Amlashi, H., Pusso, M., Steen, E. 2010. Residual Hull Girder Strength of Ships with Collision or Grounding Damages. *Proceedings of PRADS 2011 Conference, Rio de Janeiro, Brazil, pp. 941-951*
9. Koukounas D., Samuelides M. 2013. Modelling aspects of strength capacity of intact and damaged ship girders. *Proceedings of MARSTRUCT 2013 Conference 25-27 March, Espoo, Finland, pp. 157-165*
10. Pollalis C., Samuelides M. 2013. Ultimate strength of damaged hulls. *Submitted to the 6th International Conference of Collision and Grounding of Ships, Trondheim, Norway*
11. Samuelides M., Koukounas D., Pollalis C. 2013. Residual strength of damaged ship's hull. *Proceedings of the PRADS2013 Conference, 20-25 October, CECO, Changwon City, Korea*
12. ABAQUS 6.13. Analysis User’s Guide, Vol. 2: Analysis. Chapter 6.3.3
13. ABAQUS 6.13. Getting Started with Abaqus/Interactive Edition. Chapters 8.1 & 8.2
14. Alsos H.S., Amdahl J., Hopperstad, O.S. 2009. On the resistance to penetration of stiffened plates, Part II: Numerical Analysis. *International Journal of Impact Engineering, 36 (2009) 875-887*

15. Τσαμασφύρος Γ. Μηχανική Παραμορφώσιμων Σωμάτων ΙΙ. p*g. 8-14, ΕΚΔΟΣΕΙΣ ΣΥΜΜΕΤΡΙΑ*
16. Κορουλάκης Π 2014. Μέγιστη αντοχή πλοίου στην άθικτη κατάσταση και σε καταστάσεις μετά από βλάβη. *Διπλωματική εργασία για το Δίπλωμα του Ναπυηγού Μηχανολόγου Μηχανικού ΕΜΠ*
17. International Ship and Offshore 2006 (ISSC 2006). August 20-25, Southampton
18. Timoshenko S. (1953). The Strength of Materials. Mc-Graw-Hill Company
19. Common Structural Rules for Double hull Oil Tankers. Sections 6.1, 7.2 & 8.1

APPENDIX

SHIP DRAWINGS

MIDSHIP SECTION-SHIP I

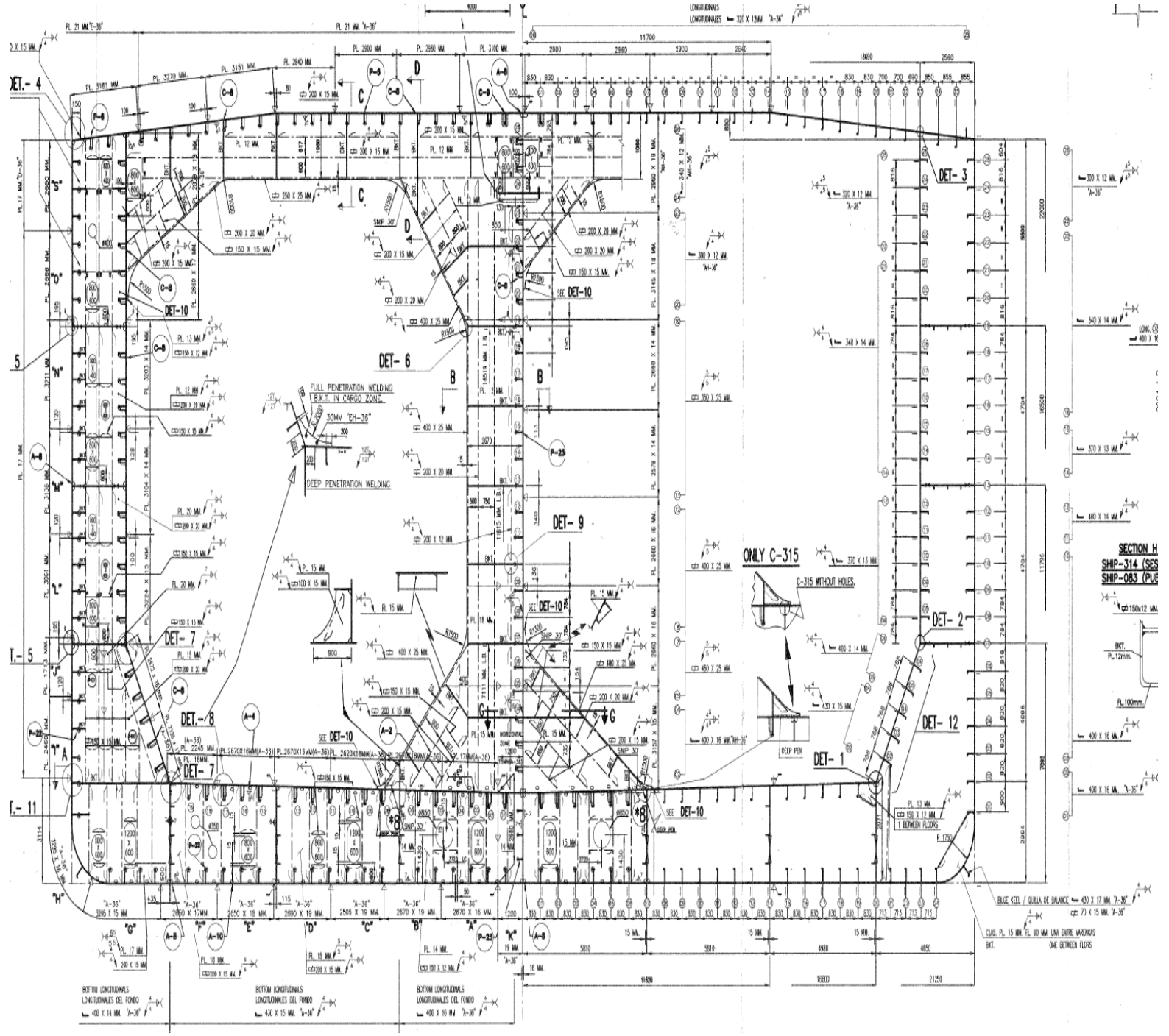

MIDSHIP SECTION-SHIP II

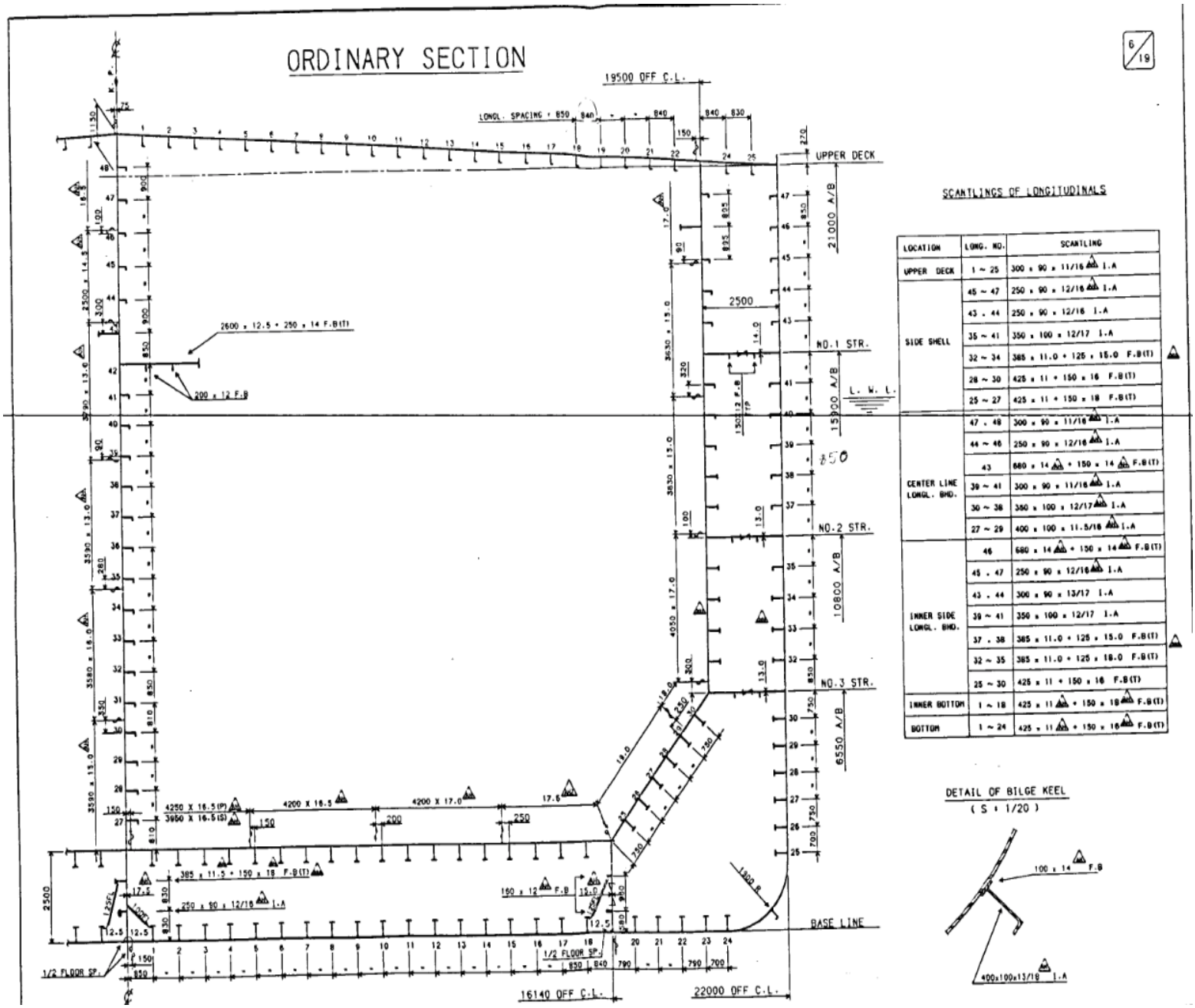

SCANTLINGS OF LONGITUDINALS

LOCATION	LONG. NO.	SCANTLING
UPPER DECK	1 ~ 25	300 x 90 x 11/16 I.A
SIDE SHELL	45 ~ 47	250 x 90 x 12/16 I.A
	43 . 44	250 x 90 x 12/16 I.A
	35 ~ 41	350 x 100 x 12/17 I.A
	32 ~ 34	385 x 11.0 + 125 x 15.0 F.B(T)
	28 ~ 30	425 x 11 + 150 x 16 F.B(T)
	25 ~ 27	425 x 11 + 150 x 18 F.B(T)
CENTER LINE LONGL. BHD.	47 . 48	300 x 90 x 11/16 I.A
	44 ~ 46	250 x 90 x 12/16 I.A
	43	680 x 14 + 150 x 14 F.B(T)
	39 ~ 41	300 x 90 x 11/16 I.A
	30 ~ 38	350 x 100 x 12/17 I.A
	27 ~ 29	400 x 100 x 11.5/16 I.A
INNER SIDE LONGL. BHD.	46	680 x 14 + 150 x 14 F.B(T)
	45 . 47	250 x 90 x 12/16 I.A
	43 . 44	300 x 90 x 13/17 I.A
	39 ~ 41	350 x 100 x 12/17 I.A
	37 . 38	385 x 11.0 + 125 x 15.0 F.B(T)
	32 ~ 35	385 x 11.0 + 125 x 18.0 F.B(T)
	25 ~ 30	425 x 11 + 150 x 18 F.B(T)
INNER BOTTOM	1 ~ 18	425 x 11 + 150 x 18 F.B(T)
BOTTOM	1 ~ 24	425 x 11 + 150 x 18 F.B(T)

DETAIL OF BILGE KEEL
(S = 1/20)